5-1999

CLOSE-RANGE AND SATELLITE REMOTE SENSING OF ALGAL BIOMASS IN THE IOWA GREAT LAKES

Eric A. Wilson
University of Nebraska-Lincoln

CLOSE-RANGE AND SATELLITE REMOTE SENSING OF ALGAL BIOMASS IN THE IOWA GREAT LAKES

by

Eric A. Wilson

A THESIS

Presented to the Faculty of

The Graduate College at the University of Nebraska

In Partial Fulfillment of Requirements

For the Degree of Master of Arts

Major: Geography

Under the Supervision of Professor Donald C. Rundquist

Lincoln, Nebraska

May, 1999

CLOSE-RANGE AND SATELLITE REMOTE SENSING OF ALGAL BIOMASS IN THE IOWA GREAT LAKES

Eric A. Wilson, M.A.

University of Nebraska, 1999

Advisor: Donald C. Rundquist

The utility of both close-range and satellite remote sensing for assessing inland water quality was examined in the Iowa Great Lakes. The water quality of this system is of considerable interest because of its status as an environmental, recreational, and therefore, economic resource. The broad range of optical conditions present in the lakes and the wealth of literature on the system make it an ideal environment for water quality remote sensing research. The goal of this research was to survey the water quality of the Iowa Great Lakes via remote sensing, evaluate different predictive algorithms, and map the distribution of algal biomass.

In situ sampling was carried out on Spirit, West Okoboji, and East Okoboji lakes, concurrent with a SPOT-2 satellite overpass, August 13, 1997. A total of 26 sample sites were visited. Measurements included chlorophyll *a*, turbidity, vertical attenuation, hyperspectral radiance/reflectance, and GPS. Aerial photographs were taken later in order to illustrate the spatial characteristics of various aquatic features.

Empirical relationships between chlorophyll and both close-range (hyperspectral) and satellite (broad-band) data, were evaluated using correlation and regression

techniques. Results suggest that low chlorophyll concentrations are difficult to estimate, while moderate to high biomass levels can be accurately modeled using either close-range or satellite data. The near-infrared portion of the optical spectrum proved the single most useful spectral region for estimating chlorophyll concentration. Due to their ability to correct for nonalgal scattering, the NIR:Red ratio ($r^2 = 0.997$) and the Baseline Sum ($r^2 = 0.998$) algorithms, proved the most effective for estimating chlorophyll in hypereutrophic East Okoboji Lake.

Chlorophyll *a* maps were developed by applying an algorithm based on near-infrared band radiance magnitude ($r^2 = 0.833$) to the SPOT imagery. The distribution of algal biomass is predominantly homogeneous in West Okoboji and Spirit lakes, but extremely patchy in Lake East Okoboji. This spatial heterogeneity of water quality constituents may be a significant source of error for monitoring programs based solely on point sampling.

ACKNOWLEDGMENTS

The list of people who have assisted me during my graduate career is extensive and diverse. First, I recognize my committee members, Dr. Kyle Hoagland, Dr. Sunil Narumalani and Dr. James Merchant. They have been a great asset to me in my research and coursework endeavors. Special thanks go to my advisor, Dr. Donald Rundquist, who has provided me with opportunities that amaze me to this day. I came to the University of Nebraska with the hopes of working at the Center for Advanced Land Management Information Technologies and Dr. Rundquist made that possible and much more. A more conducive environment to learning and growing I cannot imagine. Dr. Stephen Lavin, who was my initial contact here at UNL, deserves acknowledgment. He played a significant role in my enrollment at UNL. My personal and professional growth was positively impacted by Dr. John Schalles and my Israeli mentors and friends Dr. Anatoly Gitelson, Dr. Yosef Yacobi, and the "wanna be" Ph.D.'s, Robi Stark, Yoav Zur, Dror Etzion and their families.

My thesis research and various class projects benefited greatly from the help I received from John Holtz and Kris Fisher, as well as the student employees and staff at CALMIT, particularly, Dave Derry, Rick Perk, Brian Tolk, Bryan Leavitt and Stuart McFeeters. All the great people in the Conservation and Survey Division, especially Bernice Goemann the ladies in the main office, have been more than accommodating during my years at UNL. I give special thanks to Water Level Program Coordinator Mohan Khisty, Steve Payton and their respective families for their friendship and contributions to my enlightenment. Others deserving thanks include: the Iowa Lakeside Lab, Roger Patocka, Gary Phillips, Joe Larscheid, Gary Owen and Gary Koppie. Gary Koppie requires special acknowledgment for taking me up in his airplane to acquire aerial photographs of the lakes. I am especially grateful to Brian Smith and my long-time friend Ron Lane for their hospitality and comfortable, free couch up at the lakes.

Most of all I thank my parents, Roger and Rose Wilson, who made sacrifices which their children will forever benefit from. Along with my brother Brent, my family has provided me with an abundance of tangible and intangible support, including their uplifting love, profound guidance and encouragement.

TABLE OF CONTENTS

LIST OF FIGURES

LIST OF TABLES

CHAPTER 1 — INTRODUCTION

1.1 Rationale

Water is a necessity of life and therefore a fundamental natural resource. Water often attains the status of a commodity, possessing significant value or potential. This perception of water is usually a consequence of its scarcity and/or an effect of its utility. Whatever the motivating factor(s), proper management is usually deemed indispensable for restoring and/or maintaining a high level of water quality.

The success of any management paradigm requires a comprehensive understanding of system elements and their relational structure. In the context of photosynthetic populations in aquatic ecosystems, Wetzel and Likens (1991) state that "an understanding of community structure is dependent on the ability to differentiate between true population changes and variations in spatial and temporal distribution." This implies that without an understanding of spatial and temporal dynamics, true ecological conditions cannot be adequately determined, rendering the management paradigm less than optimal.

Air/space remote sensing appears to provide a useful means to adequately characterize the spatial and temporal distribution of optically active constituents in sizable bodies of water. Therefore, remote sensing may be the only practical approach for isolating transient spatial and temporal variability from long-term ecological trends.

1.2 Purpose

In the early 1970s, a comprehensive water quality study was carried out on the Iowa Great Lakes "to document ... limnological conditions in each lake and the reasons

for the differences in the degree of eutrophication among the lakes" (Jones and Bachmann, 1974). The purpose of this research is similar in concept but more focused in form. Here, the focus is on quantifying chlorophyll *a* (chl *a*) concentration by means of remote sensing. A tangential objective is to document the spatial distribution of algal biomass in the Iowa Great Lakes.

1.3 Research Questions

This thesis addresses three primary research questions.

*1. **What are the reflectance characteristics of the Okoboji lakes?***

In answering this question, I explain the hyperspectral reflectance characteristics of West and East Okoboji lakes as determined through close-range spectroradiometry. The primary emphasis is on how these lakes differ from one another spectrally and how this impacts the successful quantification of chl *a* concentration.

*2. **What empirical relationships exist between hyperspectral reflectance and chl a concentration?***

This is the principal focus of the thesis and involves the application of previously developed predictive algorithms to data collected from the wide range of optical conditions present between West and East Okoboji lakes. The end result is the determination of which techniques most accurately estimate algal biomass. The restriction of the algorithms to certain optical conditions is also discussed.

*3. **How is algal biomass distributed throughout the Iowa Great Lakes?***

This question is addressed through the analysis of the Systeme Pour l'Observation de la Terre (SPOT) imagery acquired concurrently with surface sampling. The SPOT data demonstrate the effectiveness of air/space imaging for capturing the spatial arrangement

of optically active constituents in an aquatic medium. The success of several chl *a* predictive algorithms is also reported. The most reliable algorithm is used to develop maps of chl *a* concentration.

1.4 Traditional Methods for Assessing Water Quality

Planktonic algal abundance (i.e. biomass) is the primary factor affecting water clarity in many inland water bodies, including Iowa's Great Lakes. Chl *a* concentration ($\mu g\ L^{-1}$), a popular measure of algal abundance, is often used to describe water quality. This is because chl *a* is the principal photosynthetic pigment in all algae and can be considered taxonomically independent (Stewart, 1974; Rowan, 1989; Lee, 1992).

Quantitative determination of chl *a* concentration typically takes place in a laboratory where the pigment is extracted from cells using organic solvents and then analyzed via spectrophotometry, fluorometry or high performance liquid chromatography. Although reasonably accurate and reliable, these methodologies remain less than ideal due to their reliance on point sampling, which is labor/cost intensive and seldom captures the true character of the water body. The spatial arrangement and size of the sample area ultimately determine how well the data represent actual conditions across geographic space. Even with a fine grid of sites, often logistically impractical, gaining a true representation of an aquatic environment is improbable due to the turbulent and variable nature of the medium itself.

1.5 Remote Sensing Methods for Assessing Water Quality

The direct linkages among the optical nature of the water, accepted optical definitions of water quality and our ability to collect optical information via remote

sensing, form the logical framework of a remote sensing approach. Ideally, we would like to use remote sensing to directly measure water quality parameters commonly measured in the laboratory; namely, the inherent optical properties. This is impossible, however, because the effects of scattering can neither be minimized nor held constant, spatially or temporally, in the natural environment. The reliance of remote sensing on solar illumination also prevents measurement at this fundamental level. However, subsequent determination of the inherent optical properties from volume reflectance is a current research focus (Dekker *et al.*, 1991; Van Stokkom *et al.*, 1993; Jupp *et al.*, 1994).

Reflectance (R) is a common unit of measure in remote sensing research. Kirk (1994) refers to reflectance and vertical attenuation as, "apparent" or "quasi-inherent" optical properties. These apparent optical properties are largely determined by the inherent optical properties of the aquatic medium but are minimally affected by changes in irradiance; i.e. solar zenith changes (Morel and Prieur, 1977; Kirk, 1994).

The restriction of remote sensing to the "apparent" research domain requires the employment an empirical approach for quantifying water quality indicators such as chl *a* concentration. This involves analyzing, via simple linear regression, the relationship between the radiance measured at the sensor and the water quality parameters acquired concurrently *in situ*. The strength of the relationship or, "goodness of fit," is expressed in terms of the correlation coefficient (r) or the coefficient of determination (r^2) (Chacon-Torres *et al.*, 1992; Quibell, 1992; Van Stokkom *et al.*, 1993; Kirk, 1994; Mayo *et al.*, 1995; Gitelson *et al.*, 1995). Although not universally applicable, empirically derived algorithms can, once properly calibrated, provide useful estimates of chl *a* on a site-specific basis (Mayo *et al.*, 1995; Kirk, 1994).

1.5.1 Air/Space Imaging

The synoptic view offered by airborne and satellite sensors is the advantage most often associated with remote sensing. The ability to sample an entire lake system almost instantaneously, hence capturing the spatial distribution of the optical characteristics, uniquely qualifies remote sensing for water quality assessment and monitoring. In essence, a single digital image produces one sample value for every spectral channel, for every pixel contained in the water body.

In addition to the synoptic view, multispectral and multitemporal sensor characteristics provide significant utility for water quality research. Provided the spectral bands are properly placed and sufficiently narrow, a multispectral capability allows individual absorption and/or scattering processes to be examined. Ultimately, the spectral and radiometric resolutions determine the effectiveness of a sensor for capturing wavelength specific information, while the temporal resolution (revisit cycle) determines the potential for monitoring the progression of water quality conditions.

1.5.2 Close-Range Remote Sensing

A close-range remote sensing assessment of water quality can be viewed as a hybrid approach, fusing laboratory concepts and air/space remote sensing rationale. The phrase, "close-range remote sensing," usually refers to outdoor, surface-based data collection incorporating a spectoradiometer. The numeric data output from such non-imaging sensors is similar to that of a laboratory spectrophotometer. In both cases, radiant flux is detected and quantized at numerous spectral bands or channels. When the reflectance values (%) are plotted in terms of wavelength, they assume a curvilinear appearance and are referred to as a "spectral signature."

The precision at which the emergent flux is represented is determined by the spectral and radiometric resolutions of the sensor. A hyperspectral capability promotes the detection of individual absorption and scattering processes. This is very useful for aquatic studies where a diverse array of optical constituents produce complex spectral signatures. Such a configuration is quite different from the broad-band capability common on satellite platforms. In the case of broad bands, information on specific processes can be degraded when the signal is integrated across large spectral intervals.

Laboratory and close-range remote sensing approaches to water quality are both dependent on point sampling, a significant limitation. However, close-range remote sensing allows a nearly continuous sequence of measurements to be acquired across a broad spectral range while in the field. *In situ* measurements via close-range remote sensing therefore allow the full optical spectrum to be investigated as the phenomena exist in their natural states. The non-destructive and continuous capabilities of this measurement approach make close-range remote sensing an appealing and unique means of assessing water quality.

A final benefit of close-range remote sensing results from its relative indifference to atmospheric distortion when compared to satellite platforms. The close proximity of the sensor and target reduces potential atmospheric attenuation substantially from what is encountered by high altitude platforms. The degradation of the upwelling signal by atmospheric attenuation is especially significant to aquatic remote sensing applications because of the typically low signal strength and narrow dynamic range of aquatic targets. Similarly, Dekker *et al.* (1991) suggest the close-range approach allows the evaluation of remote sensing systems under ideal circumstances. Through spectral band simulation and

signature reconstruction (Dekker *et al.*, 1991; 1992), a process which involves the mathematical integration of the hyperspectral response to the broad bands possessed by satellite platforms, the utility of different sensors and/or band configurations can be evaluated.

1.6 The Study Area

1.6.1 General Background

The drainage basin containing the Iowa Great Lakes is located in north-central Dickinson county, Iowa (USA) and southern Jackson county, Minnesota (USA) [43° 25' 19" N latitude by 95° 07' 30" W longitude] (Figure 1-1). The climate of this region is classified as humid continental with wide daily and seasonal variations and an average annual rainfall of 69.5 cm (Bachmann and Jones, 1974).

The lakes of this system are relics of glacial retreat and are categorized as typical hard-water or bicarbonate lakes (Bachmann and Jones, 1974; Jones and Bachmann, 1978). The system falls within the boundaries of the Des Moines lobe of the Wisconsin glacial drift sheet (Jones and Bachmann, 1978). Radiocarbon dating of West Okoboji Lake sediment cores places the system at 12,700 ybp ±200 yr (Dodd *et al.*, 1968).

There are seven primary lakes in the drainage basin, five of which have separate watersheds. There are also numerous ponds, wetlands and marshes throughout the area (Table 1-1). The major lakes are: Spirit Lake, West Okoboji Lake, East Okoboji Lake, Upper Gar Lake, Lake Minnewashta, Lower Gar Lake, and Loon Lake (in Minnesota).

1.6.2 Historical Perspective

Even though there has been no indication of any systematic change in water

quality from the early 1970s to the late 1980s (Bachmann, 1990), the local citizenry have altered their behavior and organized in response to a heightened environmental awareness. The increase in awareness has prompted a more proactive management style which is aimed at improving the stability and utility of the ecosystem with a simultaneous increase in long-term viability. For example, agricultural tiling systems have been dismantled and historic wetlands re-established. Another example is the completion of a high-capacity sewage line and the associated arterials which divert more phosphorus from the watershed than enters from all of the other sources combined (Bachmann and Jones, 1974).

The improvements in awareness and understanding which have spurred these initiatives can be largely attributed to the establishment of the Iowa Lakeside Laboratory on West Okoboji Lake in 1909. The existence of this university field station has provided a means for conducting numerous scientific investigations. As a result, there is a wealth of literature addressing the flora, fauna and overall ecology of the system. This extensive base of knowledge, and the ever growing interest in improving the water quality, make current and future studies on the area even more appropriate and perhaps more sound.

1.6.3 Significant Characteristics, Trends and Processes

1.6.3.1 Nutrient Cycles

Phosphorus availability plays a significant role in determining biological productivity (Wetzel, 1983) and nutrient budgets suggest the Iowa Great Lakes act as a phosphorus trap (Bachmann and Jones, 1974). The budgets for these lakes suggest that West Okoboji Lake and Spirit Lake follow the same general pattern, while the annual

patterns of East Okoboji Lake and the Gar lakes are similar (Bachmann and Jones, 1974).

The ability to store phosphorus in the bottom sediments may be the source of the nuisance algal conditions more evident in the shallow lakes. The high level of boat traffic during the summer season may contribute to the resuspension of phosphorus in the water column. This may be one reason why past copper sulfate treatments applied to East Okoboji for controlling nuisance algae have proved ineffective over the long term.

1.6.3.2 Eutrophication

In terms of phosphorus availability, each of Iowa's Great Lakes are classified either as eutrophic or hypereutrophic (Table 1-2). In order of increasing eutrophication they are, West Okoboji, Spirit and East Okoboji lakes (Bachmann and Jones, 1974). This ranking is also valid in terms of algal abundance (Tables 1-2, 1-4). While only two trophic classes are technically represented, the Iowa Great Lakes possess a wide range of optical transparency/turbidity conditions. Each of the three lakes sampled in this investigation occupies a discrete section of a broad optical clarity gradient.

Trends in taxonomic composition and biomass distribution are also evident among the lakes in this system. As the level of eutrophication increases, there is an increasing proportion of blue-green algae. Bachmann and Jones (1974) note how these relationships are associated with the lake volume : watershed area ratio (Table 1-3).

1.6.3.3 Sedimentation

In the past, suspended inorganic matter has not been a prominent constituent in the Iowa Great Lakes (Bachmann and Jones, 1974). Jones and Bachmann (1978) found a tendency for water transparency to decrease as summer progressed for many lakes and reservoirs throughout Iowa, including the Okoboji lakes, and concluded that the

decreases were related more to algal density than to suspended inorganic matter. To a large degree, this simplifies the optical character of the lakes because particulate scattering can be attributed primarily to organic sources, i.e. algal cells.

In recent years the Iowa Great Lakes region has undergone a wetlands "renaissance" in which historic wetlands throughout the drainage basin have been restored. Given the filtering capabilities of wetland environments, improvements in agricultural practices, and heightened environmental awareness, continued low levels of suspended inorganic material should be expected.

1.6.3.4 Lake Specific Optical Properties

The lakes sampled for this research, West Okoboji, East Okoboji and Spirit lakes, each exhibit a unique hue which is clearly evident to the naked eye, in aerial photography, and in satellite imagery. This color difference is a function of the inherent optical properties of each lake, specifically the scattering and absorption coefficients. These coefficients are contingent on the cumulative absorption and scattering properties of the optically active constituents in the water column. The optical constituents of inland lakes fall into four fundamental groups; pure water, dissolved organic matter (yellow substance), tripton (non-living particulate matter), and phytoplankton (Kirk, 1994).

The Iowa Great Lakes tend to fall into the Case 1 category established by Morel and Prieur (1977) for green oceanic waters. The ideal example of a Case 1 system is where a pure culture of phytoplankton exists, absent of inorganic particles. Due to phytoplankton being the dominant optical constituent in the water column of these lakes, the color disparity results largely from differences in algal abundance and/or taxonomic

composition, with algal cell scattering and photosynthetic pigment absorption being the dominant processes. However, the inherent optical properties for phytoplankton are influenced by numerous factors including the cell or colony structure, size, shape and pigment composition. Other factors, such as the presence of gas vacuoles, common in blue-green algae, also impact the optical character of the water by enhancing the scattering process (Carr and Whitton, 1973; Kirk, 1994).

1.6.3.5 Thermal and Temporal Abundance Patterns

Individual lakes maintain very similar summer surface temperatures, but West Okoboji, with its large volume, responds more slowly to ambient thermal trends than lakes of small volume (Table 1-3). West Okoboji does thermally stratify and turns over in the spring and fall. Except for Lake Minnewashta, none of the shallow lakes thermally stratify (Bachmann and Jones, 1974).

While algal standing crops differ among the Iowa Great Lakes, the temporal pattern of chl *a* abundance is similar in all the lakes. Pigment concentrations increase throughout the summer and usually peak in September, coinciding with ambient thermal patterns. Thereafter, levels decrease to a minimum during ice cover and remain low into early May (Bachmann and Jones, 1974).

1.6.3.6 Algal Bloom Conditions

Nuisance algal levels in the Iowa Great Lakes usually result from the excessive growth of blue-green algae, specifically, *Aphanizomenon flos-aquae* (Cyanophyceae). This filamentous planktonic alga forms feathery colonies which look like "chopped grass" in the water. Typically, the colonies become concentrated near the surface due to the positive buoyancy of gas vacuoles (Carr and Whitton, 1973; Prescott, 1978; Lee,

1989). The concentration of this alga in bays and coves by wind, combined with the intense solar conditions at the surface, often leads to massive photooxidative death of the cells (Lee, 1989). There are several consequences of these mass die-offs, including the visual degradation of the water, as well as the oppressive odor produced by the decaying cells. Because the phycobilipigments are water soluble, the shoreline and surrounding water take on a distinct cyan color (Figure 1-2). A variety of endotoxins, known to be deadly when ingested by livestock and other animals, are also released into the water.

1.6.4 Specific Lakes of Interest

As introduced earlier, West Okoboji, East Okoboji and Spirit lakes, each occupy a discrete section of the total phosphorus range. Even though the lakes are connected and exchange surface water, each lake similarly maintains its own unique optical character. Bachmann and Jones (1974) suggest this is largely determined by lake morphology.

1.6.4.1 West Okoboji Lake

West Okoboji is the deepest natural lake (41.5 m) in Iowa (Bachmann, 1990) and possesses the greatest volume of the lakes in this system (Bachmann, 1966) (Table 1-3). West Okoboji has a relatively small terrestrial drainage area compared to its lake volume (Table 1-3) and possesses a unique funnel-shaped basin. West Okoboji is thought to be spring fed, but rates and fluctuations are not well understood.

West Okoboji consistently maintains the lowest phytoplankton standing crop in the system and only occasionally experiences nuisance algal conditions (Table 1-2). Blooms develop only on a localized and short-term basis, usually a product of algae being concentrated by wind. This lake is considered eutrophic but maintains a high degree of optical transparency, commonly appearing light green in color.

West Okoboji is largely homogeneous in terms of biomass distribution but heterogeneous in terms of phytoplankton taxa. Chl *a* levels of 5 μg L^{-1} are common and a fluctuating co-dominance exists between green and blue-green genera (Bachmann and Jones, 1974). The phytoplankton present on the day of data collection (8/13/97) were consistent among the sample sites and were virtually identical to those documented by Bachmann and Jones (1974). Some of the more common genera were, *Anabaena, Gleotrichia, Microcystis, Aphanizomenon, Scenedesmus, Euglena,* and *Pediastrum.*

1.6.4.2 East Okoboji Lake

A long and narrow lake, East Okoboji possesses a chain of distinct basins. These sub-basins have gradually sloping bottoms which reach a maximum depth of 6.7 m near the southern end of the lake. East Okoboji is consistently classified as hypereutrophic and possesses high chl *a* levels. The two dominant phytoplanktonic genera are *Aphanizomenon* and *Microcystis,* the former being significantly more prominent. The highest chl *a* level recorded during data collection (8/13/97) approached 600 μg L^{-1}. These high biomass levels, common in the summer and fall, give the water a deep blue-green color with very limited transparency. These dense conditions frequently culminate as surface "scums" or emergent alga blooms (Figure 1-2).

Unlike Spirit and West Okoboji, East Okoboji maintains a heterogeneous biomass distribution across its surface. At the height of the growing season, distinct patches of dense algae are often interspersed with relatively clear water (Figure 1-3). Bachmann and Jones (1974) suggest that this results from "morphological and external factors" which differentially influence water quality at various locations, a spatial dependence which should be investigated in future air/space remote sensing research. The discovery

and understanding of any biomass spatial dependency could lead to further improvements in the Iowa Great Lakes' water quality.

1.6.4.3 The Gar Chain (Upper Gar Lake, Lake Minnewashta and Lower Gar Lake)

Upper Gar Lake and Lake Minnewashta are considered to be the southern extension of East Okoboji because these lakes all share the same watershed. Although Lower Gar possesses its own watershed, it is similar to both Upper Gar and Lake Minnewashta. Together, these lakes are referred to as the "Gar Chain" and in terms of planktonic composition and spatial biomass characteristics, they mirror East Okoboji.

All surface waters of the primary lakes eventually drain into the Gar Chain and out of the drainage basin via an ungated spillway on Lower Gar Lake. This outlet was constructed in 1910 and is the only surface outlet for the Iowa Great Lakes (Bachmann and Jones, 1974). The spillway forms the source of Milford Creek, which flows into the Little Sioux River and eventually into the Missouri River.

1.6.4.4 Spirit Lake

Spirit Lake has the largest surface area of any natural lake in Iowa (Table 1-3). The morphology of this lake is characterized by a gently sloping shore and a uniform depth of approximately 6.1 m across the majority of its expanse. Spirit Lake is supplied by Minnesota lakes (Loon, Rush and Pearl) which drain in a southerly direction. Spirit Lake subsequently drains into the north end of East Okoboji Lake via a concrete outflow constructed in 1944 (Bachmann and Jones, 1974).

In terms of chl *a* levels, Spirit Lake exists between the extremes exhibited by West Okoboji, with its typically low chl *a* levels, and East Okoboji, with its typically high chl *a* levels (Tables 1-2, 1-4). Spirit Lake is considered eutrophic and the planktonic

taxa more closely resembles that of East Okoboji with blue-green genera dominating most of the year. However, Spirit Lake and West Okoboji are similar in that both possess relatively homogeneous biomass distributions (Bachmann and Jones, 1974).

1.7 Study Design

Three trips were made to the study area. The first two "reconnaissance" trips were taken for the purpose of becoming more familiar with the lake system, surveying the taxonomic composition, and determining the accuracy and reliability of the proposed Global Positioning System (GPS) community base station. The third trip to the study area was for comprehensive data collection.

1.7.1 Seasonal Considerations and Logistics

August was targeted for data collection because conditions favorable to my research typically occur during this period. Specifically, there is a higher probability of encountering a wide range of chl *a* concentrations and emergent bloom conditions. In addition, spatial patchiness is more pronounced late in the growing season. Scheduling data collection when biomass is high is also beneficial due to the potential improvement in the signal-to-noise ratio resulting from increases in particle scattering.

Fourteen potential August dates were dictated by the SPOT-2 satellite orbit cycle. The number of potential dates was reduced to four because of sensor incidence angle requirements. Due to the relatively low reflectance magnitude of water (usually <10%), a view angle of less than 10° from nadir was considered more appropriate for exploiting a weak return signal. On August 13, 1997, the weather conditions were suitable for remote sensing (Figure 1-4).

1.7.2 SPOT Satellite Imagery

The SPOT platform was selected for this research primarily because of the off-nadir viewing capability of the high resolution visible (HRV) sensor. The ability to manipulate the sensor incidence angle increases the overpass frequency. This flexibility is appealing because midwestern weather patterns are quite variable and cloud cover prevents surface features from being studied. The decision to use SPOT instead of the more commonly used Landsat Thematic Mapper (TM), increased the probability of procuring usable image data.

In addition to the higher temporal resolution, the SPOT platform possesses several other advantages. The higher spatial resolution of the SPOT HRV, 20 m versus 30 m for TM, is better suited for capturing intricate spatial patterns, such as biomass patterns on East Okoboji Lake. Second, the spectral bands commonly used for inland lake water quality assessment (green, red, near-infrared) are nearly identical between the two sensors (Dekker *et al.*, 1992; Guyot and Gu, 1994; Jensen, 1996). Finally, the excessive geographic area imaged by the Landsat TM sensor and the surplus of bands inappropriate for water quality determination, provide only an increase in financial and storage space costs with little improvement in research utility.

1.7.3 Surface Investigation

The spatial sampling regime used on August 13, 1997 (Figure 1-5), approximates that developed by Bachmann and Jones (1974). Because this spatial design was also adopted for the long-term (1974 - present) monitoring program of the system, it was appropriate that initial remote sensing research focus, at a minimum, on those general locations.

Two boats (speed and pontoon) were used for data collection. United States Geological Survey (USGS) 7.5' topographic quadrangles and Iowa Department of Natural Resources lake bathymetry maps were used for positioning the boats at the predefined sample sites. The spatial coordinates for each sample site were precisely recorded using Trimble GPS receivers capable of differential correction. The positional data for each site were differentially corrected (post processing) using a community base station located near Onalaska, Wisconsin. This base station is 322 km east of the Okoboji study site. Trimble Navigation recommends that the distance separating the rover and the base station not exceed 483 km; thus, the use of this base station was valid. The horizontal accuracy achieved through differential correction ranged from one to five meters. On January 1, 1999, the Onalaska, Wisconsin community base station was taken off-line and relocated at another site.

1.7.3.1 Spirit Lake

The speed boat was anchored at each Spirit Lake site, GPS positions logged, and water samples collected. Other ancillary information such as water temperature, depth, sky conditions, and surface characteristics were also documented. The restriction of the pontoon boat to the West and East Okoboji lakes meant that no optical data could be gathered from Spirit Lake on 8/13/97.

1.7.3.2 Okoboji Lakes

Extensive data collection was carried out on West and East Okoboji from the pontoon boat. In addition to the parameters mentioned above, *in situ* optical measurements of the water and incoming solar radiation were carried out. Attention was given to two primary parameters, hyperspectral reflectance of the water (discussed in

Chapter 2) and subsurface vertical attenuation. The latter is a direct measure of the ability of the water to bring about a diminution of radiant energy with depth through both scattering and absorption processes (Kirk, 1994). Determination of the attenuation coefficient is accomplished via the Beer-Bouguer Law:

$$\mathbf{E_{zPAR} = E_{0PAR} \exp -k_d z} \quad \text{where,}$$

E_{zPAR} = downward photosynthetically active irradiance at depth z (μmol $s^{-1}m^{-2}$ μA^{-1})

E_{0PAR} = downward photosynthetically active irradiance above surface (μmol $s^{-1}m^{-2}$ μA^{-1})

k_d = diffuse photosynthetically active irradiance attenuation coefficient (m^{-1})

z = depth (m).

Measurements of E_{zPAR} were made using a LI-COR (Lincoln, NE) underwater quantum sensor (LI-192SA) suspended from a yardarm on the boat and lowered into the water in 1 m increments down to maximum depth of 6 m. Measurements of E_{0PAR} were collected using a terrestrial quantum sensor (LI-190SA) that was mounted overhead on the boat framework. Quantifying E_{0PAR} in this manner rather than just below the air/water interface may have biased the calculated attenuation values.

1.7.4 Water Quality Ground Truth Data

Water samples were collected using the "grab" method. At each sample site, 500 ml wide-mouth amber plastic bottles were rinsed several times with lake water and then filled between the air/water interface and 40 cm in depth. The bottles were then labeled and placed in a cooler containing lake water and a small amount of ice. This helped maintain the thermal conditions of the samples.

Turbidity measurements were carried out the morning following data collection using a 2100P Portable Turbidimeter (HACH, Loveland, CO). The instrument was calibrated using HACH *StablCal* turbidity standards. A known volume of water sample

was also passed through a Gelman A/E 47 mm glass fiber filter (porosity = 0.3 μm), wrapped in foil and immediately frozen. The filters were later packed in dry ice for the trip back to Lincoln, NE.

The pigment extraction and fluorometric measurement processes took place approximately ten weeks after filtration and followed the procedures of Nusch (1980), Arar and Collins (1992), and Welschmeyer (1994). Ninety percent ethanol was used as the extracting solvent and care was taken to prevent the extracts from degrading in the ambient light. A TD-700 Fluorometer (Turner Designs Inc., Sunnyvale, CA), configured with the excitation and emission filters specified by Welschmeyer (1994) was used in this research. A single point (75 μg L^{-1}) calibration procedure using a pure sample of *Anacystis nidulans* (Sigma, St. Louis, MO) in ninety percent ethanol was used to calibrate the instrument (Turner Designs, 1995). Four standard solutions were prepared and periodically measured in order to monitor instrument drift and variability introduced by the decanting process (Table 1-5). In order to examine the reliability of the fluorescence measurements, each extract volume was split and re-measured (2-4x), often with a different ethanol dilution. Table 1-6 shows the chl *a* measurements and the associated standard deviation values. Only the four highest chl *a* measurements show a high level of variation. It is probable that this error is associated with the excessive dilution that was required to bring these extracts into the linear range of the instrument. This source of error can be avoided by filtering less sample volume at the onset.

1.7.5 Aerial Photographs

Several rolls of 35mm print and slide film were shot from an airplane at an altitude of 360 - 450 m. The fly-over took place mid-morning on August 23, ten days

CHAPTER 2 — CLOSE-RANGE SPECTRORADIOMETRY

2.1 Methods

2.1.1 Instrumentation

Upwelling spectral radiance data were collected using an SE-590 silicon diode spectroradiometer (Spectron Engineering, Inc., Denver, CO) (Figure 2-1). The SE-590 is a non-imaging, hyperspectral remote sensing instrument capable of detecting radiant flux in 252 narrow spectral bands between 365 nm and 1126 nm. The 400-900 nm range was deemed the most pertinent due to the lack of useful data and the decrease in signal integrity from atmospheric and thermally induced variation outside this spectral range (Figure 2-2). The radiometric resolution of the SE-590 is 12 bit, which translates into 4096 brightness levels. The spectral bandwidth, in terms of the spectral distance at "full width half maximum," is ~10 nm and the spectral sampling interval is ~3 nm (Starks *et al.*, 1995).

2.1.2 Configuration

The SE-590 camera was configured with a 15° optic and arranged in a nadir viewing position, 1.5 m from the starboard (right) side of the boat and 2.4 m in vertical distance from the water (Figure 2-3). This arrangement produced a 64 cm diameter instantaneous field of view or spot size. A laptop computer with custom dedicated software was used to configure the instrument, initiate the scan sequence, and subsequently store the output data.

Because aquatic targets are not perfectly Lambertian (isotropic) reflectors, data

were collected close to solar noon when changes in solar zenith angle are minimal. In addition, the bow of the pontoon boat was consistently pointed east so as to lessen the influence of the boat on downwelling and upwelling light fields.

2.1.3 Calibration

Calibration of the spectroradiometer to the ambient light conditions, and quantification of the total incoming radiant flux (direct and diffuse combined), was accomplished using a 25.4 cm by 25.4 cm white *Spectralon* reflectance standard (Labsphere, Inc., North Sutton, NH) with near Lambertian reflectance characteristics. At each site, the reference panel was positioned under the camera optic and a calibration scan sequence was initiated (Figure 2-2). Immediately upon completion, the panel was removed, and a target scan sequence was initiated. Each scan sequence took approximately ten seconds and was composed of four individual spectral measurements which were internally averaged and saved as a single data file in the computer. These upwelling spectral radiance data were converted to reflectance (%) using Microsoft (Seattle, WA) Excel spreadsheet software according to the equation:

$$\mathbf{R_\lambda\ (\%) = L_{\lambda\ water}\ /\ L_{\lambda\ panel}\ * 100}\quad \text{where,}$$

R_λ = percent reflectance per wavelength

$L_{\lambda\ water}$ = upwelling spectral radiance from the water ($\mu W\ cm^{-2}\ sr^{-1} nm^{-1}$)

$\mathbf{L_{\lambda\ panel}}$ = upwelling spectral radiance from the calibration panel ($\mu W cm^{-2} sr^{-1} nm^{-1}$)

(Morel and Prieur, 1977; Milton, 1987; Dekker *et al.*, 1991, 1992; Gitelson, 1992; Gitelson *et al.*, 1993; Gitelson *et al.*, 1995; Quibell, 1992; Lillesand and Kiefer, 1994; Rundquist *et al.*, 1995; Rundquist *et al.*, 1996; Yacobi *et al.*, 1995; Schalles *et al.*, 1998). Technically, this type of biconical measurement configuration, where the radiance

of the target is reported as a proportion of that of the reference panel, is referred to as the bi-directional reflectance factor (Milton, 1987).

2.1.4 Statistical

The evaluation of different predictive techniques was accomplished through bivariate correlation and regression analysis at a 95% confidence level. Linear and logarithmic best fit equations were used and the strength of the relationships between chl *a* concentration and hyperspectral reflectance were described by the coefficient of determination (r^2). Statistical analyses were performed in Microsoft Excel.

2.2 Data Analysis

West Okoboji and East Okoboji lakes are significantly different in terms of optical character (§1.6.3.2; §1.6.3.4). This inherent contrast of conditions encouraged the stratification of close-range data according to trophic state.

2.2.1 West Okoboji Lake Reflectance Spectra

As expected, the spatially homogeneous nature of this water body results in nearly identical reflectance spectra (Figure 2-4). These spectra are ambiguous, in that the reflectance peaks and troughs corresponding to scattering and absorption processes are poorly developed and the reflectance signatures are, for the most part, superimposed upon one another.

In the 400-450 nm range, each reflectance signature demonstrates low reflectance due to photosynthetic pigment absorption. Absorption in this spectral region corresponds to the Soret band (435 nm) of chl *a* (Kirk, 1994; Schalles *et al.*, 1998). Absorption by dissolved organic matter may also be exerting some influence in these shorter

wavelengths (Morel and Prieur, 1977; Gitelson, 1992).

Reflectance increases with wavelength beyond 450 nm in a generally consistent manner and reaches its highest level (1.5% - 2.5%) in the green portion of the visible spectrum, where photosynthetic pigments have less absorptive capacity (Morel and Prieur, 1977). The slight depression near 480 nm may be attributed to carotenoid pigment absorption (Morel and Prieur, 1977; Richardson, 1996; Schalles *et al.*, 1998). The green peak of each signature exhibits a bimodal appearance. Small peaks at 540 nm and 580 nm are separated by a small depression at 560 nm.

To the right of the green peak at 580 nm, reflectance decreases dramatically and then flattens somewhat around 610 nm. This effect is produced by an increase in the absorption coefficient of pure water with wavelength (Morel and Prieur, 1977; Mayo *et al.*, 1995). It is possible that pigment absorption focused near 630 nm (chl *a* and phycocyanin) may also contribute to this feature, but its effect on the reflectance spectra is probably less significant than that of pure water.

Between 610 nm and 735 nm, only minor deflections from a straight line or "shoulders" are distinguishable. The depression near 675 nm corresponds to the two *in vivo* absorption maxima (670 nm and 680 nm) of chl *a* (Carr and Whitton, 1973; Morel and Prieur, 1977). The shoulder near 685 nm sometimes develops into a small peak. This feature can be attributed to chl *a* fluorescence (Morel and Prieur, 1977; Gitelson *et al.*, 1993; Rundquist *et al.*, 1996; Schalles *et al.*, 1998) and is only evident in relatively clear waters. In turbid waters, more prominent absorption and scattering processes mask the effects of chl *a* fluorescence.

Beyond 735 nm, increased absorption by pure water limits reflectance. A very

small rise in reflectance occurs around 800-810 nm and corresponds to a pure water absorption minimum at that spectral location (Dekker *et al.*, 1992).

2.2.2 East Okoboji Lake Reflectance Spectra

The spectral reflectance data collected over East Okoboji Lake show fully developed peaks and troughs (Figure 2-5). Several trends between spectral reflectance and chl *a* concentration are also apparent. These characteristics and trends are most likely a product of the higher average algal abundance and the large range in chl *a* levels of East Okoboji (Table 1-4).

As with West Okoboji, absorption by algal pigments dominates the shorter wavelengths (400-500 nm) and produces the low average reflectance for all spectra. In this lake, however, carotenoid absorption near 480 nm is more pronounced. Dekker *et al.* (1992) attribute this reflectance feature specifically to β-carotene, a very prominent carotenoid in blue-green algae (Carr and Whitton, 1974). Yacobi *et al.* (1996) found that myxoxanthophyll represented nearly 50% of the total carotenoids and β-carotene was a secondary contributor at 24% for *Aphanizomenon ovalisporum*, isolated from Lake Kinneret (Israel). Yacobi *et al.* (1996) identified other carotenoids for this species, including echinenone (13%) and zeaxanthin (4.7%). Both of which have similar absorption characteristics in this spectral region.

Each reflectance signature exhibits a fully developed or unimodal green peak positioned near 550 nm resulting from the minimal aggregate absorption of all algal pigments (Schalles *et al.*, 1998) and the increase in effective scattering by particulate matter (Dekker *et al.*, 1992). The green peaks of East Okoboji spectra are symmetrically shaped, much like bell shaped curves. At the lower three chl *a* levels, the peaks tend to

be broad and shallow, but as chl *a* increases, the tails of the bell squeeze closer together, forming a sharper, more distinct peak. Using the bell curve analogy, the standard deviation decreases with chl *a* concentration.

To the right of the green peak, reflectance drops off, forming a small depression for the three lower chl *a* levels and a full reflectance trough for the three higher chl *a* levels (~630 nm). This reflectance feature coincides with the absorption maximum of the biliprotein, C-phycocyanin (Carr and Whitton, 1973; Stewart, 1974; Lee, 1989; Rowan, 1989; Dekker *et al.*, 1992; Quibell, 1992; Gitelson *et al.*, 1993; Gitelson *et al.*, 1995; Richardson, 1996). However, because chl *a* also has a "satellite" absorption peak in this spectral region, the 630 nm feature cannot be attributed solely to phycocyanin (Stewart, 1974; Rowan, 1989; Gitelson personal communication, 1998).

As wavelength increases beyond 630 nm, phycocyanin/chl *a* absorption efficiency diminishes (Carr and Whitton, 1973; Stewart, 1974; Rowan, 1989). The small peak near 650 nm results from a decrease in absorption efficiency from 630 nm upward and 675 nm downward. This decreasing inhibition of particle scattering translates into the formation of an apparent reflectance maximum (650 nm) (Jupp *et al.*, 1994). This effect is similar to the combined absorption curve concept described in the next paragraph. There is a small possibility that the peak at 650 nm could partially result from the fluorescent emission of the two biliproteins common to all cyanobacteria, phycocyanin and allophycocyanin (Carr and Whitton, 1973; Lee, 1989). Phycocyanin has an emission peak at 645 nm and allophycocyanin has an emission peak near 660 nm (Stewart, 1974; Rowan, 1989).

Absorption efficiency decreases with wavelength shortly after the chl *a* absorption

maximum centered at 675 nm. Particle scattering, predominantly from algal cells in the Iowa Great Lakes, produces the reflectance maximum near 700 nm. At lower chl *a* concentrations, gently rounded peaks are produced while at high chl *a* levels, distinct peaks are formed with magnitudes proportional to the target chl *a* concentration. In addition to the magnitude of the 700 nm peak, its spectral position is also related to chl *a* concentration. This reflectance feature is best defined as the minimum in the combined absorption curves of algae and pure water (Dekker *et al.*, 1992; Gitelson, 1992; Gitelson *et al.*, 1995) and results from decreasing chl *a* absorption efficiency and increasing pure water absorption efficiency with wavelength.

After the peak near 700 nm, absorption efficiency of pure water increases with wavelength, causing the sharp decrease in reflectance near 740 nm. A reflectance plateau between 740-775 nm results from the uniform absorptive capacity of pure water in this spectral range. Reflectance then increases again due to decreases in pure water absorption (Dekker *et al.*, 1992). The small peak near 800 nm is followed by decreasing reflectance with wavelength resulting from increases in pure water absorption.

2.2.3 Emergent Bloom Reflectance Spectra

During data collection (8/13/97), spectral reflectance measurements were taken over an emergent bloom of *Aphanizomenon flos-aquae* (Figures 1-2, 2-6). This reflectance signature is identical to that shown by Jupp *et al.* (1994) and similar to those shown by Quibell (1992) and Gitelson *et al.* (1995). In addition, the bloom signature shows the same spectral features seen in each of the East Okoboji reflectance spectra. However, two significant departures are apparent in the bloom signature; reflectance is quite high in the visible wavelengths (~10% at 550 nm) and the near-infrared response

resembles that of terrestrial vegetation (~30% plateau). Presumably, the reflectance characteristics of the emergent bloom are largely determined by its position on the surface where the absorptive influence of pure water is minimized.

Emergent blue-green alga blooms can be considered the most extreme case of degraded water quality for this lake system. As a result, the reflectance signature produced by an emergent bloom represents the upper reflectance threshold for degraded water quality. Figure 2-7 illustrates the significance of the emergent bloom signature by showing it simultaneously with the signature corresponding to the highest measured chl *a* concentration (582.72 $\mu g\ L^{-1}$).

2.2.4 Hyperspectral Reflectance Summary Statistics

2.2.4.1 Average

The average spectral reflectance signatures for the two lakes (i.e. two trophic conditions) are considerably different in magnitude and form (Figure 2-8). The average reflectance magnitude of West Okoboji (eutrophic but transparent) is considerably less than that of East Okoboji (hypereutrophic and turbid) at all wavelengths. This is due to less scattering resulting from the lower average particulate concentrations of West Okoboji Lake. The chl *a* and turbidity ground truth data support this assertion (Table 1-4). However, the higher average reflectance of East Okoboji Lake may not be due solely to higher average particulate concentrations. The dominant alga in East Okoboji, *Aphanizomenon flos-aquae*, possesses gas vacuoles which control cell/colony buoyancy. When these algae migrate to the surface, where they exploit the incoming light, scattering is enhanced, both from increased particle density and the decrease in

aqueous pathlength. Furthermore, the gas vacuoles themselves accentuate the scattering process by acting as miniature refractive lenses (Carr and Whitton, 1973; Kirk, 1994). This may be in contradiction to Quibell's (1992) finding that pure cultures of green algae scatter more efficiently than pure cultures of blue-green algae. Regardless of the scattering efficiency of the two lakes' algal suspensions, the average reflectance signature for East Okoboji Lake appears more dynamic than that for West Okoboji Lake.

2.2.4.2 Standard Deviation

The standard deviation of reflectance was calculated for each lake at each spectral band (400-900 nm). The resulting standard deviation signatures are also dissimilar (Figure 2-9). The standard deviation signature for West Okoboji Lake forms a nearly flat line, increasing slightly with wavelength and never exceeding the small level of 0.5%. This is certainly a product of the small range in chl *a* concentration and the spatial homogeneity of West Okoboji in general.

The standard deviation signature calculated from the East Okoboji Lake data appears much like a high algal biomass reflectance signature, with high variation corresponding to reflectance peaks in the green and near-infrared regions (compare Figure 2-5 with 2-9). The green peak (~550 nm) has a standard deviation magnitude of 1% and the near-infrared peak extends just above 4% at the wavelength of highest variation (720 nm). The relatively high values in these spectral regions result from scattering being less inhibited by absorption processes. As a result, these spectral regions are more sensitive to changes in particulate scattering. Therefore, it seems appropriate to use the reflectance at these spectral regions for quantifying the algal biomass of East Okoboji.

2.2.4.3 Coefficient of Variation

Along with the standard deviation, the coefficient of variation was used to determine the wavelengths most sensitive to changes in chl *a* concentration (Figure 2-10). The coefficient of variation of reflectance is determined by dividing the standard deviation of reflectance by the average reflectance on a per wavelength basis (Gitelson *et al.*, 1995). Due to differences in the two lakes optical composition, this standardized measure allows the data to be compared and evaluated more effectively.

The coefficient of variation signatures for both West and East Okoboji lakes demonstrate that the longer wavelengths of the near-infrared show the highest sensitivity to changes in chl *a* concentration. Many researchers have shown that the spectral reflectance at longer wavelengths (red and near-infrared) is more appropriate for isolating the influence of algal biomass (Gitelson, 1992; Mittenzwey *et al.*, 1992; Quibell, 1992; Schalles *et al.*, 1998). There are several physical reasons for this. First, due to the refraction of the incident light at the air/water interface, the longer wavelength radiation penetrates less, potentially avoiding the influence of the benthos. Second, absorption by gilvin (dissolved organic matter) becomes asymptotically small in the red wavelengths (Mittenzwey *et al.*, 1992) and there are no photosynthetic pigments beyond the *in vivo* absorption maximum of chl *a* near 675 nm. Pure water is the only absorbing agent in the near-infrared and can be viewed as a spatially invariant optical backdrop, although its absorption properties do vary with wavelength. Third, the red and near-infrared wavelengths are sufficiently close to one another such that any influence exerted by dissolved organic matter and, more importantly, suspended inorganic material, is nearly the same across this wavelength range (Gitelson, 1992; Gitelson *et al.*, 1993). The final

advantage of exploiting the longer optical wavelengths results from the general decrease in atmospheric attenuation with wavelength (Dekker *et al.*, 1992).

2.2.4.4 Correlation Coefficient

The correlation coefficient (r) was calculated on a per wavelength basis (400-900 nm) for each lake in order to determine the strength of the relationship between chl *a* concentration and hyperspectral reflectance (Rundquist *et al.*, 1996), and to further identify the spectral regions most useful for estimating chl *a* concentration (Figure 2-11).

The correlation coefficient signature for West Okoboji Lake shows only a small increase with wavelength. The highest correlation values between reflectance and chl *a* are located in the near-infrared, where they barely exceed $r = 0.75$. The nearly uniform nature and relatively low magnitude of these values suggest that a statistical relationship between reflectance (400-900 nm) and chl *a* concentration is lacking for West Okoboji.

The correlation coefficient signature for East Okoboji Lake assumes a form which roughly resembles an algal reflectance signature, where high and low values coincide with reflectance peaks and troughs, respectively. Notable trends include the high values ($r = 0.86$) near 550 nm associated with the green reflectance peak, and the plateau of high values ($r \approx 1.0$) across the entire near-infrared region. These spectral bands, which show high positive correlation with chl *a* concentration, hold promise for algorithm development.

Also interesting are the negative correlation values associated with pigment absorption at 630 nm ($r = -0.73$). This inverse relationship between reflectance and chl *a* concentration seems to support the conceptual model of reflectance for green oceanic waters (Case 1) given by Morel and Prieur (1977). The authors found that reflectance

tend to satisfy these shortcomings and acceptable r^2 values are achieved for several algorithms. The high scattering efficiency of bloom forming blue-green algae may also improve the ability to quantify the algal biomass of this and similar hypereutrophic lakes. When the data from both lakes are combined, the resulting r^2 values usually decrease from the levels seen when considering the East Okoboji data alone.

2.3.1 Reflectance Magnitude

Perhaps the most obvious approach to quantifying aquatic algal biomass is that which relies simply on the magnitude of reflectance. As suspended particle concentrations increase, so does particle scattering. Because particle scattering is the primary determinant of reflectance, which can be quantified via close-range spectroradiometry, particulate concentrations can be derived from changes in the magnitude of reflectance. However, scattering is inhibited by absorptive agents in the medium and by the absorptive properties of pure water itself. Therefore, reflectance magnitude measurements should be acquired at wavelengths where absorption is minimal. Avoiding wavelengths where absorption is prominent is a simple proposition with high spectral resolution instrumentation. In the case of inland lakes, reflectance peaks typically appear near 550 nm and 700 nm (§2.2.1; §2.2.2). As chl *a* concentration increases, the magnitudes of these peaks tend to increase (Gitelson, 1992; Gitelson *et al.*, 1995; Quibell, 1992; Rundquist *et al.*, 1996; Schalles *et al.*, 1998). Presumably, this relationship is asymptotic, the upper limit being demonstrated by emergent bloom conditions (Figures 2-6, 2-7).

The Reflectance Magnitude approach proved ineffective for estimating the chl *a* concentrations of West Okoboji Lake (Table 2-1). This is not surprising given the

narrow range of conditions and low particulate levels present on this lake. At such low biomass levels, and low reflectance (Figure 2-4), it is difficult to determine whether the magnitude of reflectance accurately represents the aquatic conditions or if specular reflection is corrupting the emergent signal.

For the turbid conditions of East Okoboji Lake, the magnitude of the near-infrared reflectance peak near 700 nm was the most successful (r^2 = 0.983) of the Reflectance Magnitude algorithms (Table 2-1; Figure 2-12). This is encouraging since most air/space sensor systems possess a near-infrared channel and the technique is easy to understand and adopt. When using this approach with data from other platforms, the spectral position and width of a near-infrared band will certainly influence its effectiveness. Ideally, a 10 nm band would be centered at 705 nm, much like that of the Medium Resolution Imaging Spectrometer (MERIS) to be launched by the European Space Agency in 1999.

While the magnitude of reflectance, particularly near 700 nm, provides a simple and reasonable estimate of chl *a* concentration in turbid waters, the magnitude of reflectance where pigment absorption is maximal (630 nm and 675 nm), is ineffective, regardless of how the data are stratified (Table 2-1). Schalles *et al.* (1998) also found a poor correlation between reflectance at 670 nm and chl *a* and suggest this results from roughly equal absorption and scattering processes. Yacobi *et al.* (1995) found the reflectance at 670 nm nearly constant over a wide range of chl *a* concentrations, which indicates an equilibrium between absorption and scattering. This equilibrium probably results from the interplay between the scattering and absorption processes produced by the increased pathlength photons travel upon being scattered. This longer pathlength

increases the probability that the photons will come in contact with an absorbing molecule (Dekker *et al.*, 1991; Kirk, 1994).

The distribution of points shown in Figure 2-13 for East Okoboji Lake, is very similar to that shown by Schalles *et al.* (1998) and reaffirms that reflectance is insensitive to chl *a* concentration at wavelengths where pigment absorption is maximal. This assertion is also supported by the low standard deviation and coefficient of variation values in these regions (Figures 2-9, 2-10).

2.3.2 Shift in Peak Position

As mentioned in §2.2.2, the reflectance peaks in the green and near-infrared tend to migrate along the wavelength axis according to changes in chl *a* concentration. Unlike the previously discussed Reflectance Magnitude approach, which relies on scattering processes, the position of the reflectance peak is determined solely by the absorption characteristics of the medium. It is this unique characteristic which separates the Shift in Peak Position approach from the others.

Using the position (nm) of a reflectance peak as an indicator of chl *a* concentration is appealing because it is unaffected by reflectance magnitude errors resulting from changing sky conditions and specular reflection. For example, if independent spectral measurements were collected over the same algal target, one of which was differentially biased (a cloud obscured the sun during calibration but not during the target scan) the resulting reflectance magnitude would be artificially high, but the position of the peaks should be identical.

There are several limitations to this approach, however. First and foremost, this approach requires continuous hyperspectral data, not available from air/space platforms.

Furthermore, any drift in the detector array/band centers renders the technique unreliable.

Trends apparent in the East Okoboji Lake data (8/13/97) are very similar to those reported by Rundquist *et al.* (1995), who conducted outdoor, green alga dilution experiments in artificial pools. In both instances the shift of the respective green peaks behave asymptotically beyond a chl *a* concentration of 150 $\mu g\ L^{-1}$ (Figure 2-14). This is probably due to the increase in the absorption coefficient of pure water between 580 nm and 610 nm (Kirk, 1994), and suggests a lack of utility for high biomass waters. Interestingly, the direction of the green peak shift documented by Rundquist *et al.* (1995), is toward the longer wavelengths with increasing chl *a* concentration, exactly opposite of that seen in the East Okoboji data (8/13/97) and shown by Schalles *et al.* (1998).

The green peak shift towards longer wavelengths for green algae (Rundquist *et al.*, 1995) results from chl *a* absorption incrementally surpassing that of pure water as pigment abundance increases. While the absorption signature of pure water remains constant, the absorption signature of green algae (lacking biliproteins) increases in magnitude. In situations where the green peak shifts toward shorter wavelengths, the effect is associated with an increase in the abundance or proportion of blue-green algae. Higher concentrations of phycocyanin produce an accentuated absorptive capacity on the right side of the green peak. The absorption of more energy by phycocyanin encourages the lateral erosion of the right side of the green peak, which produces an apparent leftward shift in the peak position (Schalles *et al.*, 1998). Schalles *et al.* (1998) discuss how the shift to shorter wavelengths is influenced by the seasonal changes in carotenoid and phycocyanin concentration, a consequence of species dominance changing from diatoms to blue-green algae.

In the case of the near-infrared peak, the literature is consistent concerning the direction of the shift, always toward longer wavelengths with increases in chl *a* (Figure 2-15) (Gitelson, 1992; Gitelson *et al.*, 1993; Rundquist *et al.*, 1995; Yacobi *et al.*, 1995; Schalles *et al.*, 1998). The physical reason for the shift in near-infrared peak is fundamentally the same as the green peak shift. Recall that the reflectance peak in the near-infrared is explained by the combined absorption curve concept (§2.2.2). As biomass increases, the absorption signature of chl *a* incrementally overwhelms the absorption signature of pure water and the peak subsequently appears to move toward longer wavelengths. A shift by the near-infrared peak toward shorter wavelengths with increasing chl *a* is impossible, due to the lack of absorbing pigments beyond 675 nm.

Figures 2-14 and 2-15 demonstrate how the green peak shifts toward shorter wavelengths and the near-infrared peak shifts toward longer wavelengtbs with increases in chl *a* concentration. In both cases, logarithmic equations best fit tbe data, resulting in an $r^2 = 0.716$ for the green shift and an $r^2 = 0.997$ for the near-infrared shift. For the same reasons mentioned with regard to transparent waters in §2.3, no systematic shift in green or near-infrared peak position is evident in the West Okoboji Lake data.

2.3.3 Sum and Height Above an Artificial Baseline

The success of the Artificial Baseline approach results from phytoplankton reflectance being isolated from the composite signal and quantified separately. The baseline approach is explained visually in Figures 2-16 and 2-17, and by Gitelson *et al.* (1995), Yacobi *et al.* (1995), and Schalles *et al.* (1998). It consists of constructing a straight line of negative slope between the reflectance trough near 675 nm (chl *a*) to the first tangential point in the near-infrared of each spectral signature. Due to variations in

spectral signature (peak shape and position), the near-infrared endpoints for the Okoboji data (8/13/97) lie between 720-970 nm, where pure water absorption becomes dominant. This required data outside the previously stated 400-900 nm spectral range to be incorporated. Once the limits have been determined, the reflectance data must be processed in a customized spreadsheet "macro." The values output by the program correspond to the area and height of the ~700 nm peak bounded by the spectral signature and the artificial baseline. The Artificial Baseline approach has been applied successfully to a wide variety of aquatic environments, under variable tripton levels and has been shown to be seasonally and geographically robust (Schalles *et al.*, 1998).

The performance of the baseline algorithms is shown in Table 2-1. Although the r^2 values for West Okoboji Lake are very low, the baseline sum algorithm performs better than any other algorithm for the turbid conditions of East Okoboji Lake (r^2 = 0.998) (Figure 2-18). The poor performance of the baseline algorithms in the context of West Okoboji was foreseeable due to the reasons discussed in §2.3. Furthermore, the "peak" between 675 nm and 700 nm in the West Okoboji spectra probably results from chl *a* fluorescence, a subtle process not easily detected nor quantified with close-range spectroradiometry.

2.3.4 Reflectance Ratio

Several band ratio combinations were examined for their ability to estimate chl *a* concentration. Individual band combinations were selected both on the basis of prominent reflectance features/optical processes, and their agreement with the spectral bands possessed by the SPOT HRV sensor (see Chapter 3). The ratios incorporate the reflectance values (%) of the green peak near 550 nm, the red trough near 675 nm, and/or

the near-infrared peak near 700 nm. In addition to simple band ratios, the normalized difference vegetation index (NDVI=[(NIR-Red)/(NIR+Red)]) was examined, simply because of its popularity as an indicator of terrestrial vegetative "greenness."

The near-infrared reflectance:red reflectance (NIR:Red) ratio technique has been widely successful at predicting aquatic chl *a* concentration (Gitelson, 1992; Mittenzwey *et al.*, 1992; Rundquist *et al.*, 1995; Yacobi *et al.*, 1995; Rundquist *et al.*, 1996). In this simple approach, the effects of nonalgal scattering in the numerator and denominator cancel one another out, leaving only the effects of algal scattering. Schalles *et al.* (1998) explain this concept in the context of the Artificial Baseline approach; "To subtract the impact of nonalgal seston on total scattering by particulates, an index for chl *a* estimation should include the spectral range where dependence of reflectance on phytoplankton density is minimal." The reflectance at 670 nm (red) has been determined to be insensitive to chl *a* concentration (Figure 2-13; Table 2-1; §2.3.1), but largely dependent on inorganic and detrital seston (Yacobi *et al.*, 1995; Schalles *et al.*, 1998). It appears that the success of the NIR:Red ratio results from the normalization of the near-infrared reflectance (from seston scattering) by the red reflectance (from tripton scattering).

For the turbid conditions of East Okoboji Lake, the NIR:Red ratio performs better than all other ratio algorithms and nearly as well as the baseline sum algorithm, and with less data processing (Figure 2-19; Table 2-1). By relying on the relationship between spectral features within individual reflectance signatures, rather than on their absolute values, errors arising from changing sky conditions and specular reflection (§2.3.2) are minimized and higher r^2 values can be achieved.

When comparing Figure 2-19 with Figure 2-12, it seems that the normalization

process of the NIR:Red ratio improves estimation at the lower chl *a* levels (8.77 μg L^{-1} - 25.33 μg L^{-1}). However, Mittenzwey *et al.* (1992) found increasing levels of uncertainty at low chl *a* levels and suggest the minimum threshold of accurate estimation for this technique is 10 μg L^{-1}. Regardless, the NIR:Red ratio, and the ratio algorithms in general, do provide higher r^2 values for West Okoboji (chl $a < 10$ μg L^{-1}) (Table 2-1). Interestingly, the NDVI performs slightly better ($r^2 = 0.753$) than the NIR:Red ratio ($r^2 = 0.750$), for the transparent waters of West Okoboji (Figure 2-20).

2.4 Conclusions

2.4.1 Summary of Results

Close-range spectroradiometry has proven to be an effective method for estimating algal biomass in the turbid waters of the Iowa Great Lakes. This is evident from the fact that any of several spectral indices can be used to adequately predict the chl *a* concentration of East Okoboji Lake from hyperspectral reflectance:

- **Sum of reflectance above an artificial baseline**
  Chl a = (0.743 * SUM (%)) + 14.277 ($r^2 = 0.998$)
- **Near-infrared reflectance : Red reflectance ratio**
  Chl a = (94.114 * (NIR_{peak} / Red_{trough})) - 96.187 ($r^2 = 0.997$)
- **Shift in near-infrared reflectance peak position**
  Chl a = EXP [(0.168 * NIR Peak Position (nm)) - 114.06] ($r^2 = 0.997$)
- **Near-infrared peak reflectance magnitude**
  Chl a = (54.959 * NIR peak magnitude (%)) - 127.14 ($r^2 = 0.983$)

While the determination of which algorithm is ultimately the "best" is determined by the research objectives, the selection of one algorithm over another may also be influenced by time and technological limitations.

The results of this research support findings published by other authors. First, the green through near-infrared wavelengths are important for the assessment chl *a* from turbid inland waters. More importantly, the near-infrared is the most useful optical region for chl *a* estimation, as demonstrated by its inclusion in each of the four algorithms mentioned above. Second, models incorporating spectral bands where scattering is minimally inhibited by absorption, are better suited for estimating the chl *a* concentration of productive inland lakes. However, prediction is often improved by including bands which are not sensitive to chl *a*, such is the case with the baseline algorithms and the NIR:Red ratio technique. Research findings also suggest that close-range hyperspectral remote sensing may be used to monitor algal species dominance via the shift in the green peak.

The utility of close-range spectroradiometry for estimating algal biomass in the transparent waters of the Iowa Great Lakes is less obvious. In a monitoring context, the interest lies in fast and efficient *in situ* determination of chl *a* and other optically active constituents. This is problematic in West Okoboji Lake, because conditions of low and uniform algal abundance are not favorable to statistical description. However, the simple examination of the reflectance signatures provides objective certainty that the water quality is good, in optical terms, and investigations beyond simple spectral inventories may not be necessary in such waters.

2.4.2 Improvements in Study Design

There are several shortcomings in the close-range component of this thesis. Refinement of the study design in the areas specified below should lead to more definitive conclusions in future research efforts.

2.4.2.1 Methodological

When the goal is to obtain an accurate hyperspectral measurement of volume backscattering, the vehicle transferring information about the aquatic medium, a geometric scanning configuration which minimizes the amount of specular reflection that enters the sensor optic should be adopted. An off-nadir approach where the optic is aligned parallel to the direct solar beam (azimuth and zenith) (Yacobi *et al.*,1995) should be used when it is inappropriate to submerge the optic for subsurface measurements (Dekker *et al.*, 1991, 1992; Schalles *et al.*, 1998). The subsurface technique is more appealing due to the complete avoidance of specular reflection and the diffuse nature of the light field below the air/water interface (Kirk, 1994). Acquiring spectral measurements from an isotropic light field promotes the level of measurement from the bi-directional reflectance realm mentioned in §2.1.3, to one of true volume backscattering.

Every effort should be made to minimize the elapsed time between measurements at each sample site and to assure that all measurements correspond to exactly the same target. In deep water locations, where anchoring the boat is impractical, a surface drag anchor, much like a small parachute, should be used to prevent boat drift. It is incorrect to assume that algal density, and other parameters, are homogeneous and static in the general proximity of the boat. Yacobi *et al.* (1995) found significant variation in reflectance spectra over short time spans (minutes) and space (meters) during times of *Peridinium* bloom on Lake Kinneret. Thus, water samples should be taken directly under the sensor optic immediately before or after the scan sequence. Yacobi *et al.* (1995) further recommend vertical sampling at several stations in order to estimate the degree of

vertical stratification. Similarly, collecting spectral and ground truth data near solar noon is always encouraged, not only because of the sun-sensor-target geometry considerations, but because it helps to control for the diurnal vertical migration of algal communities.

2.4.2.2 Ground Truth

In future research efforts, more water quality parameters should be measured. At a bare minimum, this should include measurements of seston and tripton. Ideally, the inherent optical properties should be determined. Collecting these data would allow the validity of several assumptions to be confirmed. Similarly, the impact of individual constituents on spectral reflectance could be ascertained and compiled for a multivariate modeling approach.

In addition to laboratory derived information, efforts should be made to incorporate a wider array of *in situ* optical measurements, specifically hyperspectral attenuation. While broad-band PAR attenuation measurements (§1.7.3.2; Table 1-4) are useful in quantifying optical clarity and also provide a standard for chl *a* and turbidity comparisons, incorporating a hyperspectral instrument could provide a means for estimating the concentration accessory pigments (Gitelson *et al.*, 1995). A hyperspectral approach to measuring attenuation would be particularly well suited for transparent waters where constituent levels are low, and the resulting backscattering is weak. Furthermore, hyperspectral attenuation measurements are appealing due to the more sensitive and consistent nature of the method, one which exploits light that is transmitted and scattered forward. This technique would also allow the optical characteristics of the water column to be examined at sites where bottom reflectance and/or submerged aquatic vegetation are significant.

2.4.2.3 Statistical

A larger number of samples is necessary to adequately represent these lakes. This is particularly important for West Okoboji Lake, where the range of conditions is narrow and relationships between spectral reflectance and chl *a* concentration are less conspicuous. Although strong relationships were found for East Okoboji Lake with the same small number of sites, increasing the number of sites would improve the probability of capturing a more continuous range of biomass levels. Most importantly, the predictive models developed here (§2.4.1) need to be validated by a second, independent dataset. This is the only way to determine the stability of the coefficients, and therefore, the overall effectiveness of the algorithms.

2.4.2.4 Temporal

It has been put forth that the lakes of this system are trophically, and therefore spectrally, autonomous. Complicating matters still further is the possibility that seasonal variation in the coefficients, even for the most robust algorithms, will emerge in the presence of a temporally rigorous remote sensing analysis. The seasonal instability of the coefficients could result from variations in taxonomic composition, physical attributes of the phytoplankton, and/or changes in the proportion of other optically active constituents within each of the lakes. Therefore, it is important to carry out close-range investigations which span the entire growing season. This would allow the variability of the coefficients to be analyzed. If the coefficients are not reliable intraseasonally, perhaps season specific coefficients would prove valid.

2.4.3 Future Research

Perhaps the most apparent research avenue deserving attention deals with the

development and validation of empirical models capable of predicting chl *a* and other water quality parameters in waters possessing a high degree of optical clarity. Being able to successfully model these conditions is important because it is in this realm that the precursors to bloom formation operate. Similarly, determining the minimal level of chl *a* capable of being detected by remote sensors is a fundamental question which has yet to be answered.

The effects of scattering and absorption efficiency on close-range radiometric data should be aggressively pursued. It is inappropriate to assume that variation in scattering and/or absorption for the same unit chl *a* is insignificant at this scale of inquiry.

CHAPTER 3 — SPOT IMAGE ANALYSIS

The basics of SPOT satellite imagery were introduced in §1.7.2, but the characteristics of the system have not been sufficiently discussed. The SPOT HRV sensor can operate in two spectral modes; panchromatic, at a 10 m spatial resolution, and multispectral (XS), at a 20 m spatial resolution (4.13° instantaneous field of view). This research incorporates only XS image data. In XS mode, the HRV sensor detects radiant flux at an 8 bit radiometric resolution (256 brightness levels) in three wide spectral bands:

- XS1: 0.50-0.59 μm (green)
- XS2: 0.61-0.68 μm (red)
- XS3: 0.79-0.89 μm (near-infrared).

Although the spectral resolution of the HRV sensor is quite coarse, the three main spectral regions important for inland water quality assessment are represented.

The SPOT-2 satellite overpass of the Okoboji study area took place at 17:17 GMT (12:17 CDT) on 8/13/97. Centered over 43° 25' 19" N latitude by 95° 07' 30" W longitude, the HRV-1 was programmed with a near nadir sensor incidence angle of -9.7°. This resulted in an imaged area of roughly 60 by 64 km (Figure 3-1).

The image data were preprocessed to Level 1A, the most "raw" format available from the SPOT Image Corporation. In Level 1A processing, only deteetor normalization is performed, while Level 1B processing also incorporates a standard geometric correction which accounts for distortions resulting from earth rotation effects and panoramic distortion introduced by high sensor incidence angles (http://www.spot.com). Level 1A processing was selected because, "the combined conversion and resampling of any data Level 1B and higher results in significant data entropy" (Messina, 1996) when

subsequent radiometric transformation is performed (Verdin, 1984; Chacon-Torres *et al.*, 1992). The scene header file/ephemeris data, as well as the raw image (filename: imag_01.img) statistics and histograms are reported in Appendix 1.

3.1 Image Characteristics and Preprocessing

3.1.1 General Appearance

The Okoboji SPOT scene does contain some cloud cover (Figure 3-1), but is still useful for this research. The lower left quadrant is visibly degraded by what appears to be a jet aircraft contrail. There are also patches of haze in the same general area, visible only at high magnification. Luckily, these atmospheric features and their shadows do not occur inside the boundaries of the Iowa Great Lakes.

At high magnification, vertical or along-track striping is evident throughout the image. This noise pattern can be accentuated by inspecting the bands individually and applying different contrast enhancement techniques. The striping problem will be discussed more completely in §3.1.3.

Also evident in the full Okoboji SPOT scene is the dominance of row crop agriculture in the lakes region. This has enduring ramifications for lake water quality due to the potential flow of nutrient rich runoff water from agricultural lands within the drainage basin into the lakes.

3.1.2 Radiometric and Geometric Correction

To account for the exact form of the analog-to-digital response functions for the sensor (Lillesand and Kiefer, 1994), the per-pixel digital numbers for each SPOT band were converted to values of SPOT equivalent radiance, which is the mean spectral

radiance taken for the interval defined by a particular SPOT band (Messina, 1996). This transformation of the data to the same physical units also accounts for differences in spectral bandwidth and therefore facilitates band to band comparisons. The equation used for the transformation was taken from Messina (1996) but variations of it can be found in Begni (1982), Price (1987), Santer *et al.* (1992), Chacon-Torres *et al.* (1992), and Guyot and Gu (1994). The equation is:

$$\mathbf{L_k = X_k / A_k} \qquad \text{where,}$$

L_k = SPOT equivalent radiance (real number, mW cm^{-2} sr^{-1})

X_k = digital number or brightness value (integer, 0-255)

A_k = absolute calibration coefficient (XS1: 0.85883; XS2: 1.00772; XS3: 1.17835)

k = SPOT band.

In order to locate the image pixels corresponding to surface sites where water samples were acquired, it was necessary to geometrically rectify the image. The geometry of the image was made planimetric through an image-to-map rectification (Jensen, 1996). First, a rectangular study area, land and lake pixels, were subset from the larger image to facilitate the process. Thirty-four ground control points (GCPs) were selected from seven USGS 7.5' quadrangles and digitized using ARC/Info geographic information system (GIS) software. The GCPs were located at road intersections and distributed in a grid-like fashion throughout the study area (Figure 3-2). Only road intersections that were clearly visible on both the maps and the image were selected. The Earth Resources Data Analysis System (ERDAS) *Imagine* digital image processing/GIS software (v.8.3) was used to carry out the actual correction procedure. The SPOT geometric correction model built into *Imagine* was applied to the image. This model accounts for the curvature of the earth and produced a total control point error (root mean

square) of 0.474. This translates into an accuracy level of less than half a pixel ($\leq$10 m). The projection, datum and spheroid used in the process were, the Universal Transverse Mercator (zone 15), NAD 27 and Clarke 1866, respectively. Finally, the nearest neighbor interpolation method was used and the pixels were resampled to a 20 m spatial resolution.

Once the image was rectified, the lakes were isolated from the terrestrial surroundings using a subset routine with the seed properties (area of interest) option in *Imagine*. The goal was to include all water pixels regardless if they were "contaminated" by terrestrial features adjacent to the shoreline. Upon being removed from the terrestrial surroundings, the color patterns within the lakes became much more pronounced, a result of the upper (terrestrial) end of the histogram being removed and the lower (aquatic) end of the histogram being preferentially stretched. The results of this operation can be seen in Figure 3-3. This rendition of the data uses the default, two standard deviation contrast stretch and a six pixel black buffer has been added around the lakes to accentuate the periphery pixels.

3.1.3 Image Noise

The true character of the lake imagery is better understood by examining each SPOT band individually in gray scale display mode (Figures 3-4, 3-5, 3-6). Brightness patterns can be further accentuated by applying additional contrast enhancement techniques such as histogram equalization (Figures 3-7, 3-8, 3-9). The along-track striping in each of the three SPOT bands is quite conspicuous in these display modes. It is difficult to judge which band is most degraded, but a side by side comparison of the default and histogram equalized images suggests that XS1 (Figures 3-4, 3-7) and XS2

(Figures 3-5, 3-8) possess similar striping patterns, and XS3 (Figures 3-6, 3-9) is more unique.

The striping problem is not uncommon nor restricted to SPOT imagery. Lathrop and Lillesand (1989), Chacon-Torres *et al.* (1992), Van Stokkom *et al.* (1993), Mayo *et al.* (1995), and Yacobi *et al.* (1995) all report image striping. This effect is usually attributed to the non-conformity of the detectors (Chacon-Torres *et al.*, 1992; Lillesand and Kiefer, 1994; Yacobi *et al.*, 1995; Jensen, 1996), however, the striping in the Okoboji SPOT scene exhibits neither a perfectly continuous, nor periodic pattern throughout the full extent of the image. An alternative effect that could be contributing to this problem is similar to what happens to the human eye when exposed to a camera flash. As the SPOT platform proceeds in a north to south orbital direction, the detectors drag some of the charge across pixel boundaries. This effect might be accentuated when going from the "hot" (highly reflective) land pixels to the "cold" (highly absorptive) water pixels (Van Stokkom *et al.*, 1993). Regardless of the cause, a noise removal algorithm was not applied to the imagery because the suitability of such a procedure is in question when quantitative biophysical information is to be extracted (Jensen, 1996 adapted from Crippen, 1989).

3.1.4 Lake Subset Statistics

The high absorptive capacity of pure water causes the emergent flux from any aquatic medium to be weak, relative to terrestrial targets, and results in a poor signal-to-noise ratio. In addition, the optically complex nature of most aquatic media, requires narrow and strategically placed spectral bands for adequate characterization of individual absorption and/or scattering processes. Unfortunately, most satellite based imaging

systems, including the SPOT HRV, have been optimized for terrestrial targets and possess broad spectral bands which integrate the aquatic response across optical process boundaries and/or are not positioned to take full advantage of specific optical processes. For example, Figures 3-10 a,b,c,d show the hyperspectral reflectance signatures for various chl *a* concentrations superimposed on the simulated SPOT band response achieved by integrating the hyperspectral data to the wavelength intervals of the individual SPOT bands, a process Dekker *et al.* (1991, 1992) refer to as "spectral band simulation and signature reconstruction." Figure 3-10b best shows how the red band (XS2) is biased because of its wide spectral interval. Because XS2 extends well below the absorption maximum of chl *a* at 675 nm, a counteraction effect is produced which results in an elevated measurement. Perhaps more important is the placement of the near-infrared band (XS3) far into the wavelengths where pure water absorption is more pronounced (Figure 3-10c). The spectral position of XS3 hinders its ability to differentiate between small changes in radiant flux emerging from the aquatic medium. Clearly, narrow spectral bands placed at 675 nm and near 700 nm would be more appropriate for monitoring specific optical processes.

Due to limitations in spectral resolution and sensor optimization, the range in pixel values recorded for the Iowa Great Lakes as a whole is quite small in each of the SPOT bands. Statistical information and histograms for the lake subset image (filename: lakes.img) can be found Appendix 2. The similarity of the minimum, mean, median and mode statistical values for each of the bands (Figure 3-11), and the relatively small deviation/variation values (Figure 3-12), suggest that there is a low degree of contrast within each band of the lake subset image. However, the near-infrared band possesses

the highest variation values and therefore shows the greatest potential for capturing the spectral nuances of the water.

3.2 Additional Processing and Modeling

Unlike the continuous nature of the close-range hyperspectral data, the coarse spectral resolution of SPOT imagery limits the manner in which the data can be used in biophysical modeling. For example, SPOT data cannot be used in an "artificial baseline" or "shift in peak position" approach. As a result, only algorithms based on band radiance magnitude and band ratios, including the NDVI, were examined.

As with each of the major image processing procedures, the *Model Maker* spatial modeling analysis tool in *Imagine* was used to perform arithmetic functions on the imagery. Using the *Model Maker* is advantageous because there is a permanent record of all operations and files involved, thus promoting sound data lineage.

3.2.1 Compilation and Statistic Extraction

The extraction of pixel values corresponding to the surface sites can be a time consuming proposition, especially if there are a large number of sites. Therefore, it is desirable to carry out this operation only once. After the ratio and NDVI calculations were completed, all the relevant layers were compiled into a single composite file using the layer stack model in *Imagine*. The result was a multilayer file from which the statistics were extracted. This approach also assured that the values were extracted from the same exact pixels in each layer.

When extracting pixel values an analyst usually incorporates a 3x3 or 5x5 pixel window surrounding the sample site and then averages the values for each site. My confidence in the GPS data lead me to extract the values from individual pixels for many

sites. At sites where boat drift occurred, I traced the path of the boat and averaged the values of the pixels through which the boat drifted.

3.2.2 Sample Site Statistics

The data extracted from the composite image were imported into Microsoft Excel where they were graphed and analyzed. As introduced in §3.1.4, the coefficient of variation for the lake subset image (all water pixels) was somewhat low; XS1=0.09; XS2=0.18; XS3=0.58 (Figure 3-12). Similarly, extracted radiance values also possess a low degree of variation. Figure 3-13 shows the nearly uniform nature of the radiance values for each SPOT band versus the corresponding chl *a* measurements (ranked). More encouraging is that the radiance data extracted from the sample sites do a reasonably good job of representing the conditions of the lakes as a whole (Figure 3-14). The coefficients of variation for the sample site data (Figure 3-14, values in white) are similar to those for the lake subset image (Figure 3-12, values in white). In addition, Figure 3-14 indicates that XS3 (near-infrared) possesses the highest variation for the sample sites on each of the lakes and the radiance values extracted from East Okoboji Lake consistently show the highest variation.

3.2.3 Modeling Results

The evaluation of different predictive models, based on radiance magnitude and band ratios, is accomplished using the methods described in §2.1.4. Algorithm performance (r^2) appears in Table 3-1.

When the data were considered on an individual lake basis, the eutrophic lakes, West Okoboji and Spirit, proved difficult to model. This is similar to what was encountered with the close-range hyperspectral reflectance data. In the case of Spirit

Lake, however, the r^2 values are generally lower than those of West Okoboji, even though there were more sample sites, a higher average chl *a* level, and a larger range in chl *a* concentration (Table 1-4). If the camera flash analogy described in §3.1.3 is accurate, this discrepancy could be a product of more noise across Spirit Lake (Figures 3-4 to 3-9). Perhaps the position of Spirit Lake (most northern) and/or its configuration (size and shape) accentuated the striping problem.

Ratioing individual bands was more effective than single band magnitudes for estimating the chl *a* concentrations of West and East Okoboji lakes. This was not the case for the Spirit Lake data, which show weak statistical relationships in every case. Confusingly, the algorithm which performed the "best" for Spirit Lake, uses the red band radiance magnitude ($r^2 = 0.429$). Recall that hyperspectral reflectance in this region has been shown to be insensitive to chl *a* concentration (§2.3.1).

Similar to the results of the close-range investigation, several algorithms proved reasonably effective for estimating chl *a* in hypereutrophic East Okoboji Lake. Contrary to the close-range results, the NDVI ($r^2 = 0.946$) approach narrowly outperformed all other tested algorithms, including the NIR:Red ratio ($r^2 = 0.919$). This may be related to the less than ideal spectral resolution of the HRV sensor (§3.1.4; Figures 3-10 a,b,c,d).

When the data are considered altogether, the near-infrared magnitude algorithm produces the highest coefficient of determination ($r^2 = 0.833$) (Figure 3-15; Table 3-1). Lathrop and Lillesand (1989) also found a strong positive relationship ($r^2 = 0.948$) between chl *a* and the near-infrared band from the SPOT-1 platform. The success of the near-infrared magnitude algorithm, over the green and red magnitude algorithms, is not surprising given the higher degree of variation in the near-infrared band (Figures 3-12,

3-13, 3-14). However, the success of the near-infrared magnitude algorithm over the ratio based algorithms is a surprise, and probably results from image noise. While the ratioing of image bands is useful for discriminating subtle spectral variations, such procedures enhance noise. Furthermore, ratio images are "intensity blind," in that different targets possessing different absolute radiances can produce identical quotients when the bands are ratioed (Lillesand and Kiefer, 1994). The difference in brightness between the lakes, apparent in Figures 3-3 to 3-9, and the previously discussed striping problem, confirms that the Okoboji SPOT image is prone to both of these effects, thus limiting the utility of predictive techniques incorporating band ratios.

The application of an aggregate algorithm, rather than a suite of trophically targeted algorithms, is acceptable if we assume that the HRV sensor is oblivious to spectral differences resulting from variations in algal scattering and absorption efficiency. This is reasonable given the limited spectral resolution of the HRV sensor, the degradation of the emergent signal by the atmosphere, and the generalization of the target in terms of scale or pixel integration. With this assumption, maps of chl *a* concentration for the Iowa Great Lakes on August 13, 1997, were developed using the near-infrared radiance magnitude algorithm:

- **Chl *a* = EXP [(0.2632 * (XS3 radiance)) - 0.9585]** .

Figure 3-16 shows the distribution and concentration of chl *a* in seven gradations. Seven gradations allowed better differentiation of the chl *a* classes. Figure 3-17 uses the same equation and color scheme but is scaled to accentuate the higher chl *a* levels.

3.2.4 Map Interpretation

Several interesting features are evident in the quantified chl *a* maps. The high chl

a levels exhibited by the extreme shoreline pixels (Figure 3-16) result from several different but coincident factors. First, the deciduous trees which run adjacent to the shoreline presumably contaminate the true water pixels. Second, biological productivity is more prominent in shallow waters where light is abundant and temperatures are higher. In these shallow water pixels, attached algae and submerged macrophytic vegetation can have a significant impact on the emergent flux. The effects of submerged macrophytic vegetation are particularly prominent in Miller's Bay which is located in the west-central portion of West Okoboji Lake (Figures 1-6, 3-16). Finally, the influence of the highly reflecting rock and sand bottom in these shallow zones can enhance backscattering, thereby resulting in artificially high chl *a* values.

Despite the uncertainty of the shoreline pixels, the spatial biomass patterns exhibited by West Okoboji and Spirit lakes, are relatively uniform and roughly coincide with the respective bathymetric pattern of each lake. This corroborates conventional and documented knowledge (Bachmann and Jones, 1974) of these lakes' homogeneous nature. However, the quantification model seems to be overestimating the chl *a* levels of West Okoboji Lake. In Figure 3-16, the majority of the lake is classed as blue or cyan (5-10 and 10-15 $\mu g\ L^{-1}$ respectively), whereas historical and ground truth data (Tables 1-2, 1-4) suggest the lake should be dominantly classed as violet and blue (0-5 and 5-10 $\mu g\ L^{-1}$ respectively).

Major expanses of East Okoboji Lake and the Gar Chain exhibit extremely high chl *a* levels. In East Okoboji, algal biomass appears to be concentrated in coves, presumably a product of the wind action on 8/13/97. During data collection, the wind originated from a northeasterly direction. This is evident by the drift in the position of

the pontoon boat, documented by the GPS data. The effects of wind action are quite prominent in the two northern basins of East Okoboji Lake. In the northernmost basin, biomass is concentrated in the western bay and at the basin constriction in the south (Figure 3-16). Color/density gradients can be seen in both instances. One basin south, there is a wide band of dense algae traveling in-mass across the basin (Figure 3-17). This basin also constricts to a narrow channel, conveniently known as "The Narrows" (Figure 1-3). These basin constriction points act as a bottlenecks which concentrate the algae and promote the formation of emergent alga blooms. Similar to the northern basins, the area where East Okoboji and Upper Gar lakes connect shows similar biomass build up. Figure 3-18 provides a more detailed view of this bloom susceptible area. In each of these instances, water volume flow may also be playing a role in concentrating the algae. Recall from §1.6.4.3 that the predominant flow of the primary lakes is in the southerly direction out through the Gar Chain.

Both Upper and Lower Gar lakes exhibit high levels of chl *a* while Lake Minnewashta possesses more moderate levels. Most interesting is the intricate spatial biomass pattern present in Lower Gar Lake (Figure 3-17). We know this feature to be real and not simply a product of image processing because it appears in Figure 3-6, and patterns of similar scale were documented with aerial photography (Figure 3-19). This feature in Lower Gar, as well as those in the northern basins of East Okoboji Lake, confirm the ability of SPOT imagery to capture fine spatial features. However, the striping noise which is carried through into the final chl *a* maps continues to hinder interpretation.

FIGURES

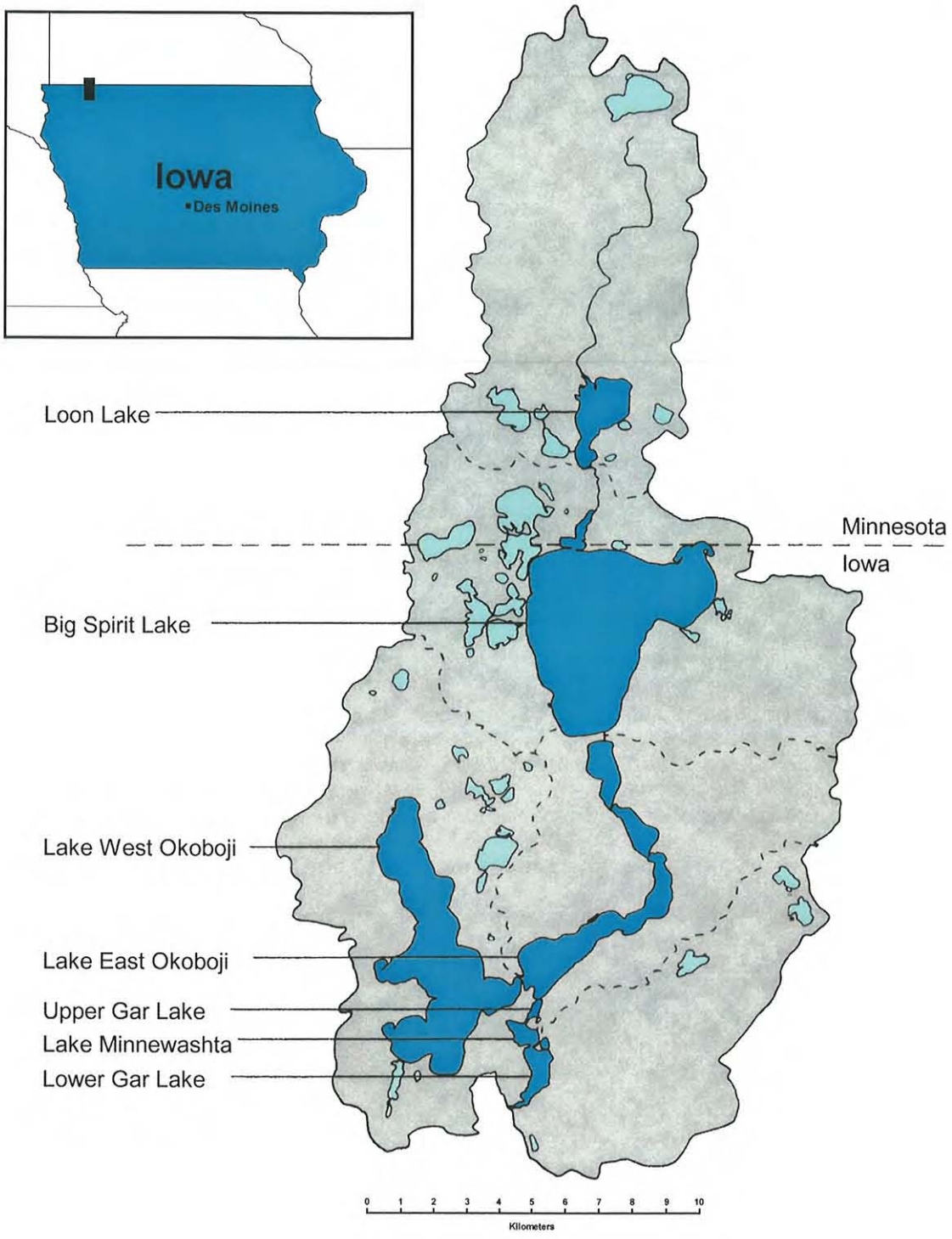

Figure 1-1. The Iowa Great Lakes drainage basin is located in northwest Iowa and southwest Minnesota. Dashed lines indicate the individual watershed boundaries (adapted from Bachmann and Jones, 1974).

Figure 1-2. These images show the degraded water quality resulting from an emergent blue-green alga bloom.

Figure 1-3. These aerial photographs demonstrate the heterogeneous biomass patterns of Lake East Okoboji. Pronounced masses of blue-green algae are evident in each image. These pictures show opposing views of "The Narrows," where the highest chl *a* measurement (582.7 $\mu g\ L^{-1}$) was acquired.

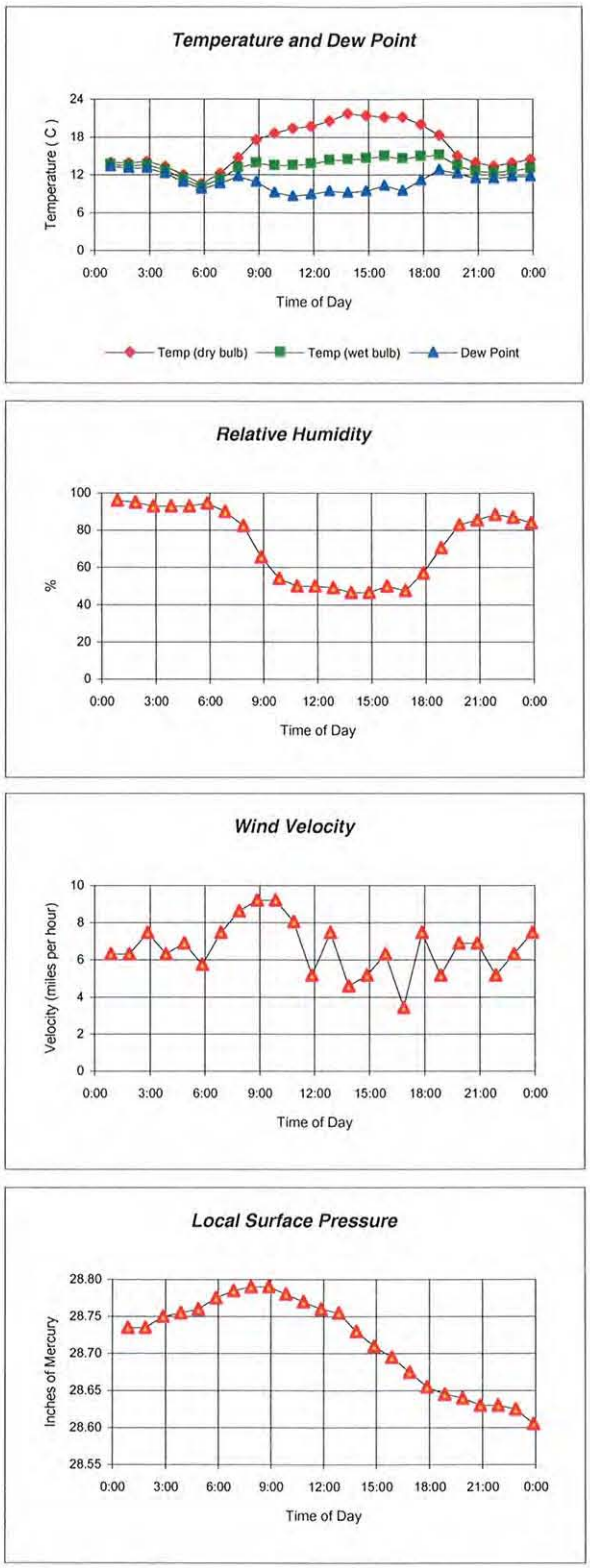

Figure 1-4. These charts show the climatological conditions during data collection (8/13/97). These hourly observations were acquired by automated weather stations in Spencer and Estherville, Iowa. The data were purchased from the National Climate Data Center (NOAA).

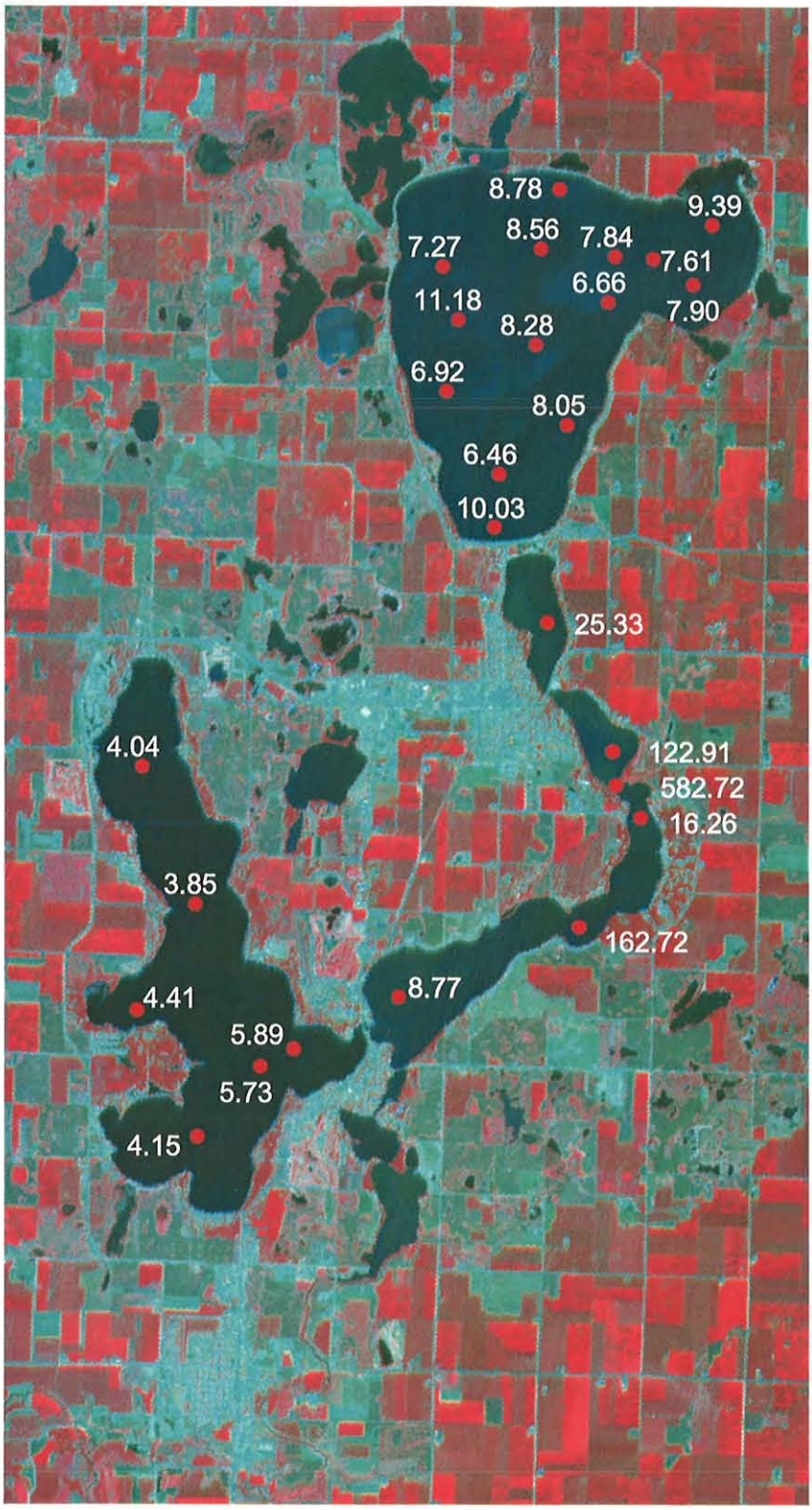

Figure 1-5. This is the Okoboji study area (8/13/97) with the sample sites denoted as red dots. Chlorophyll a concentrations are shown in white.

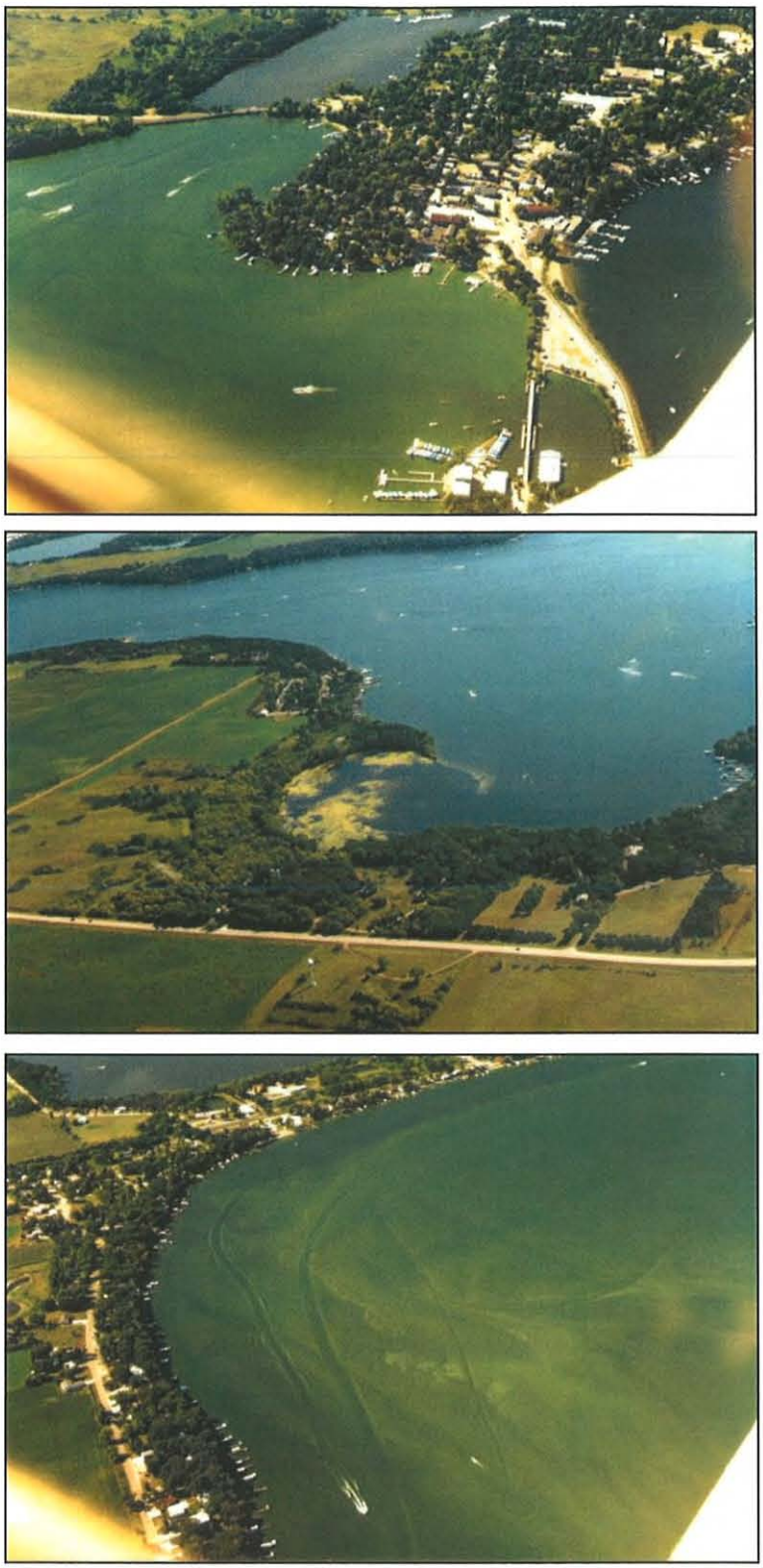

Figure 1-6. These aerial photographs show an emergent bloom near "The Grade" (top), beds of aquatic macrophytes in Miller's Bay (middle), and boat tracks through the algae on south eastern Spirit Lake (bottom).

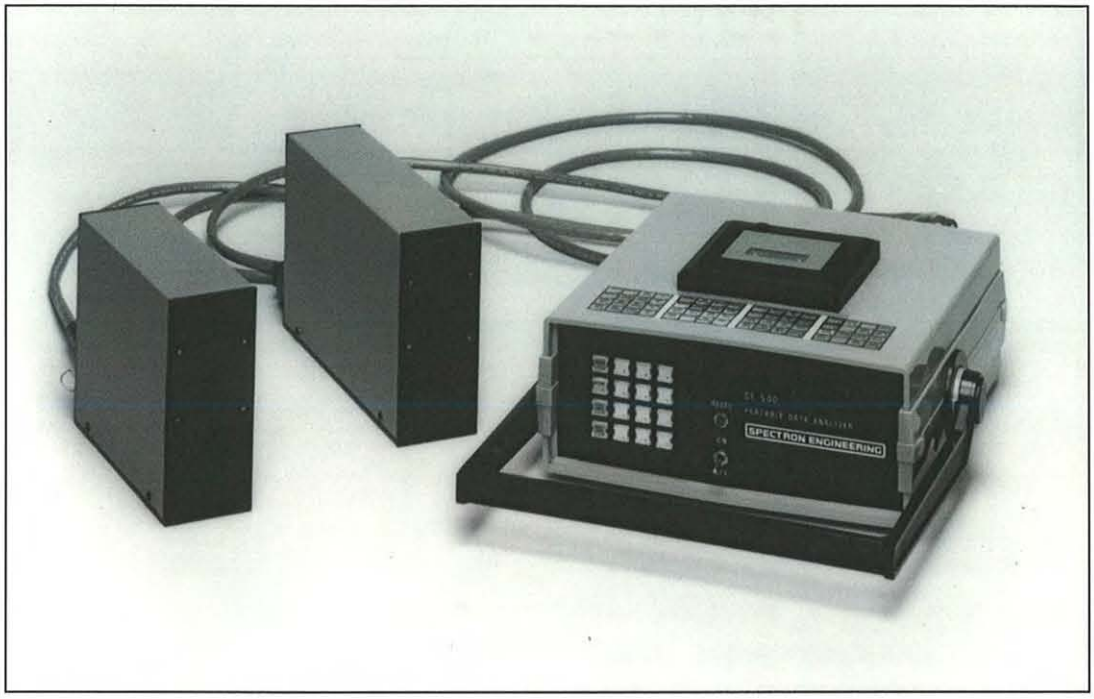

Figure 2-1. Spectron Engineering SE-590 spectroradiometer; cameras and controller

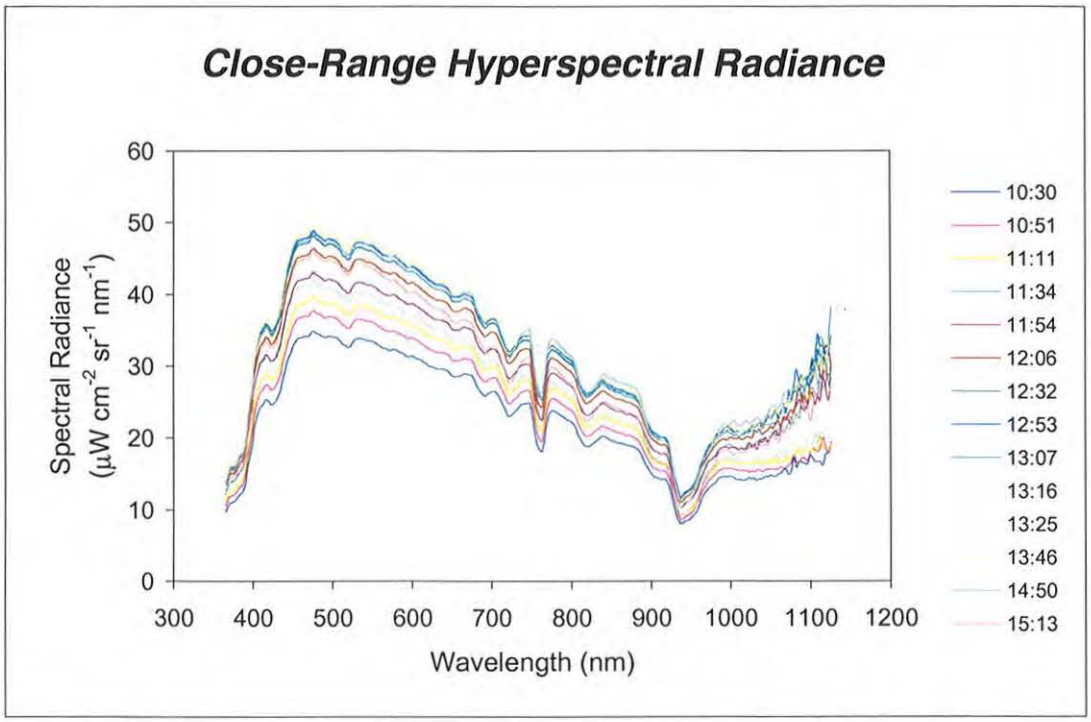

Figure 2-2. These white Lambertian panel scans were taken throughout the day (8/13/97) for calibration purposes and later used in the percent reflectance calculation.

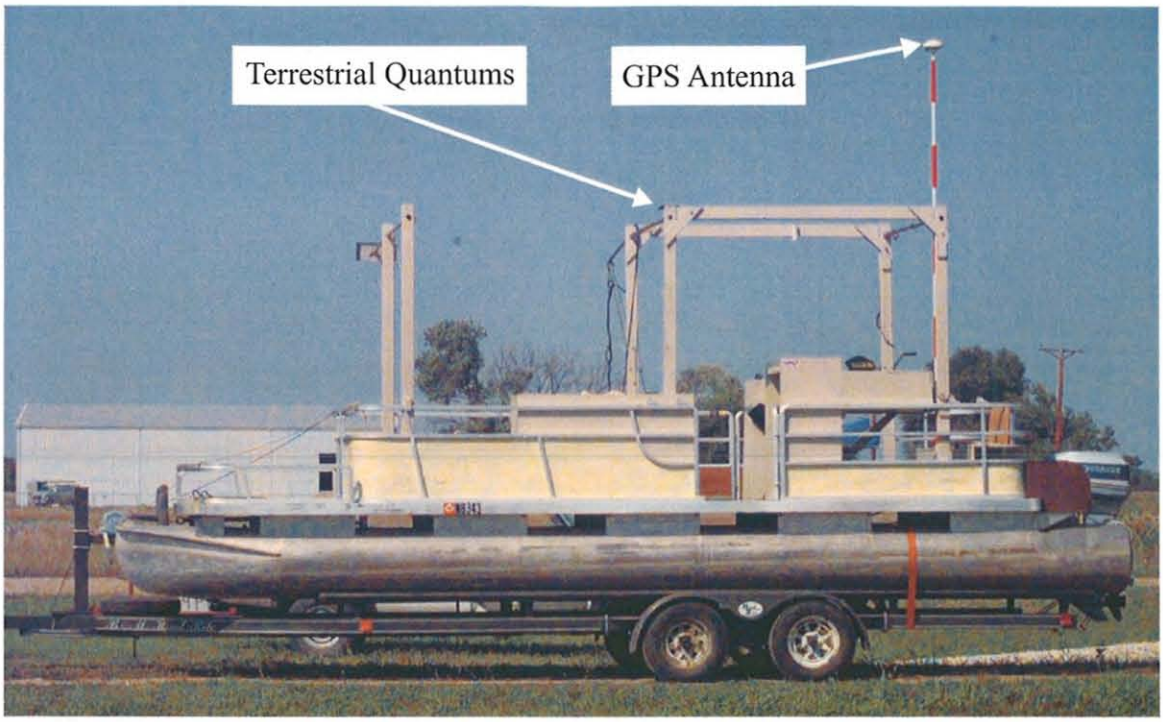

7.6 m

1.5 m

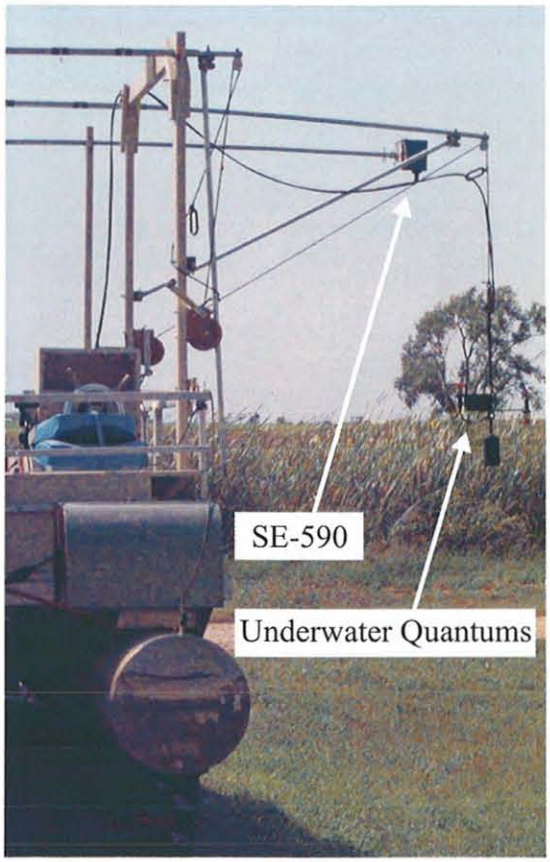

2.4 m

Figure 2-3. Optical measurements were made on West and East Okoboji lakes from a pontoon boat.

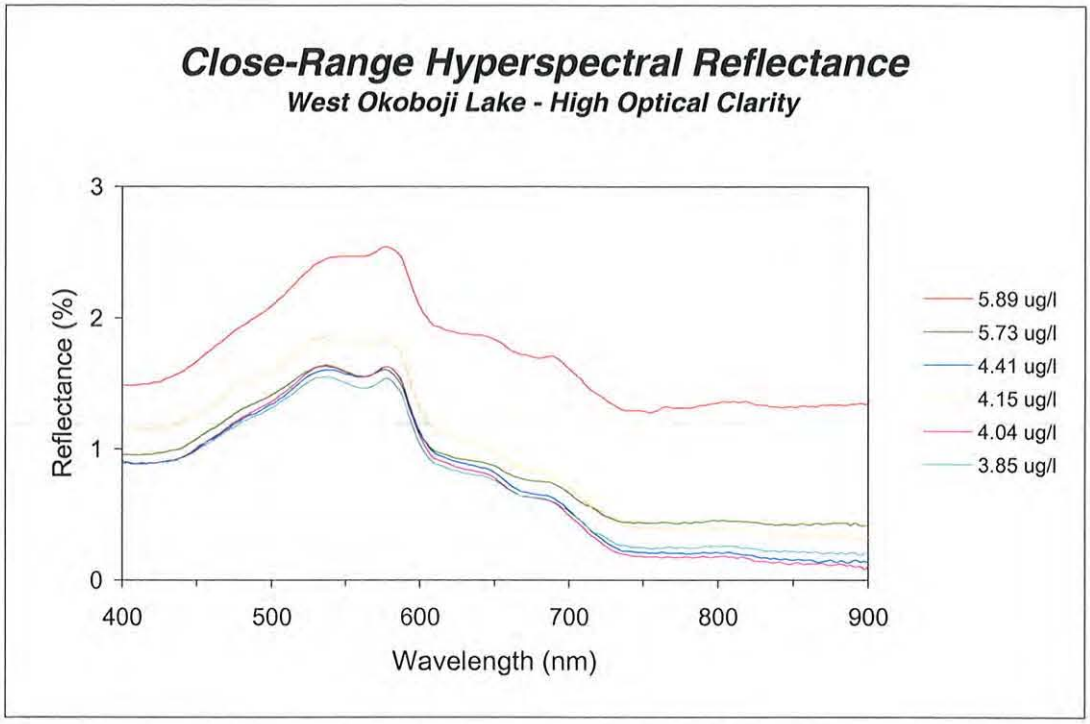

Figure 2-4. The hyperspectral reflectance signatures for the highly transparent waters of West Okoboji possess poorly developed spectral features.

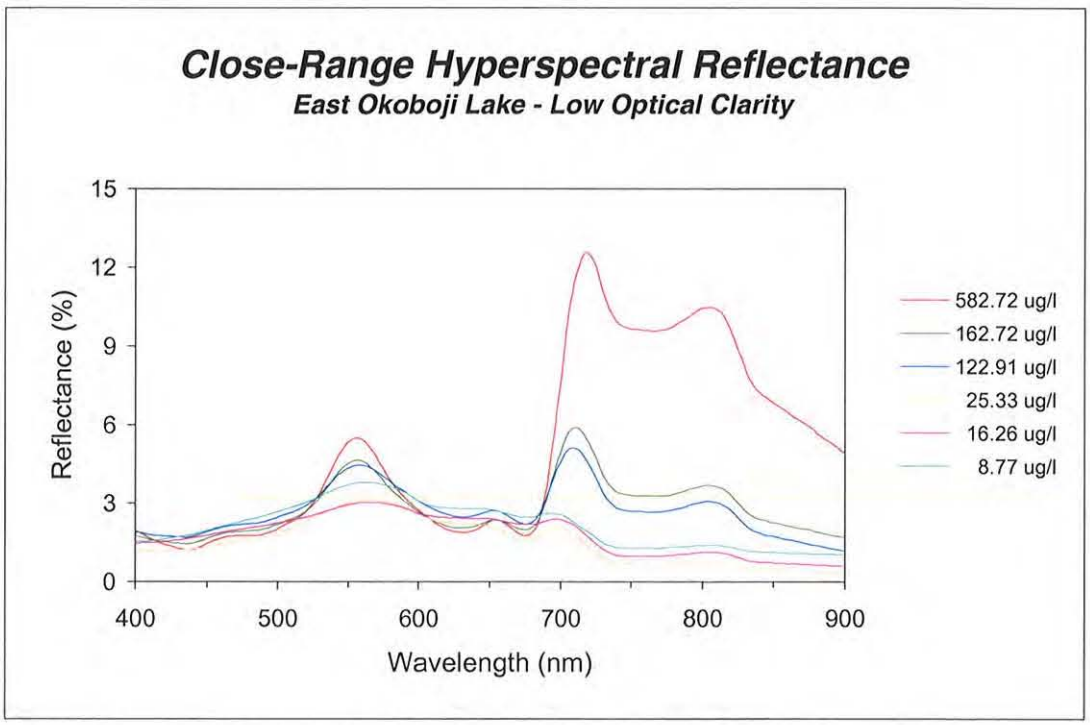

Figure 2-5. The hyperspectral reflectance signatures for the highly turbid waters of East Okoboji possess distinct spectral features which correspond to prominent absorption and scattering processes.

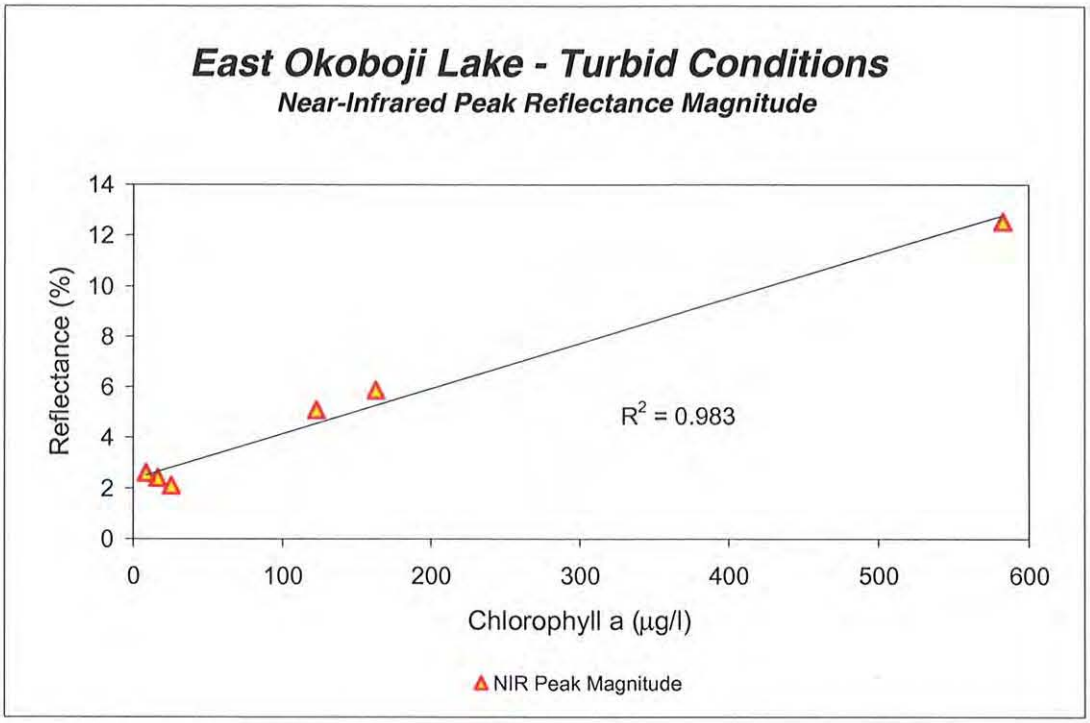

Figure 2-12 The turbid conditions of East Okoboji Lake can be effectively modeled simply on the basis of the magnitude of the reflectance peak near 700 nm.

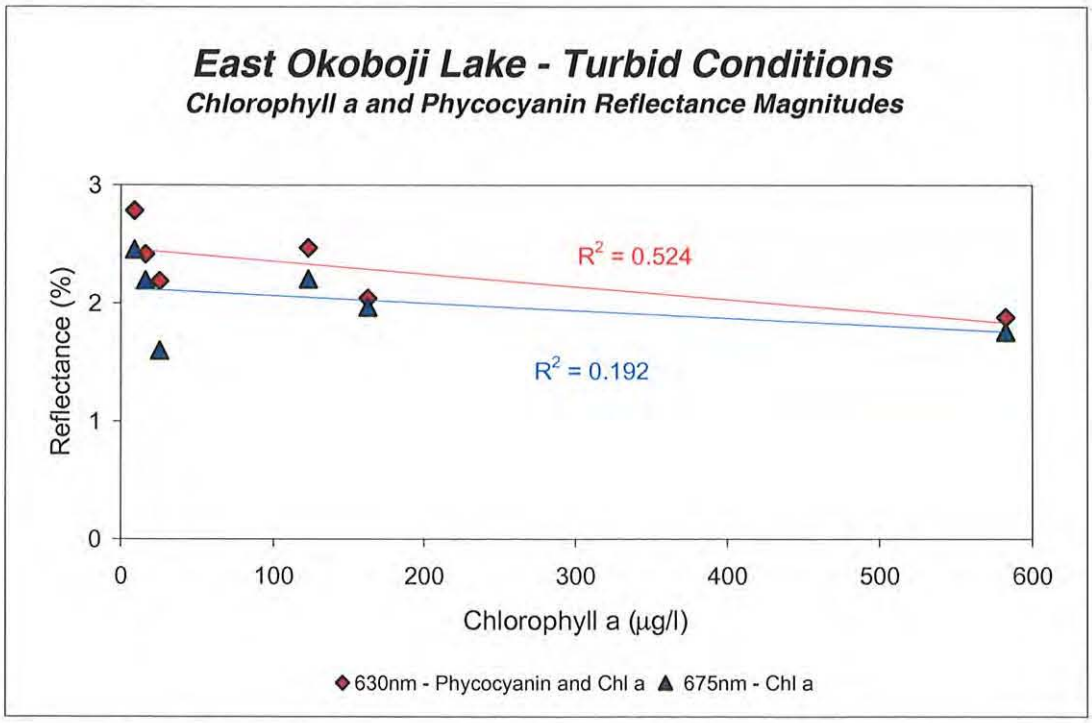

Figure 2-13 In regions where pigment absorption in maximal, spectral reflectance is not sensitive to changes in algal biomass.

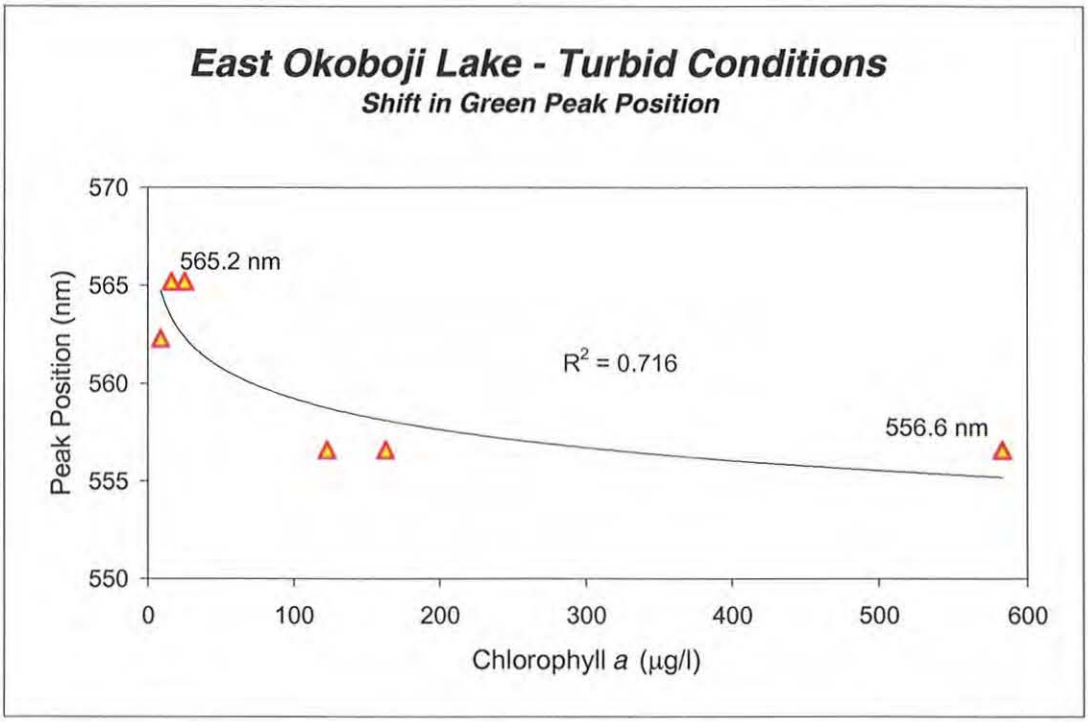

Figure 2-14 While the shift of the green peak toward shorter wavelengths saturates at 150 $\mu g\ L^{-1}$, it might be useful as a temporal indicator of species dominance.

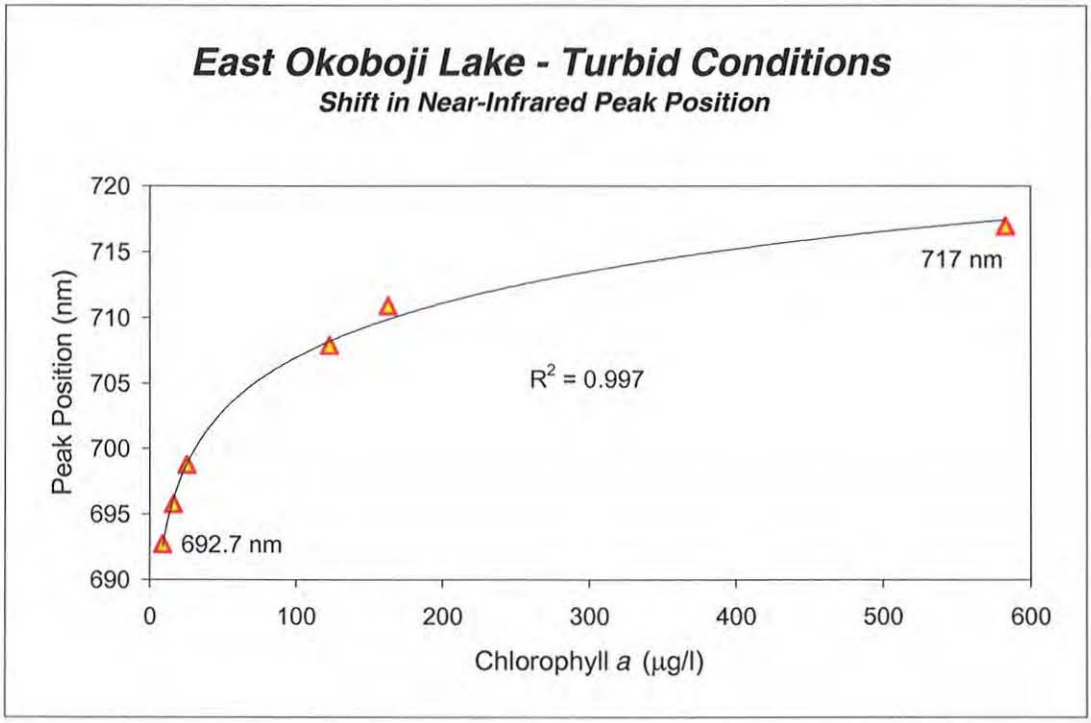

Figure 2-15 Due to the lack of photosynthetic pigments beyond 675 nm, the shift of the near-infrared peak is always toward the longer wavelengths with increases in biomass. An algorithm based on the position of the peak near 700 nm is appealing because its position is determined solely by the absorption properties of the medium.

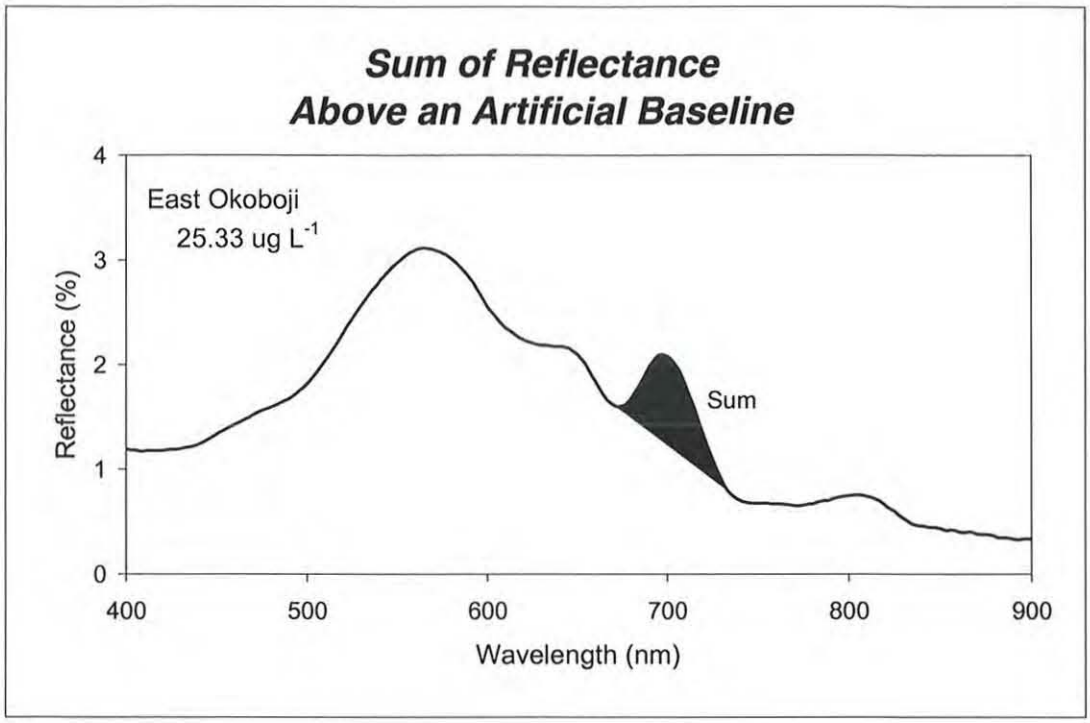

Figure 2-16 This chart illustrates the Baseline Sum concept.

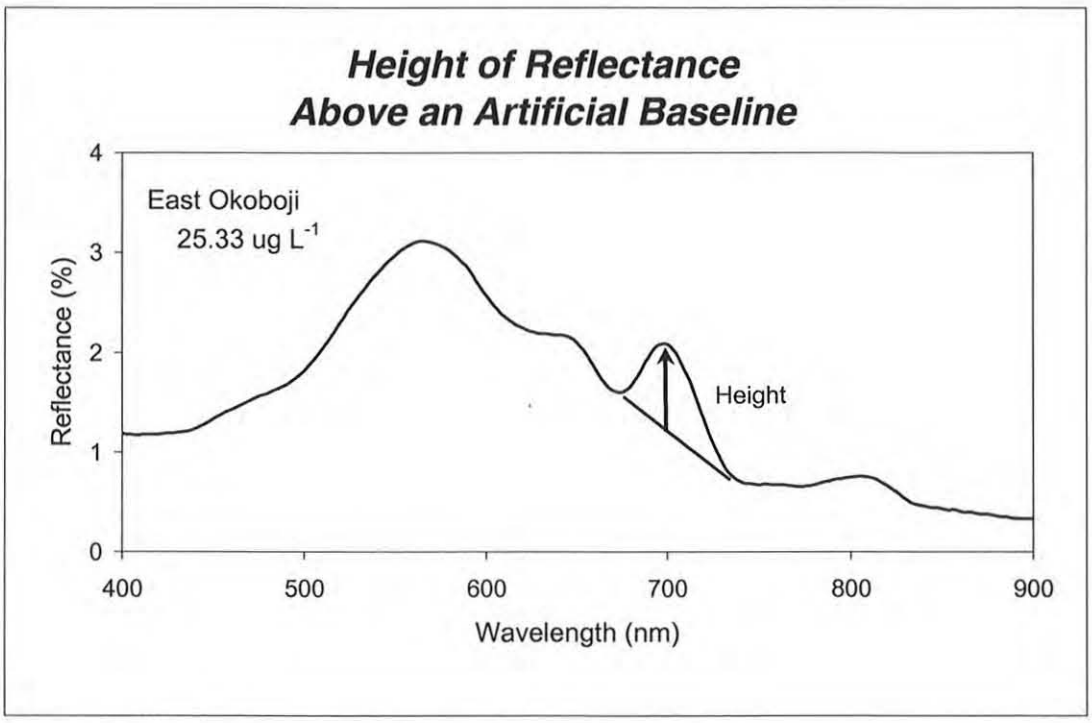

Figure 2-17 This chart illustrates the Baseline Height concept.

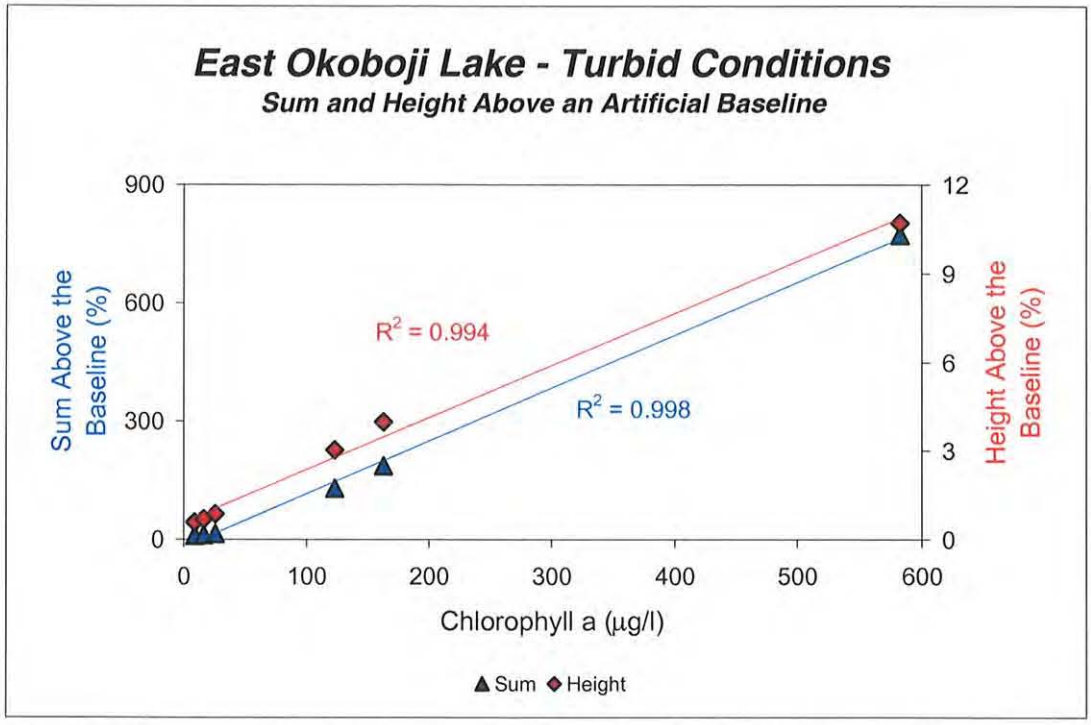

Figure 2-18 The success of the baseline algorithms is based in their ability to isolate the fraction of light scattered by phytoplankton from the total composite signal.

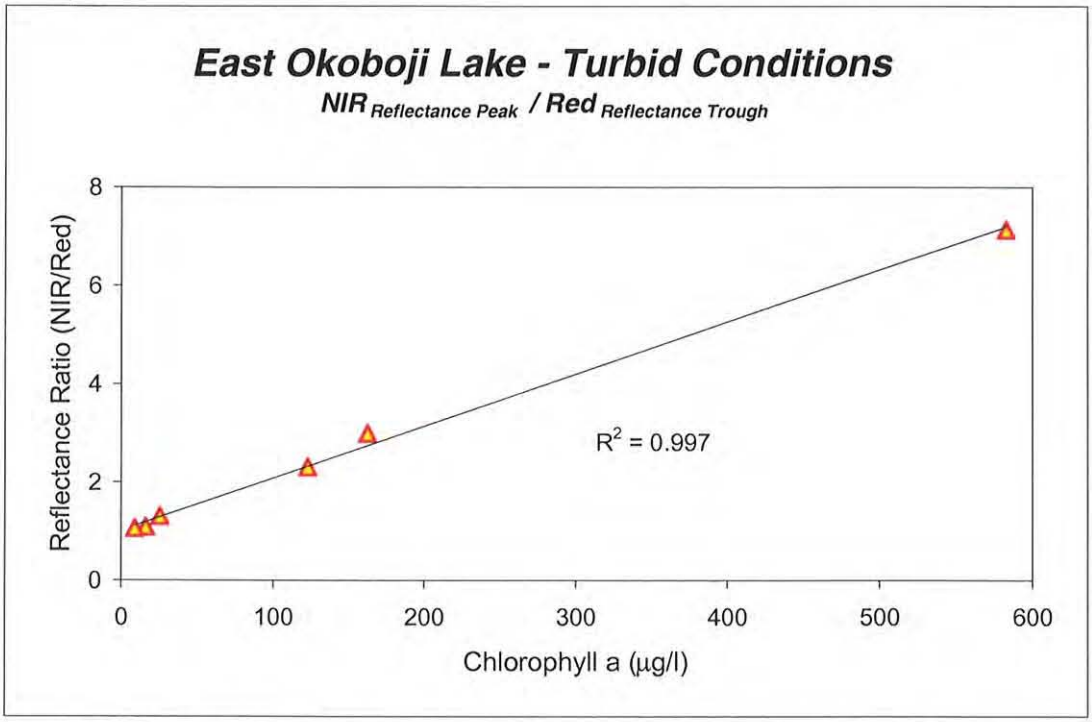

Figure 2-19 The NIR:Red ratio is a simple and effective approach. Similar to the baseline algorithms, the normalization of the near-infrared response corrects for non-algal scattering.

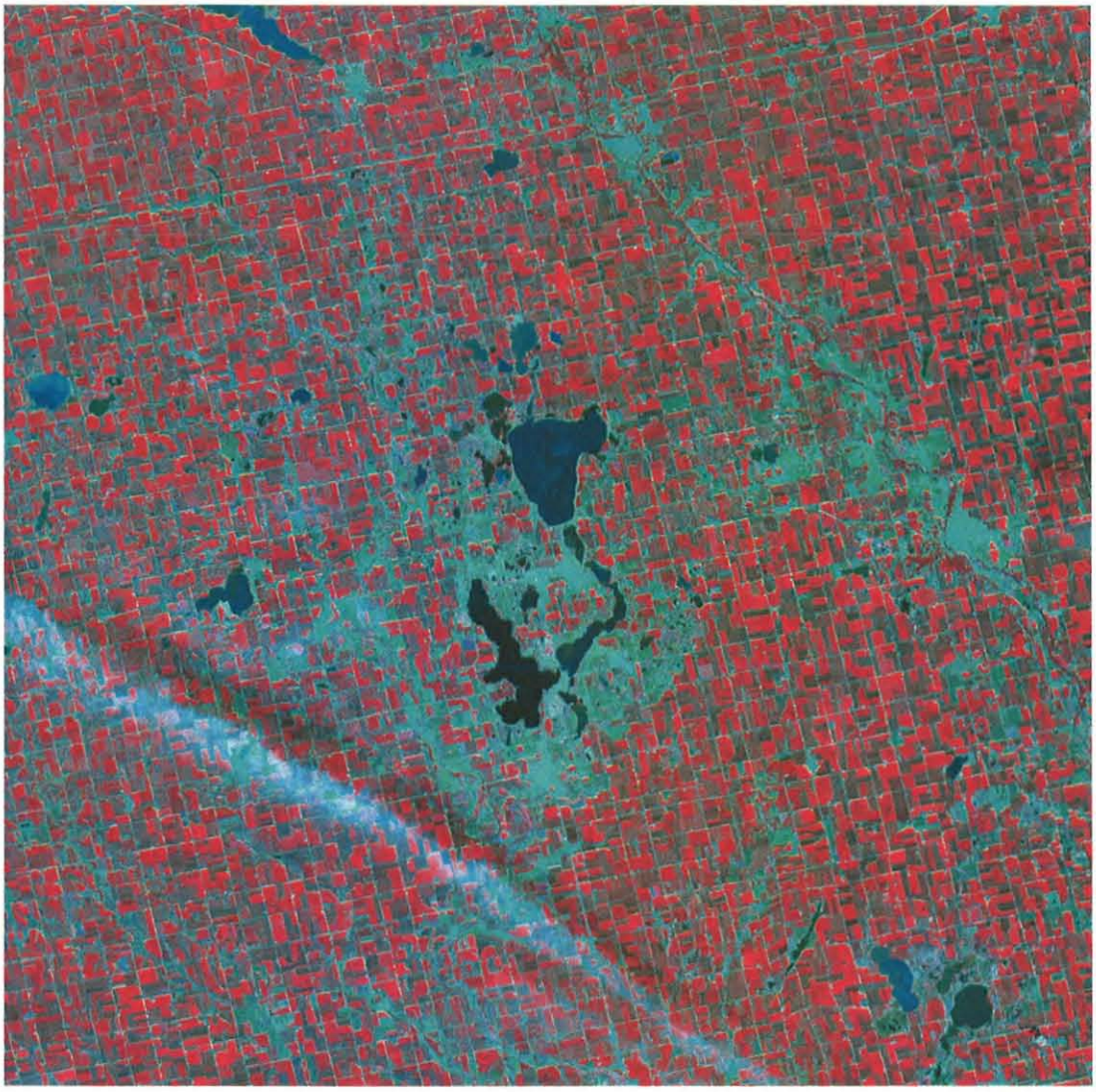

Figure 3-1. The Iowa Great Lakes are positioned in the center of this raw SPOT scene. In this false color composite, SPOT bands XS3, XS2, and XS1 are directed to the red, green, and blue color guns respectively. With this arrangement, lush vegetation appears red while bare ground and urban areas appear cyan.

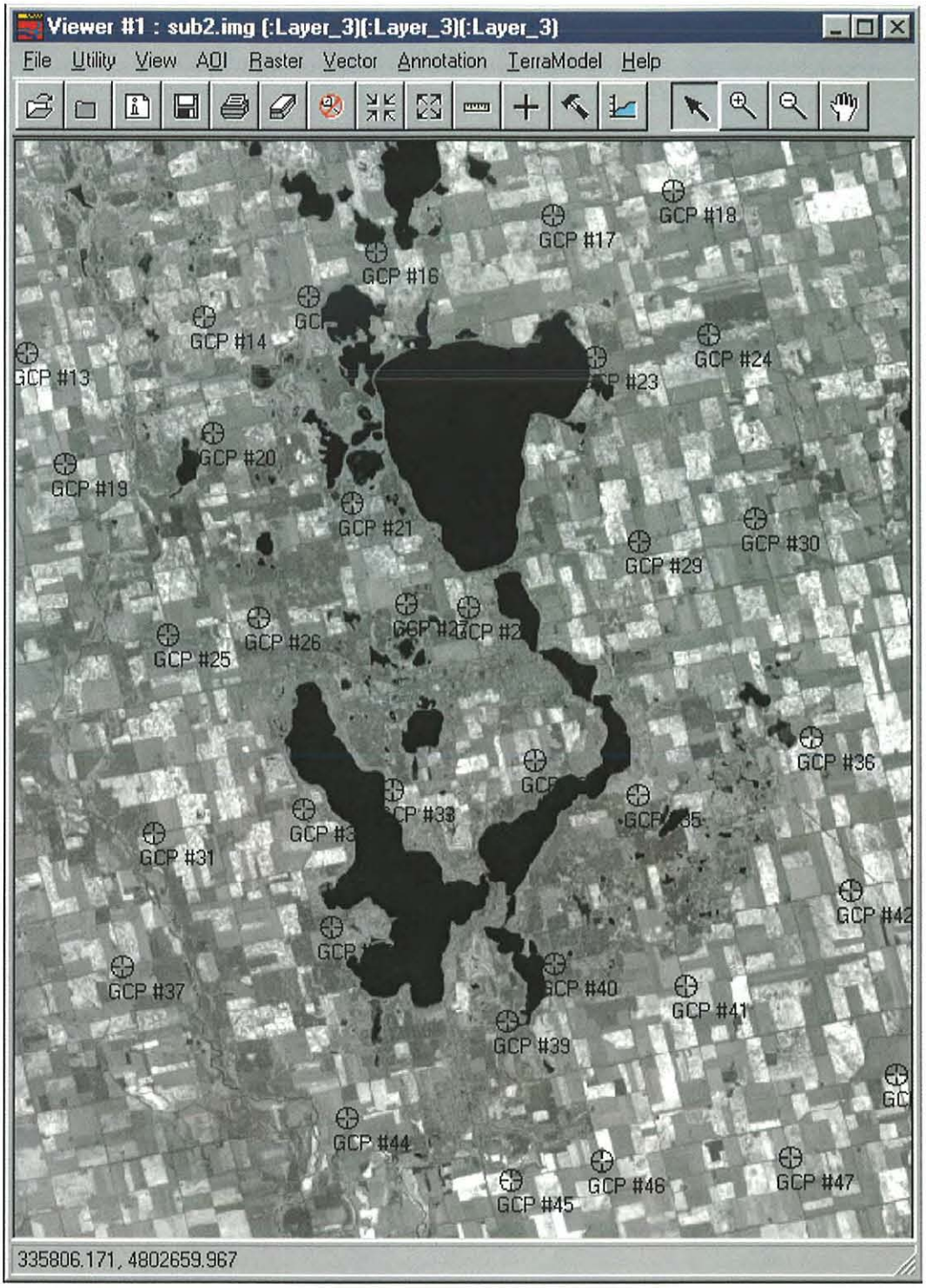

Figure 3-2. Thirty-four ground control points were used to geometrically correct the Okoboji study area image. The individual points are shown in black.

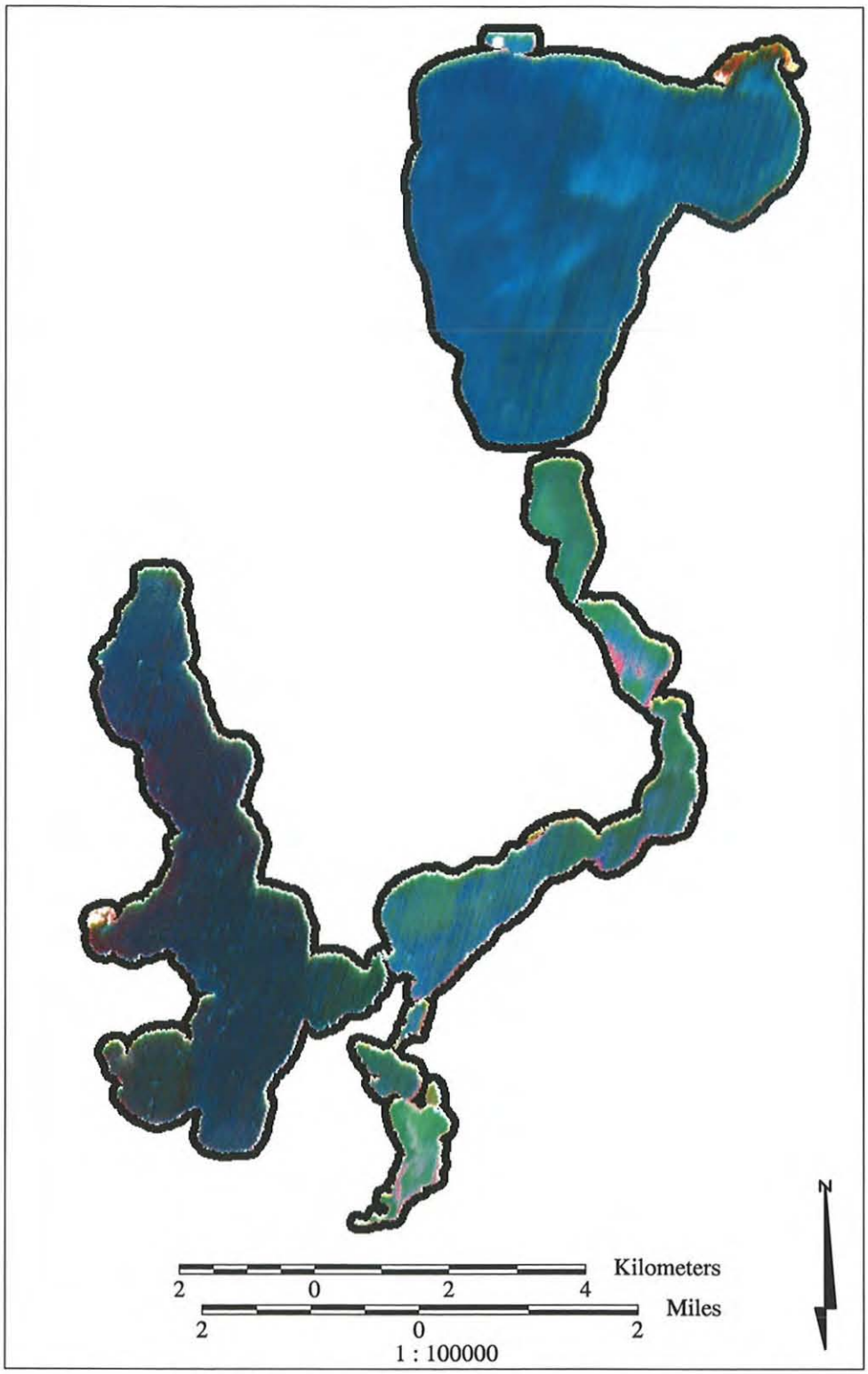

Figure 3-3. The lake subset image is shown using a 3,2,1 band combination and the default two standard deviation contrast stretch. This radiometrically and geometrically corrected image also has a six pixel black buffer to accentuate the periphery pixels.

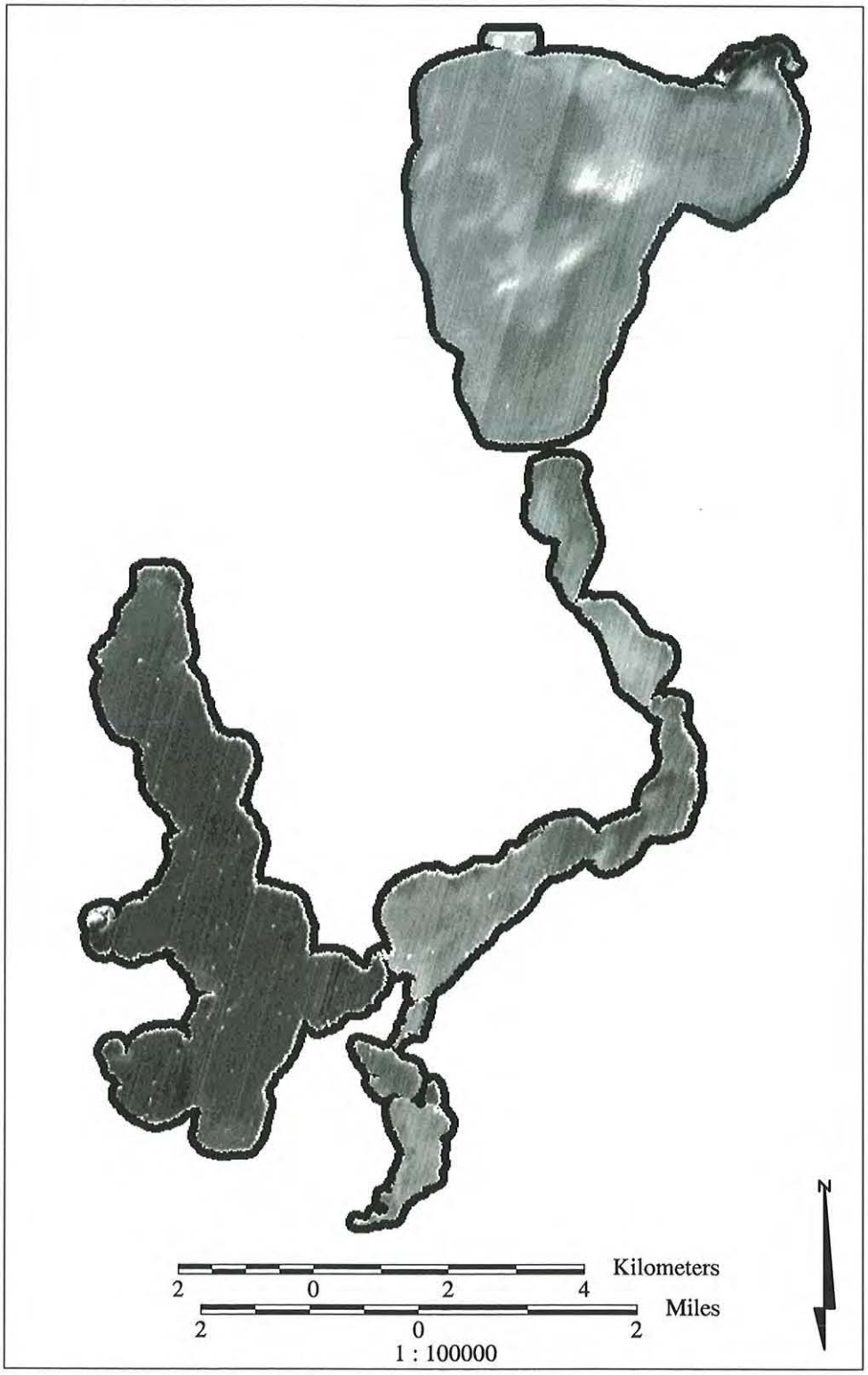

Figure 3-4. SPOT band 1 (0.50 - 0.59 um) of the lake subset image is displayed in gray scale mode with the default two standard deviation contrast stretch.

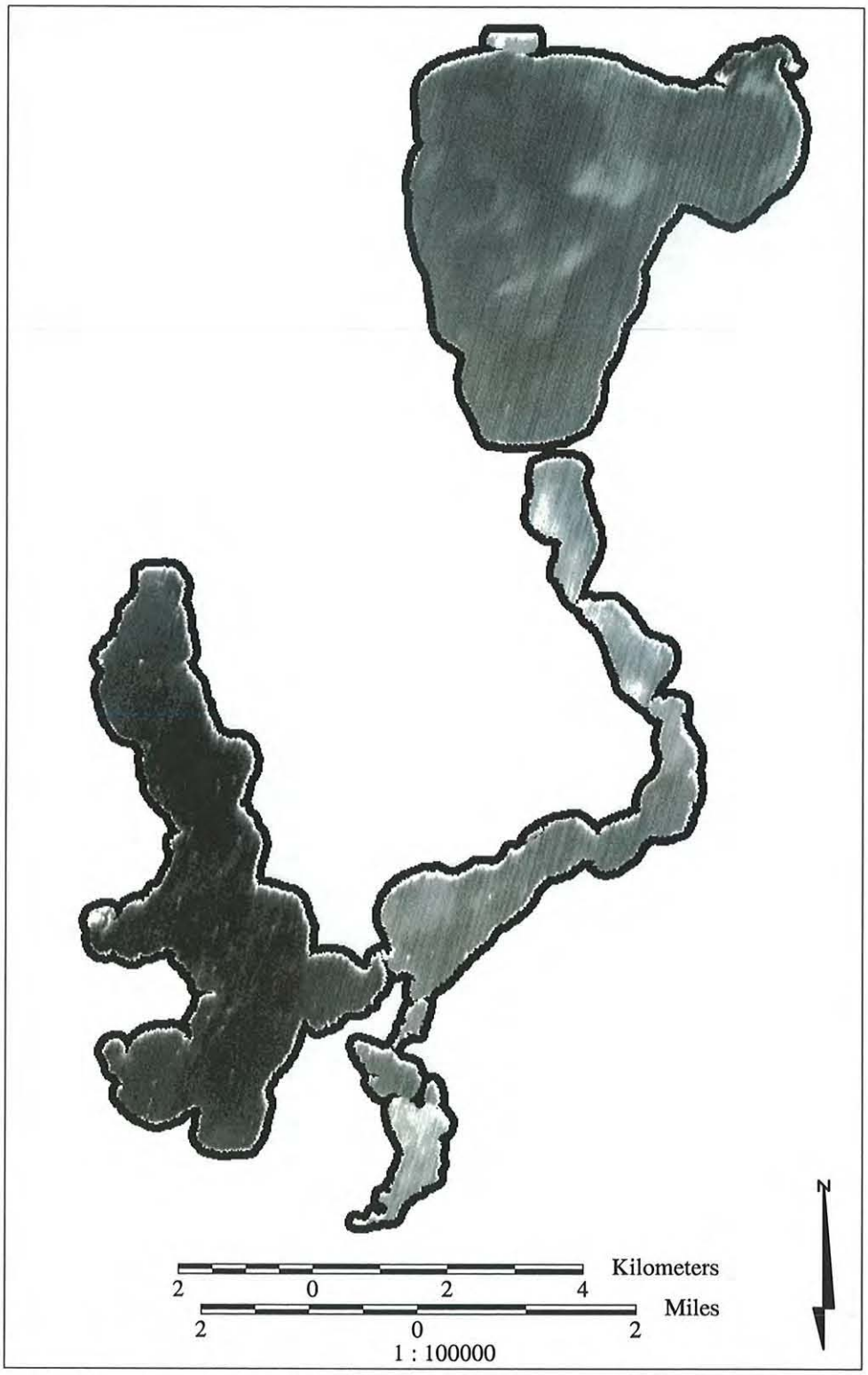

Figure 3-5. SPOT band 2 (0.61 - 0.68 um) of the lake subset image is displayed in gray scale mode with the default two standard deviation contrast stretch.

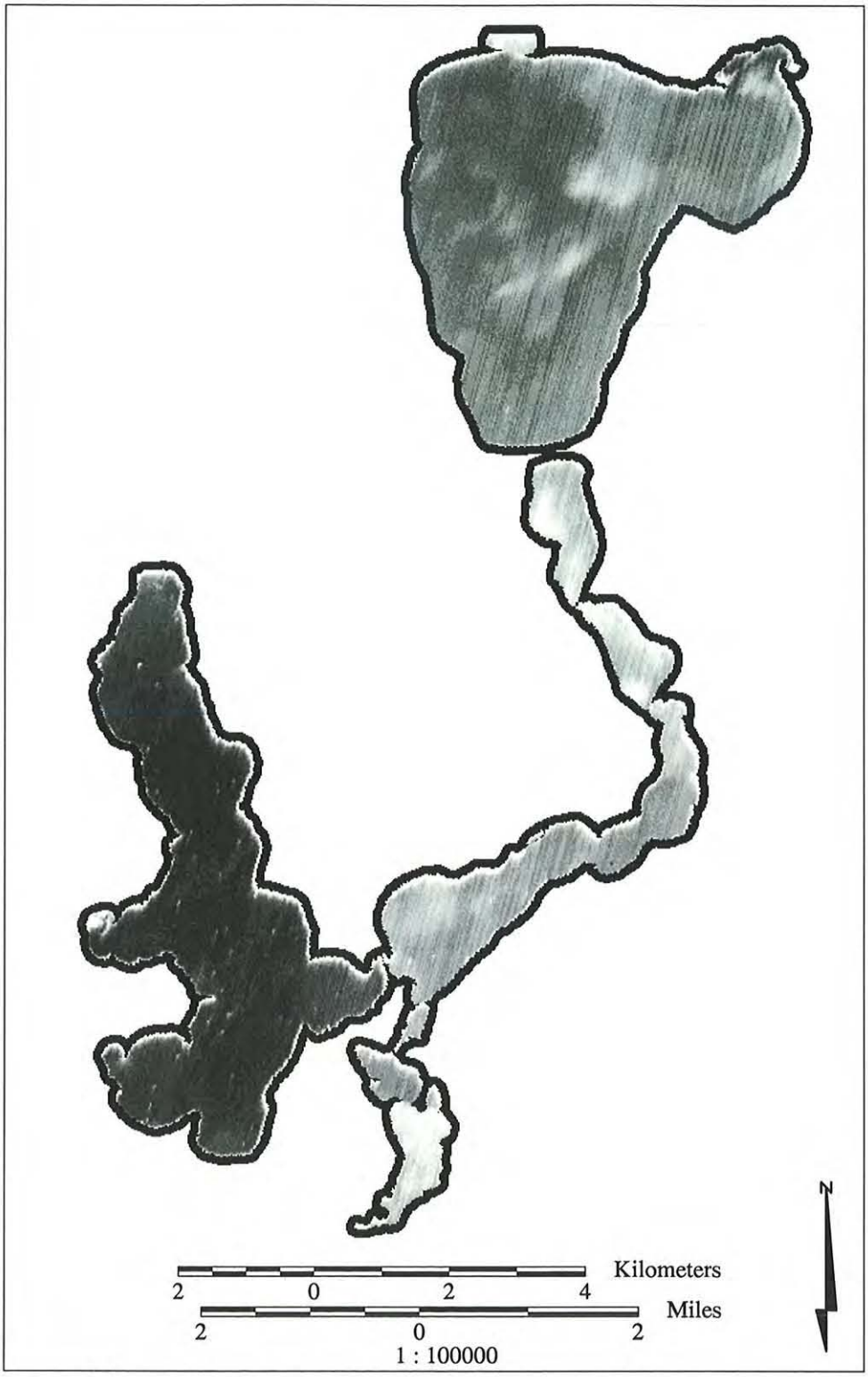

Figure 3-8. SPOT band 2 (0.61 - 0.68 um) of the lake subset image is displayed in gray scale mode with a histogram equalization contrast stretch.

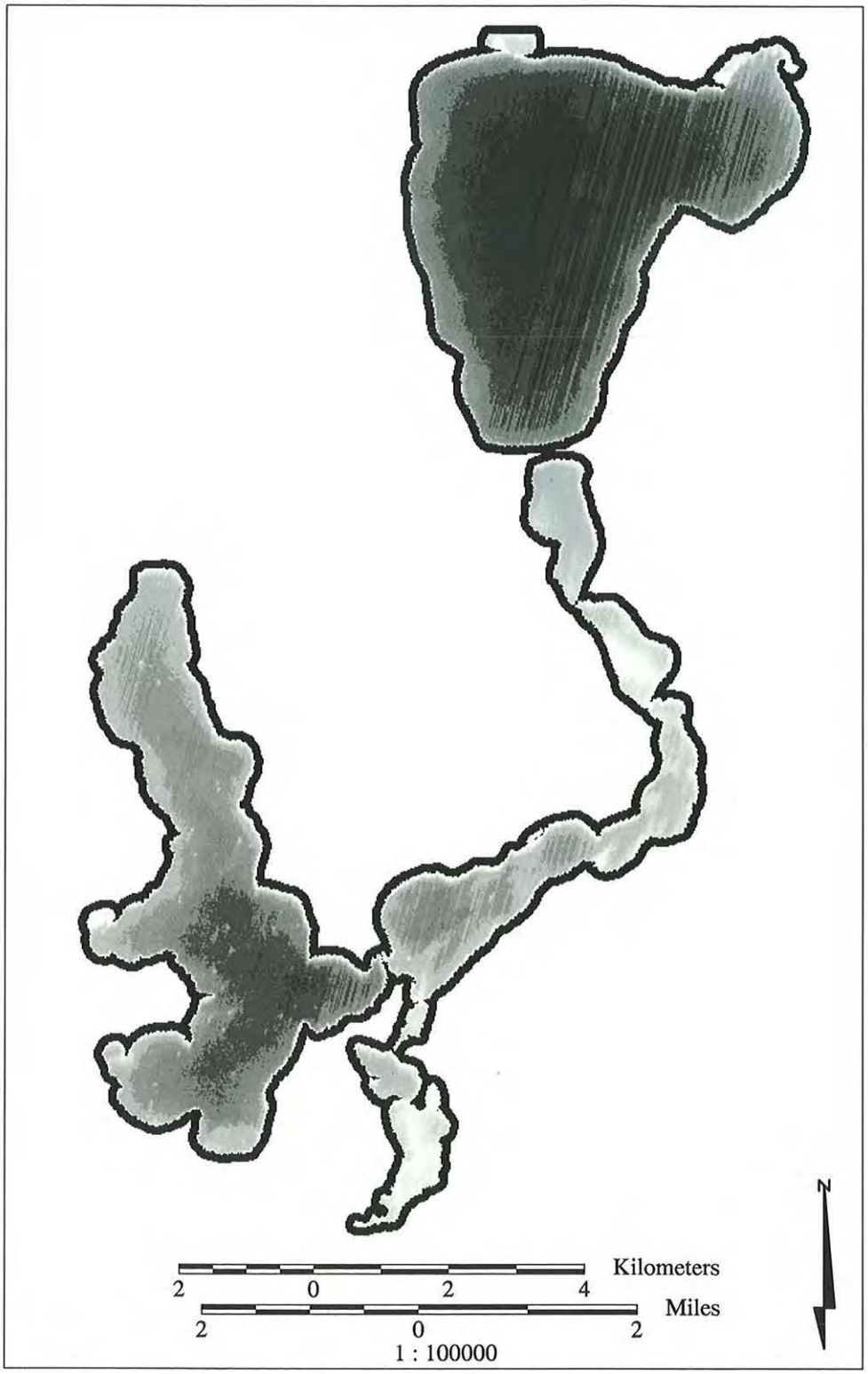

Figure 3-9. SPOT band 3 (0.79 - 0.89 um) of the lake subset image is displayed in gray scale mode with a histogram equalization contrast stretch.

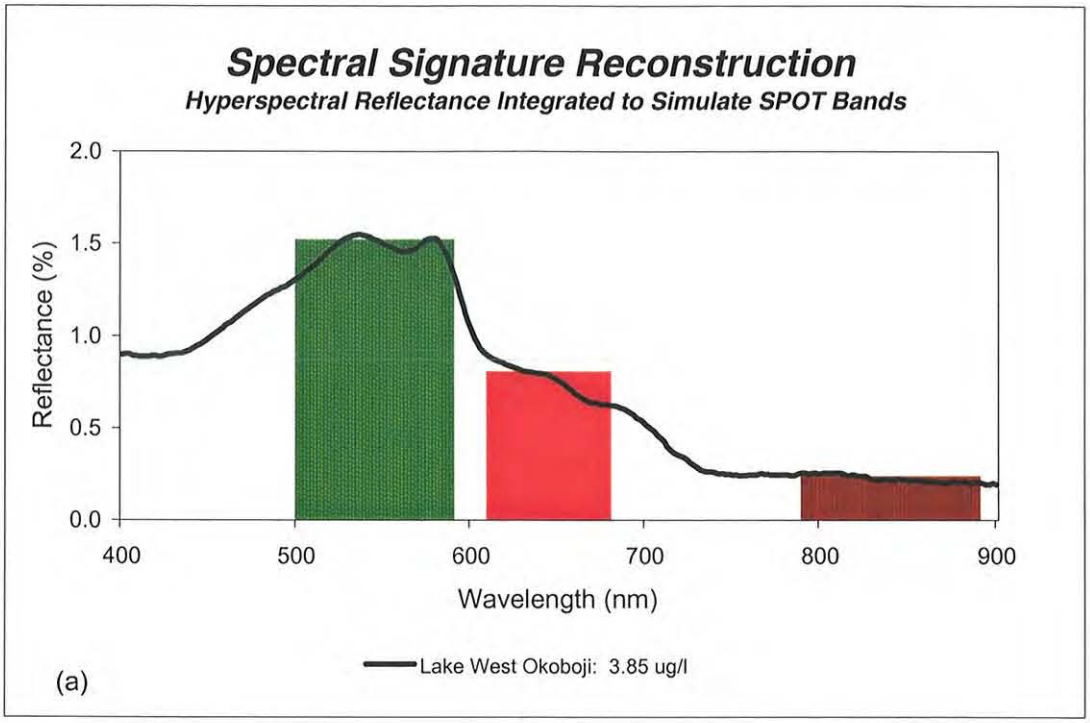

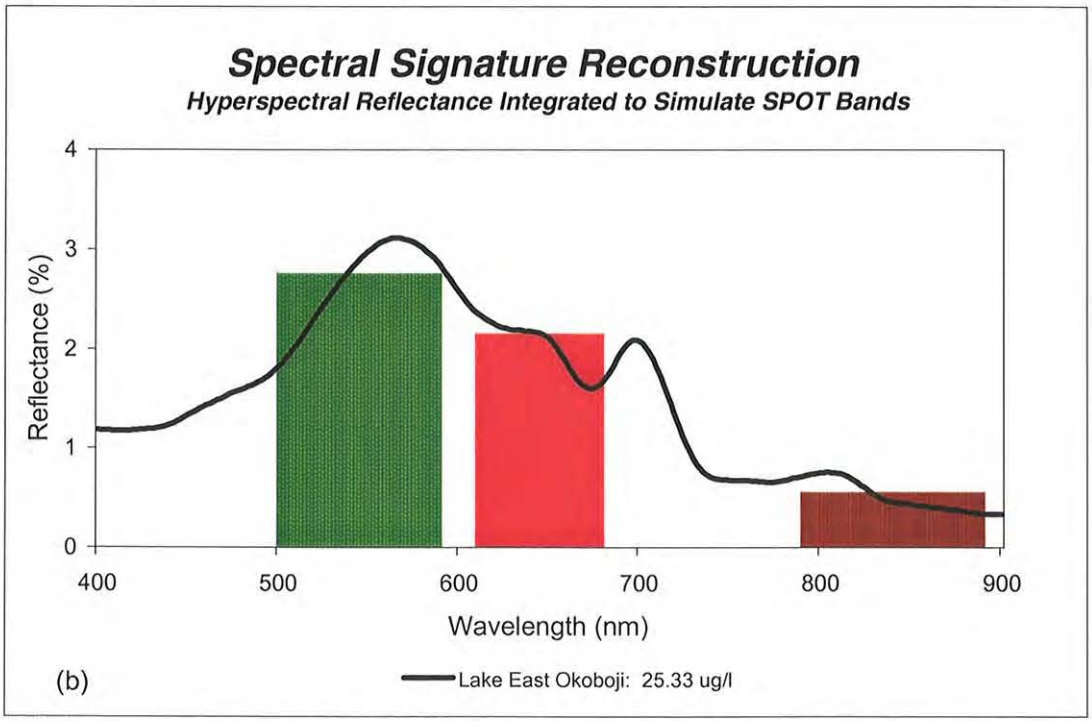

Figure 3-10 The width and placement of spectral bands largely determine the ability of a sensor to detect and quanitfy specific optical processes.

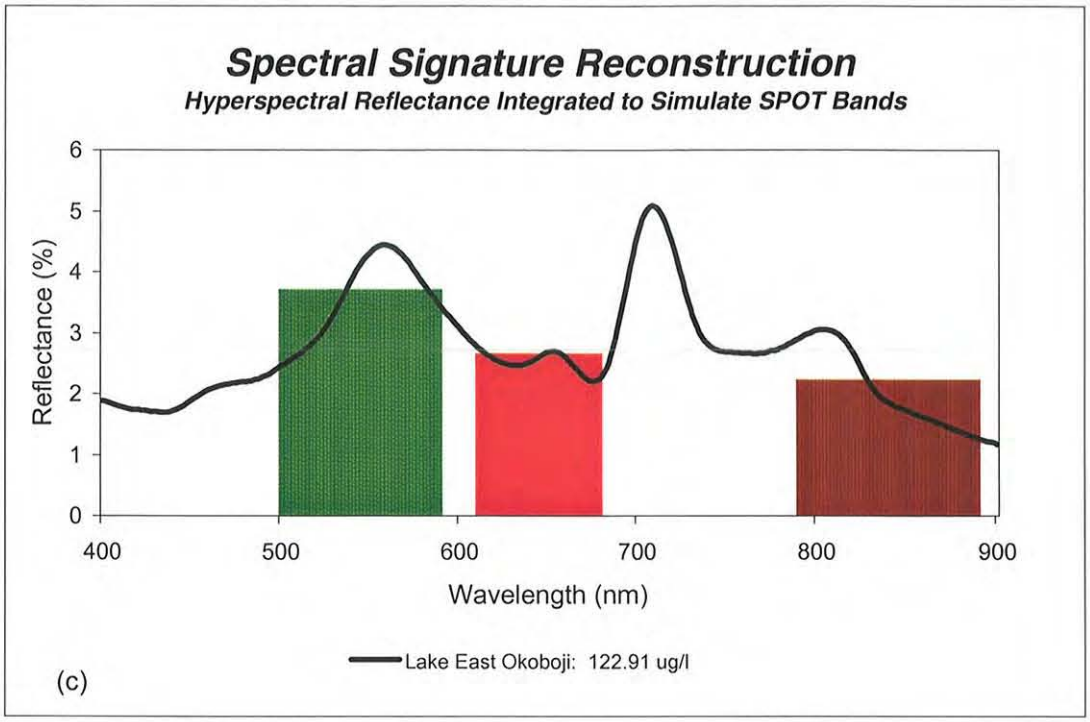

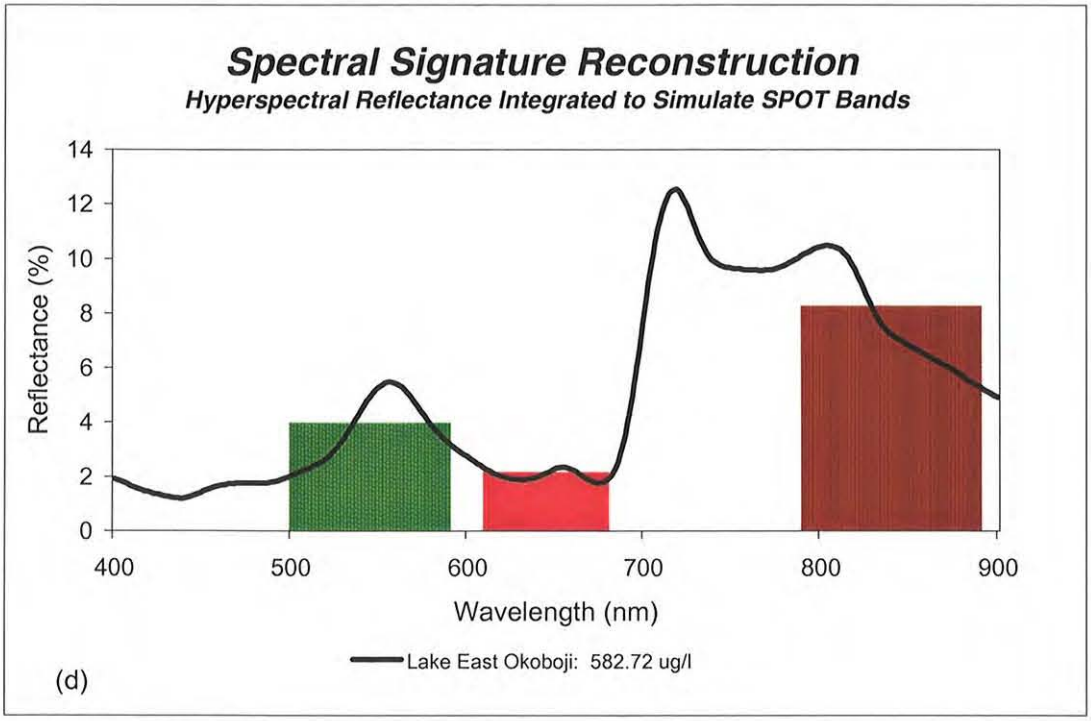

Figure 3-10. continued

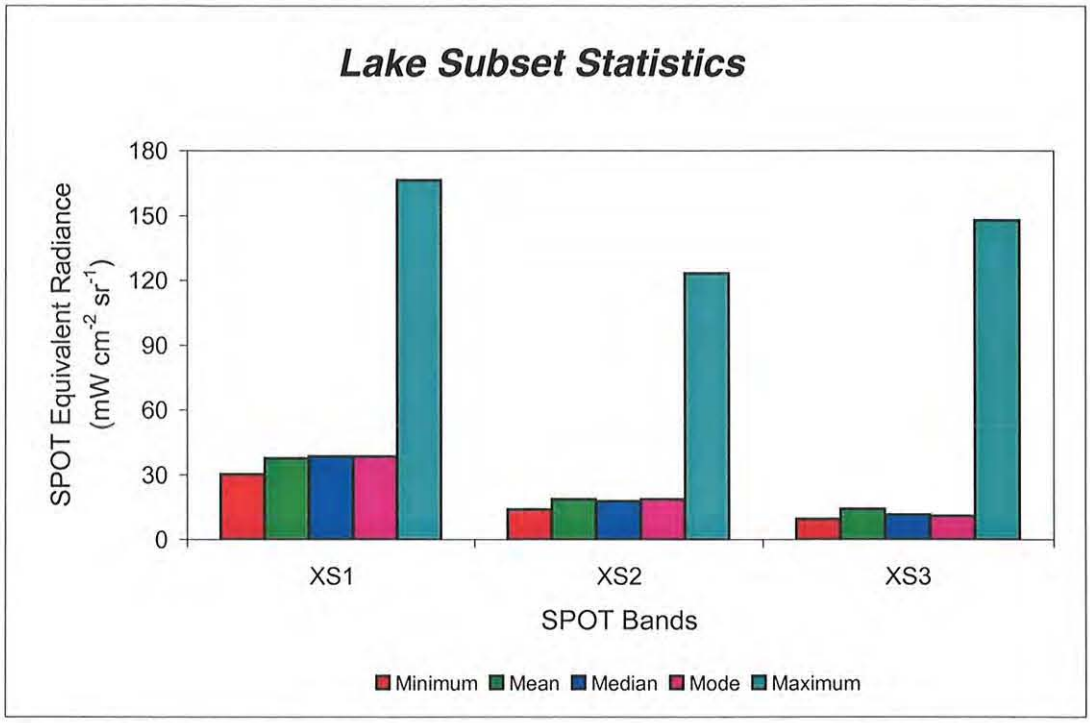

Figure 3-11 The statistics for all the lake pixels are very similar in each of the SPOT bands. The high "maximum" values are biased from the contaminated shoreline pixels.

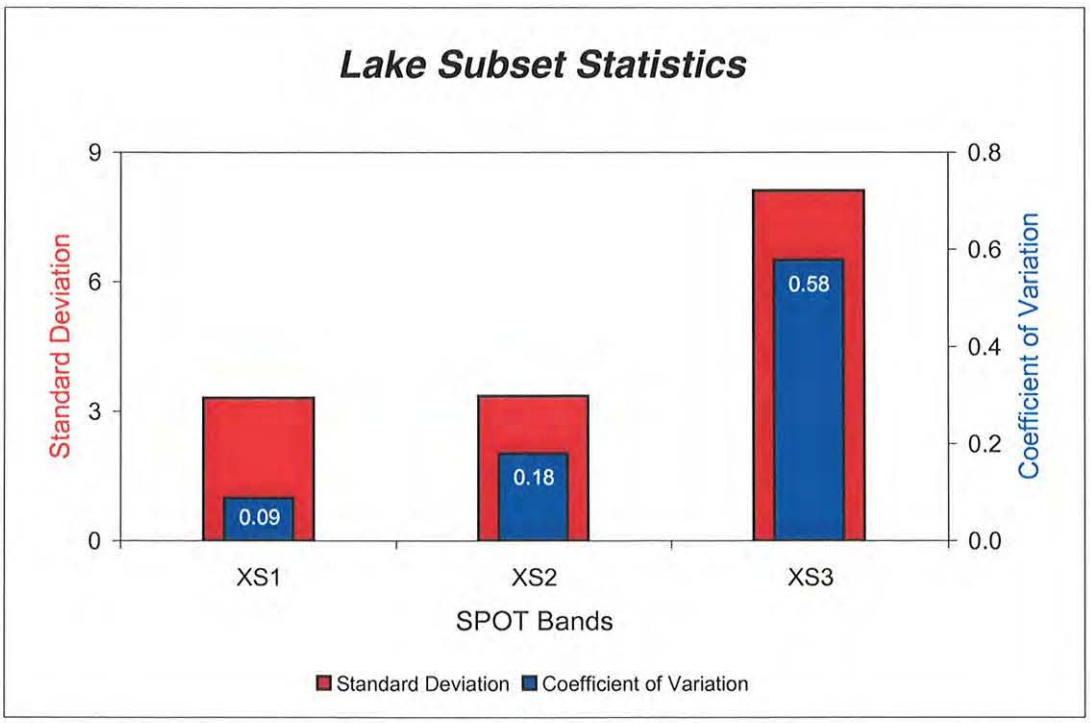

Figure 3-12 The variation among all water pixels is quite low relative to typical terrestrial targets. While this hinders statistical modeling, the near-infrared band (XS3) shows the highest level of variation.

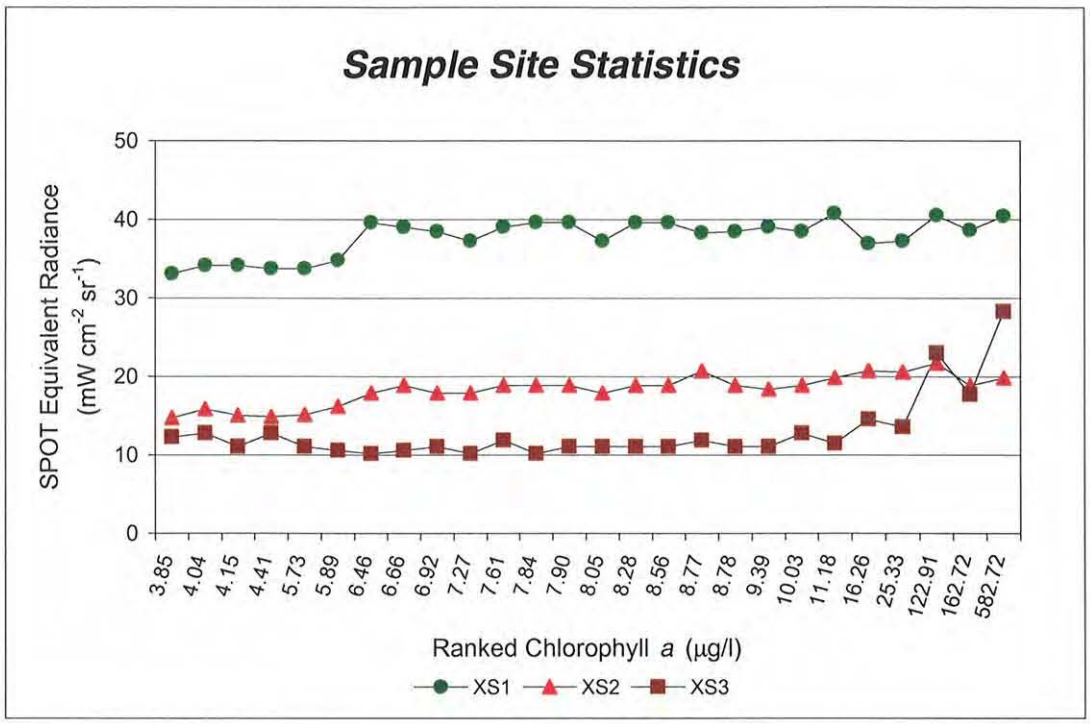

Figure 3-13 The nearly uniform nature of the extracted radiance values suggests the HRV sensor is limited in its ability to detect differences in radiant flux emerging from the water.

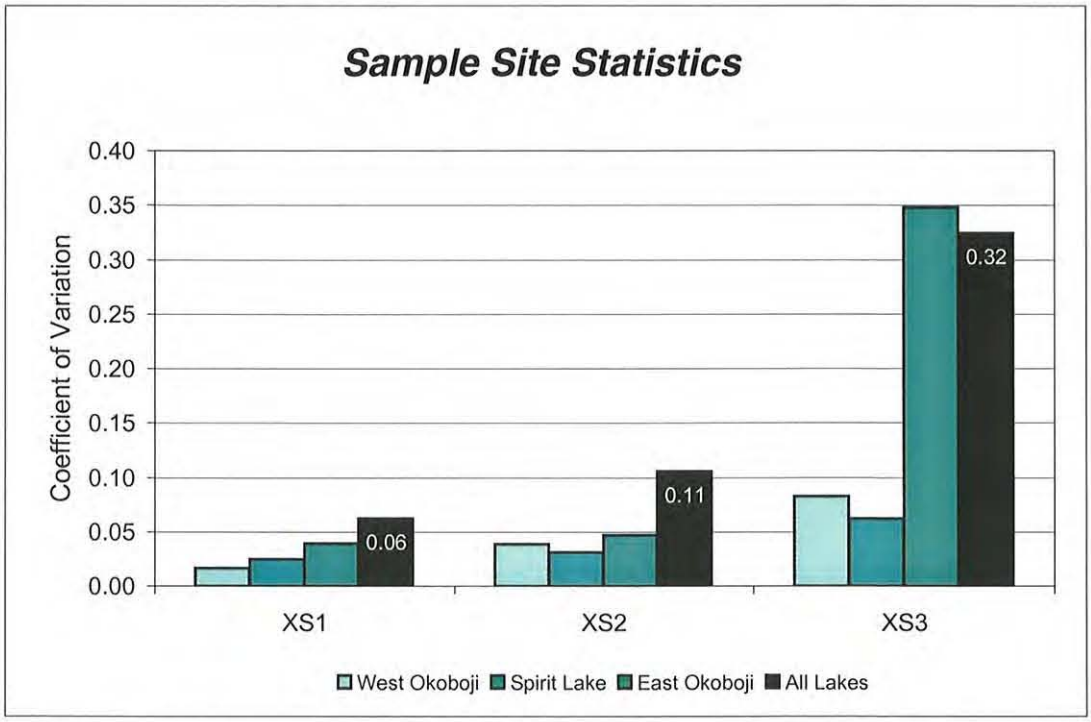

Figure 3-14 The sample site data extracted from the lake subset image adequately represent the optical conditions of the lakes as a whole. In addition, XS3 (near-infrared) possesses more "contrast" than the other SPOT bands.

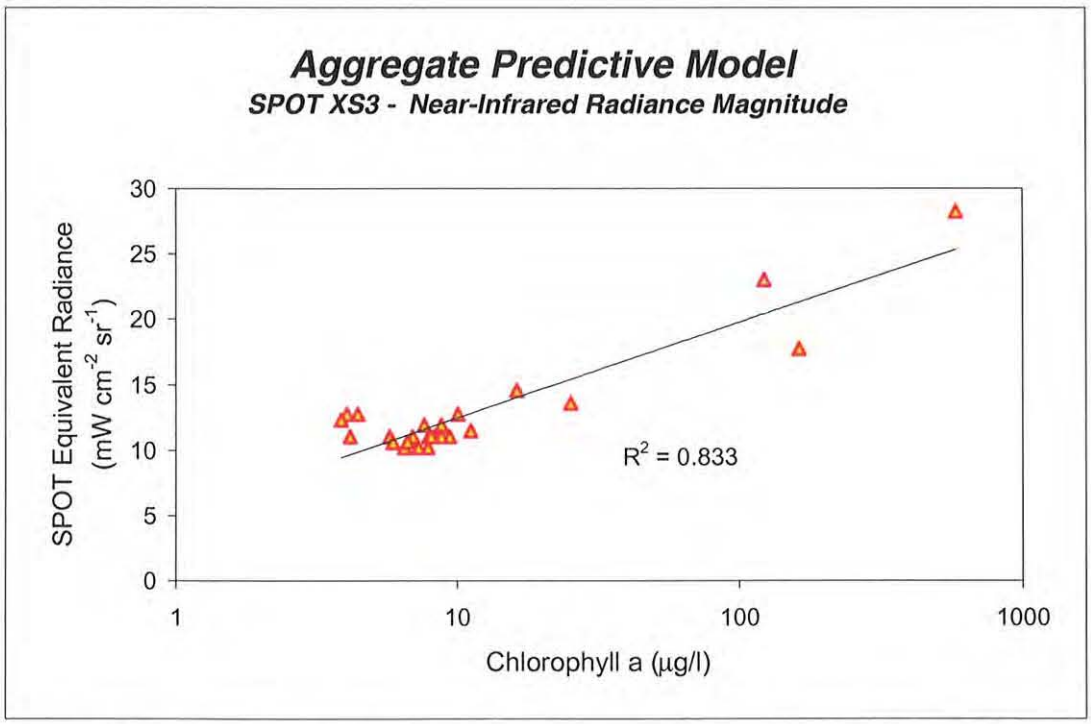

Figure 3-15 The relationship between the SPOT radiance data extracted from the sampled pixels and the ground truth chl *a* data produced the highest r^2 and was used to create maps of chl *a*.

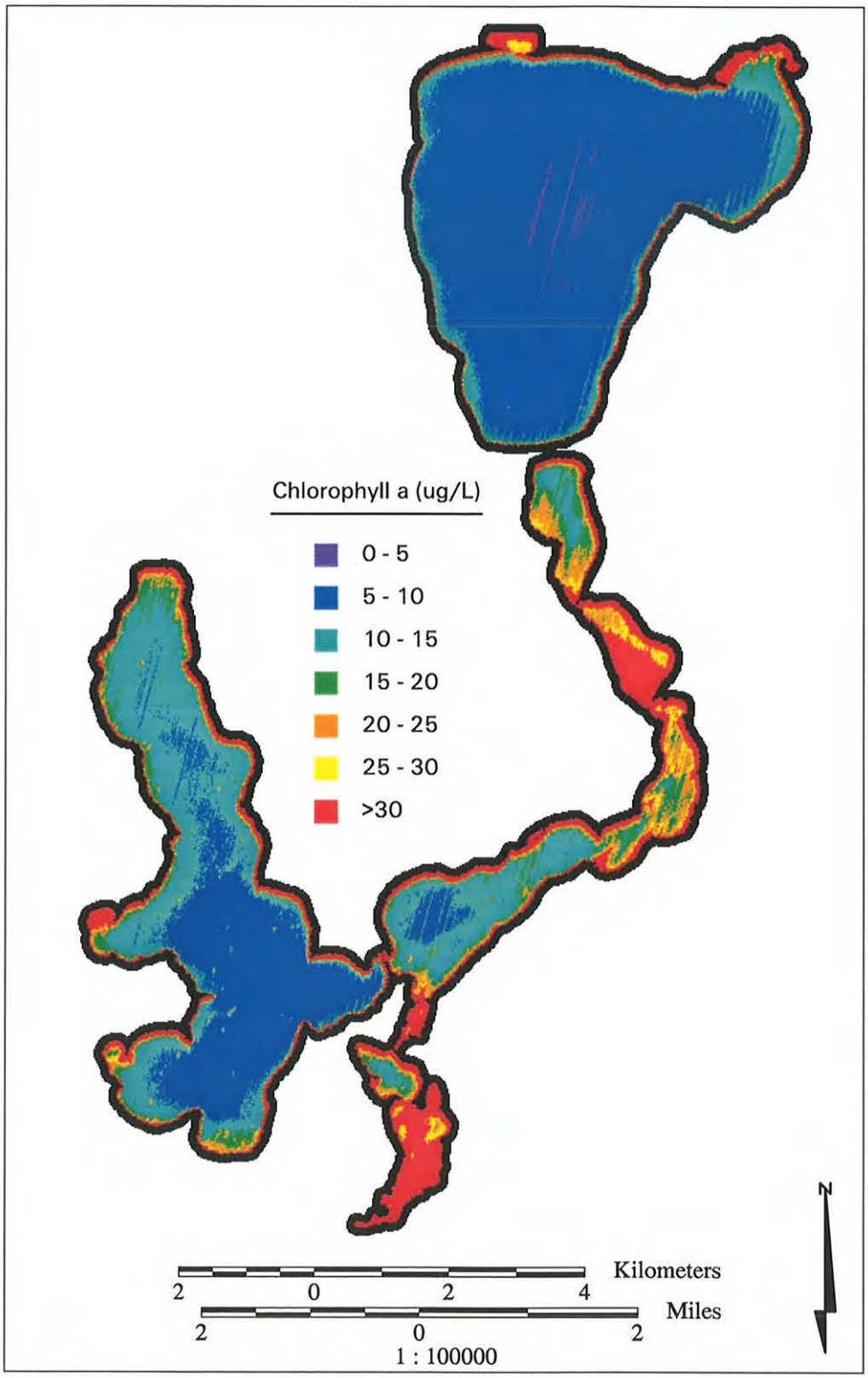

Figure 3-16. This quantified chlorophyll map is scaled to accentuate the lower chlorophyll a levels.

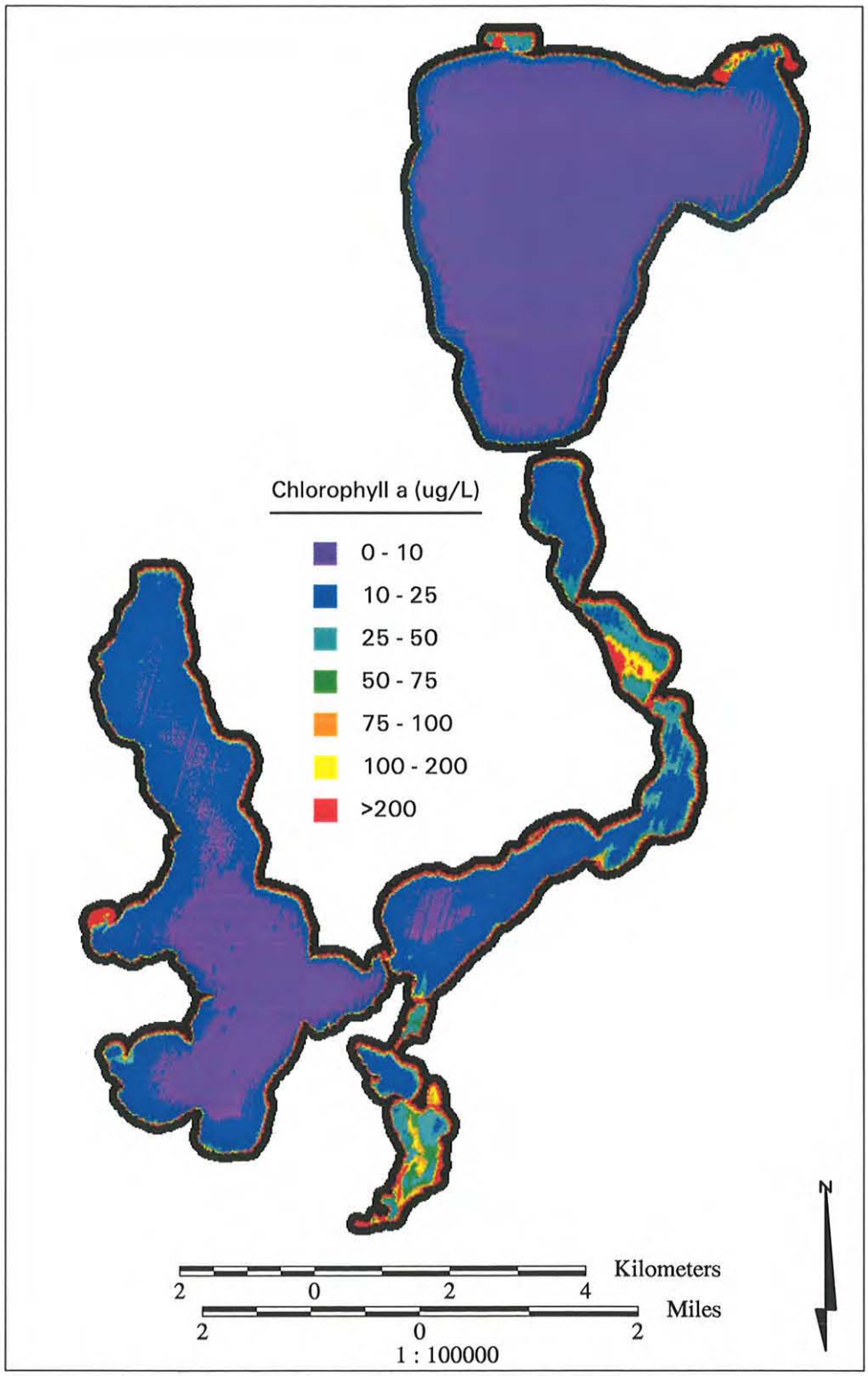

Figure 3-17. This quantified chlorophyll map is scaled to accentuate the higher chlorophyll a levels.

Figure 3-18. This aerial photograph gives a detailed view of the channel connecting the southern end of East Okoboji and Upper Gar lakes. Emergent blue-green alga blooms are common at this bottleneck and in the cove at the upper left of the this image.

Figure 3-19.

These aerial photographs of Lower Gar Lake show fine scale biomass patterns. The similarity of the patterns seen here and in Figure 3-17, suggests SPOT's 20 m spatial resolution is sufficient for mapping dense concentrations of chl *a*.

TABLES

	Drainage Basin	West Okoboji Watershed	East Okoboji Watershed	Spirit Lake Watershed	Lower Gar Watershed
Total Area (ha)	36218	7698	5903	9962	4720
Land Area (ha)	29380	5808	5062	6935	4195
Area of Lakes Ponds and Marshes (ha)	6839	1890	841	3009	526
Ratio of Land Area to Total Area	0.811	0.755	0.858	0.696	0.889

Table 1-1. Iowa Great Lakes watershed characteristics (adapted from Bachmann and Jones, 1974)

	West Okoboji	Spirit Lake	East Okoboji	Lower Gar Lake
Total Phosphorus (mg L^{-1})	0.033	0.041	0.165	0.222
Nitrate Nitrogen (mg L^{-1})	0.009	0.017	0.085	0.145
Ammonium Nitrogen (mg L^{-1})	0.11	0.239	0.468	0.644
COD (mg L^{-1})	20.5	24.9	46.5	56.5
Chlorophyll *a* (mg m^{-3})	4.28	27.5	122.2	226.8
Secchi Disk Depth (m)	3.2	1.7	0.9	0.4

Table 1-2. Chemical composition of Lake West Okoboji, Spirit Lake, Lake East Okoboji (which includes Upper Gar Lake and Lake Minnewashta), and Lower Gar Lake These measurements are mean summer values for the years of 1971-1973 (adapted from Bachmann and Jones, p.2, 1974).

	West Okoboji	Spirit Lake	East Okoboji	Lower Gar Lake
Watershed Area (ha)	7698	9962	5903	4720
Lake Area (ha)	1540	2168	764	98
Lake Volume (1 x 10^6 m^3)	184.0	111.9	21.2	1.1
Maximum Depth (m)	41.5	7.3	6.7	2.0
Mean Depth (m)	11.9	5.2	2.8	1.1
Ratio of Watershed Area to Lake Volume (m^2 m^{-3})	0.33	0.69	2.42	42.0
Turnover Time (years)	20	5.5	1.2	0.3

Table 1-3. Morphological comparison of Lake West Okoboji, Spirit Lake, Lake East Okoboji (which includes Upper Gar Lake and Lake Minnewashta), and Lower Gar Lake (adapted from Jones and Bachmann, 1974)

West Okoboji	Chlorophyll *a* ($\mu g\ L^{-1}$)	Turbidity (NTU)	Depth (m)	Attenuation Coefficient (at 1 m)
49.2	3.85	1.63	18.7	0.250
49.1	4.04	2.79	11.7	0.567
49.4	4.15	1.78	7.7	0.564
49.3	4.41	1.69	8.6	0.318
49	5.73	1.17	38.7	0.559
50	5.89	1.86	7.9	0.622
$\bar{x}$	4.7	1.8	15.6	0.5
SD	0.9	0.5	12.1	0.2

East Okoboji	Chlorophyll *a* ($\mu g\ L^{-1}$)	Turbidity (NTU)	Depth (m)	Attenuation Coefficient (at 1 m)
57	8.77	8.86	5.4	1.18
56	16.26	28.70	1.9	2.29
55	25.33	9.57	1.9	2.05
55.1	122.91	52.40	1.8	3.06
56.1	162.72	18.00	3.5	2.29
Narrows	582.72	50.90	1.5	10.04
$\bar{x}$	153.1	28.1	2.7	3.5
SD	219.8	19.6	1.5	3.3

Spirit Lake	Chlorophyll *a* ($\mu g\ L^{-1}$)	Turbidity (NTU)	Depth (m)	Attenuation Coefficient (at 1 m)
SL-8	6.46	3.65	6.2	-
54	6.66	3.15	6.4	-
54.3	6.92	2.73	6.1	-
54.2	7.27	4.20	6.1	-
SL-6	7.61	5.55	5.0	-
SL-3	7.84	5.76	5.2	-
SL-4	7.90	5.44	6.2	-
54.4	8.05	5.31	5.8	-
SL-2	8.28	4.31	4.9	-
SL-9	8.56	5.00	5.9	-
54.1	8.78	5.20	6.1	-
SL-5	9.39	4.68	5.2	-
SL-1	10.03	5.68	4.6	-
SL-7	11.18	4.85	5.5	-
$\bar{x}$	8.2	4.7	5.6	-
SD	1.3	1.0	0.6	-

Table 1-4. These parameters for West Okoboji, East Okoboji and Spirit lakes were acquired on August 13, 1997.

Chlorophyll *a* ($\mu g\ L^{-1}$)	12:10	12:34	15:50	16:50	18:00	$\bar{x}$	SD
5	---	---	5.12	5.07	5.16	5.12	0.045
25	25.30	25.30	25.10	25.40	25.10	25.24	0.130
75	---	74.30	73.90	74.30	73.90	74.10	0.191
100	---	99.80	99.00	100.00	100.00	99.70	0.472

Table 1-5. Change in chlorophyll *a* concentration in standard solutions over time

Sample Site	Chl a ($\mu g\ L^{-1}$)	SD
49.2	3.85	0.15
49.1	4.04	0.16
49.4	4.15	0.29
49.3	4.41	0.00
Miller's Bay	5.17	0.03
49	5.73	0.13
50	5.89	0.14
SL-8	6.46	0.33
54	6.66	0.29
54.3	6.92	0.19
54.2	7.27	0.33
SL-6	7.61	0.42
SL-3	7.84	0.54
SL-4	7.90	0.24
54.4	8.05	0.55
SL-2	8.28	1.22
SL-9	8.56	0.25
57	8.77	0.36
54.1	8.78	0.35
SL-5	9.39	1.15
SL-1	10.03	1.02
SL-7	11.18	0.50
56	16.26	0.57
55	25.33	1.73
55.1	122.91	11.73
56.1	162.72	21.50
Grade	304.00	49.78
Narrows	582.72	34.02

Table 1-6. Estimation of variability in chlorophyll *a* data

Reflectance Magnitude	West Okoboji (r^2)	East Okoboji (r^2)	Lakes Combined (r^2)
Green Peak vs Chl a	0.381	0.751	0.576
Green Peak vs ln Chl a	0.373	0.789	0.880
630 nm vs Chl a	0.457	0.524	0.047
630 nm vs ln Chl a	0.445	0.634	0.301
675 nm vs Chl a	0.500	0.192	0.081
675 nm vs ln Chl a	0.486	0.232	0.358
NIR Peak vs Chl a	0.508	0.983	0.938
NIR Peak vs ln Chl a	0.494	0.813	0.868

Peak Shift	West Okoboji (r^2)	East Okoboji (r^2)	Lakes Combined (r^2)
Green Shift vs Chl a	0.500	0.428	0.373
Green Shift vs ln Chl a	0.500	0.716	0.786
NIR Shift vs Chl a	0.000	0.731	0.717
NIR Shift vs ln Chl a	0.000	0.997	0.992

Artificial Baseline	West Okoboji (r^2)	East Okoboji (r^2)	Lakes Combined (r^2)
Sum vs Chl a	0.001	0.998	0.998
Sum vs ln Chl a	0.002	0.718	0.669
Height vs Chl a	0.106	0.994	0.987
Height vs ln Chl a	0.106	0.814	0.802

Band Ratio	West Okoboji (r^2)	East Okoboji (r^2)	Lakes Combined (r^2)
Green/Red vs Chl a	0.677	0.873	0.370
Green/Red vs ln Chl a	0.662	0.863	0.104
NIR/Green vs Chl a	0.638	0.980	0.915
NIR/Green vs ln Chl a	0.622	0.830	0.883
NIR/Red vs Chl a	0.750	0.997	0.997
NIR/Red vs ln Chl a	0.732	0.787	0.749
NDVI vs Chl a	0.753	0.824	0.829
NDVI vs ln Chl a	0.735	0.978	0.959

Table 2-1. Close-range Hyperspectral Reflectance Algorithm Performance

Indicates the highest overall r^2 for trophic group

Indicates the highest r^2 for trophic group and algorithm set

Radiance Magnitude	West Okoboji (r^2)	East Okoboji (r^2)	Spirit Lake (r^2)	Lakes Combined (r^2)
Green vs Chl a	0.291	0.493	0.105	0.090
Green vs ln Chl a	0.298	0.603	0.086	0.234
Red vs Chl a	0.218	0.145	0.429	0.075
Red vs ln Chl a	0.210	0.154	0.414	0.337
NIR vs Chl a	0.535	0.792	0.363	0.797
NIR vs ln Chl a	0.525	0.854	0.369	0.833

Band Ratio	West Okoboji (r^2)	East Okoboji (r^2)	Spirit Lake (r^2)	Lakes Combined (r^2)
Green/Red vs Chl a	0.120	0.572	0.311	0.029
Green/Red vs ln Chl a	0.110	0.681	0.334	0.243
NIR/Green vs Chl a	0.563	0.801	0.198	0.733
NIR/Green vs ln Chl a	0.555	0.864	0.213	0.710
NIR/Red vs Chl a	0.587	0.868	0.096	0.734
NIR/Red vs ln Chl a	0.574	0.919	0.103	0.573
NDVI vs Chl a	0.598	0.787	0.093	0.609
NDVI vs ln Chl a	0.585	0.946	0.101	0.498

Table 3-1. SPOT Equivalent Radiance Magnitude and Ratio Algorithm Performance

Indicates the highest overall r^2 for trophic group

Indicates the highest r^2 for trophic group and algorithm set

APPENDIX 1

Contents of :SPOT_Header (filename: imag_01.img)

```
struct SpotHeader {
   char scnname[15] = "SPN04326W09507"
   double scncenlat = 43.436111
   double scncenlon = -95.117222
   double scncor1lat = 43.751111
   double scncor1lon = -95.405278
   double scncor2lat = 43.645
   double scncor2lon = -94.657222
   double scncor3lat = 43.225833
   double scncor3lon = -95.578611
   double scncor4lat = 43.120556
   double scncor4lon = -94.836944
   long scncenline = 1500
   long scncenpixel = 1500
   long scncor1line = 1
   long scncor1pixel = 1
   long scncor2line = 1
   long scncor2pixel = 3000
   long scncor3line = 3000
   long scncor3pixel = 1
   long scncor4line = 3000
   long scncor4pixel = 3000
   double scnorientangle = 11
   double angleofinc = 9.7
   double sunazimuth = 147.5
   double sunelevation = 58.2
   char scncentime[17] = "17:17 08/13/1997"
   char sensorid[4] = "HRV1"
   char specmode[3] = "XS"
   long revolutionnum = 302
   char playback[2] = "DT"
   char preprocesslevel[9] = "1A"
   enum correction = EMSC_TRUE
   long deconvolution = 0
   char resampling = " "
   long ulxmap = 0
   long ulymap = 0
   long lrxmap = 0
   long lrymap = 0
   long xpixelsize = 0
   long ypixelsize = 0
   double mapxpixelsize = 64336
   double mapypixelsize = 59978
   char mapprojid[32] = "                    "
```

2274, 2316, 2357, 2399, 2440, 2482, 2523, 2565, 2607, 2648, 2690,
2731, 2773, 2814, 2856, 2897, 2939, 2981, 0
long yawspeed[73] = 40, -180, -160, -80, 60, 100, 40, -280, -240,
0, 60, 160, 120, -60, 40, 120, 180, 20, -180, -80, 0, 120, 100,
-40, -60, -160, 60, 120, 100, 0, 40, 200, 180, 40, -260, -260,
-100, -20, 60, -20, -160, -220, -100, -20, -20, -100, -160, 0,
200, 80, 100, 20, 60, -20, 140, -40, -120, -40, 60, 100, 180, 20,
-100, -20, -20, 120, 100, 40, -100, 0, 140, 40, 0
long avgrollspeed[73] = -20, 0, 80, 100, 140, -80, -20, -100, 60,
120, 60, -140, 0, -120, -20, 0, -60, -100, 0, 100, 120, 0, -80,
-40, 180, 80, 140, 0, -80, -180, -20, 20, -60, -20, -20, -20, 20,
40, 60, 40, 80, 140, 20, 40, 40, 20, 80, 120, 20, -160, -80, -100,
60, 40, 80, -40, -60, -40, 60, -80, -60, -100, 20, 40, 40, 0, -80,
-20, 20, 120, 80, -20, 0
long avgpitchspeed[73] = 140, 120, 0, 40, -260, -240, 60, -140, 60,
-20, -480, -20, -100, -120, -120, -260, -200, 160, -60, -140, -280,
-420, 100, 120, -160, -80, -80, 80, 100, 100, -280, -160, 220, 300,
0, 0, 60, 80, 280, 80, 100, -220, -20, 340, -80, -100, -500, -540,
-160, 40, -160, -340, -320, -340, 300, -60, -340, -320, -220, 100,
120, -100, -100, -80, 80, 340, 280, -120, -100, -20, 220, 560, 0
double lookangles[4] = -0.50027778, -0.50555556, -6.4833333, -10.604167
double polynomial1[4] = -0.45739424, 0.9996731, -2.0087265e-08,
3.2763686e-12
double polynomial2[4] = -0.037985648, 1.0382252, -4.8410737e-06,
6.5583868e-11
double polynomial3[4] = 0.45362108, 1.000327, 1.9870218e-08,
-3.3095453e-12
double polynomial4[4] = 0.03712556, 0.96317533, 4.2829457e-06,
-2.4099975e-11
double polynomial5[4] = 144.46397, -0.04812894, -1.8256511e-07,
1.5751293e-13
char level2quality[17] = " "
char dateofdarkcal[17] = "19960601 "
long ephemerislength = 3960
long ephemerisnumber = 1
long numberofgcps = 0
char GRSdesignator[17] = " "
char referencesensorid[17] = " "
char referencespecmode[17] = " "
char referenceprocesslevel[17] = " "
long numberlostlines = 0
long numberlostdetectors = 0
char sceneidentification[17] = "S2H1970813171705"
double GRSlatdelta = -0.23805556
double GRSlondelta = -0.11916667
long gainnumber = 6

```
double xpixelsized = 0
double ypixelsized = 0
double urxmap = 0
double urymap = 0
double llxmap = 0
double llymap = 0
char *datum[0] = ""
struct SpotCanHeader {
   double nom_interpixel_dist = 0
   double nom_interline_dist = 0
   double image_skew = 0
   double orbital_inclination = 0
   double sat_ascending_node = 0
   double satellite_altitude = 0
   double sat_ground_speed = 0
   double satellite_heading = 0
   double satellite_latitude = 0
   double satellite_longitude = 0
   double acrosstrackFOV = 0
   double semi_major_axis = 0
   double bandgain[16] = 0, 0, 0, 0, 0, 0, 0, 0, 0, 0, 0, 0, 0, 0, 0, 0
   enum LGSOWG = EMSC_FALSE
} canheader
struct GeoSpotHeader {
   enum geospotformat = EMSC_FALSE
   char *geospotversion[0] = ""
   long bandrowbytes = 0
   char byteorder = ""
   long numbits = 0
   char *correction_level[0] = ""
   double deltax_origin = 0
   double deltay_origin = 0
   char *contact_info[0] = ""
   char *easting_size_units[0] = ""
   char *northing_size_units[0] = ""
   double grid_declination = 0
   char *job_id[0] = ""
   char *location[0] = ""
   double magnetic_declination = 0
   double mag_decl_annual_chg = 0
   char *mag_decl_date[0] = ""
   char *map_name[0] = ""
   char *map_number[0] = ""
   char *meridian_name[0] = ""
   double meridian_origin = 0
   double origin_x_coord = 0
```

```
    double origin_y_coord = 0
    char *production_date[0] = ""
    char *product_id[0] = ""
    char *proj_code[0] = ""
    char *proj_id[0] = ""
    double proj_lat_true_scale = 0
    double proj_meridian = 0
    double proj_parallel = 0
    double proj_scale_factor = 0
    double proj_std_parallel_I = 0
    double proj_std_parallel_II = 0
    long proj_zone = 0
    double raster_x_origin = 0
    double raster_x_size = 0
    double raster_y_origin = 0
    double raster_y_size = 0
    double sheet_rect_elevation = 0
    char *sheet_rect_type[0] = ""
    double spheroid_flat = 0
    double spheroid_maj_axis = 0
    double spheroid_min_axis = 0
    char *spheroid_name[0] = ""
  } geospotheader
} SpotHeader
```

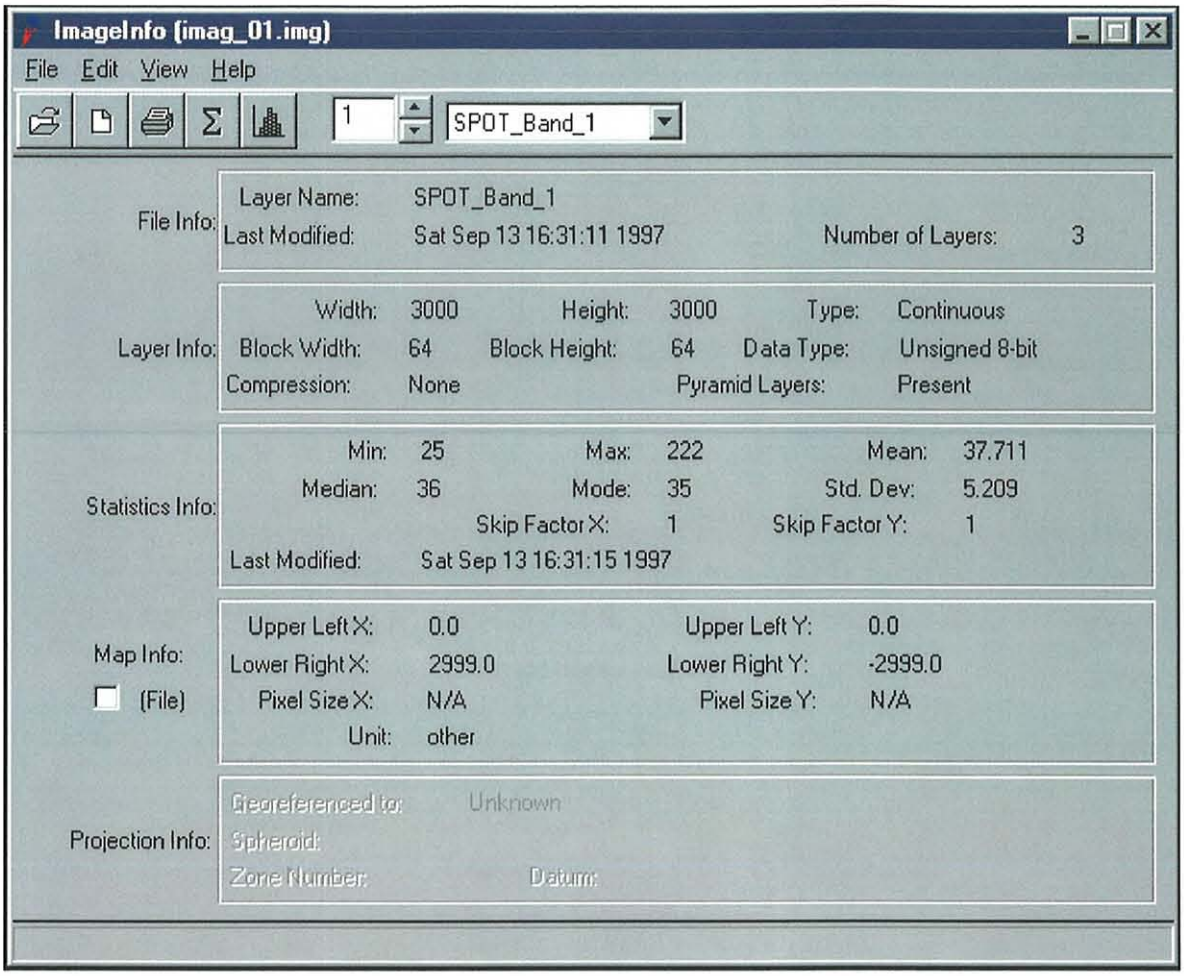
ImageInfo (imag_01.img)
File Edit View Help
1
SPOT_Band_1
File Info:
Layer Name: SPOT_Band_1
Last Modified: Sat Sep 13 16:31:11 1997
Number of Layers: 3
Layer Info:
Width: 3000
Height: 3000
Type: Continuous
Block Width: 64
Block Height: 64
Data Type: Unsigned 8-bit
Compression: None
Pyramid Layers: Present
Statistics Info:
Min: 25
Max: 222
Mean: 37.711
Median: 36
Mode: 35
Std. Dev: 5.209
Skip Factor X: 1
Skip Factor Y: 1
Last Modified: Sat Sep 13 16:31:15 1997
Map Info:
(File)
Upper Left X: 0.0
Upper Left Y: 0.0
Lower Right X: 2999.0
Lower Right Y: -2999.0
Pixel Size X: N/A
Pixel Size Y: N/A
Unit: other
Projection Info:
Georeferenced to: Unknown
Spheroid:
Zone Number:
Datum:

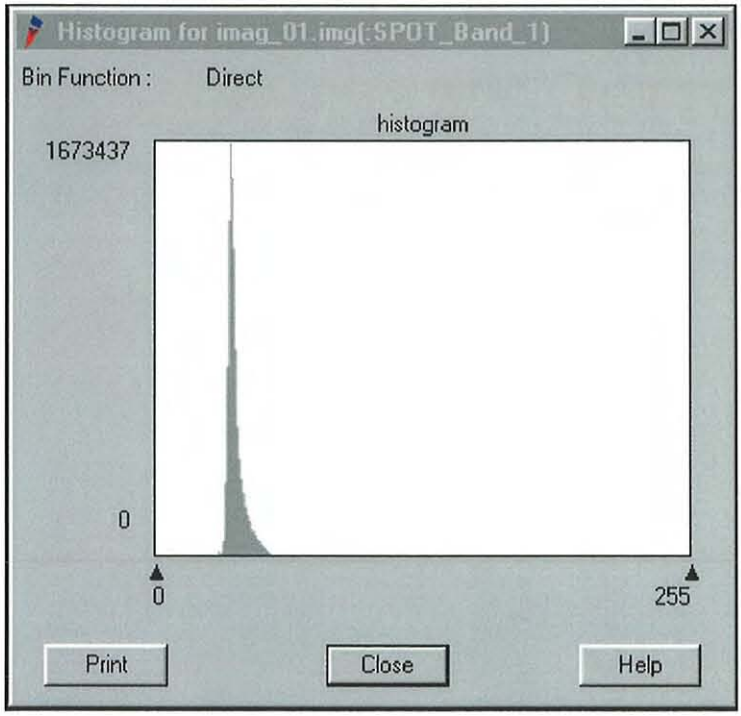
Histogram for imag_01.img(:SPOT_Band_1)
Bin Function : Direct
histogram
1673437
0
0
255
Print
Close
Help

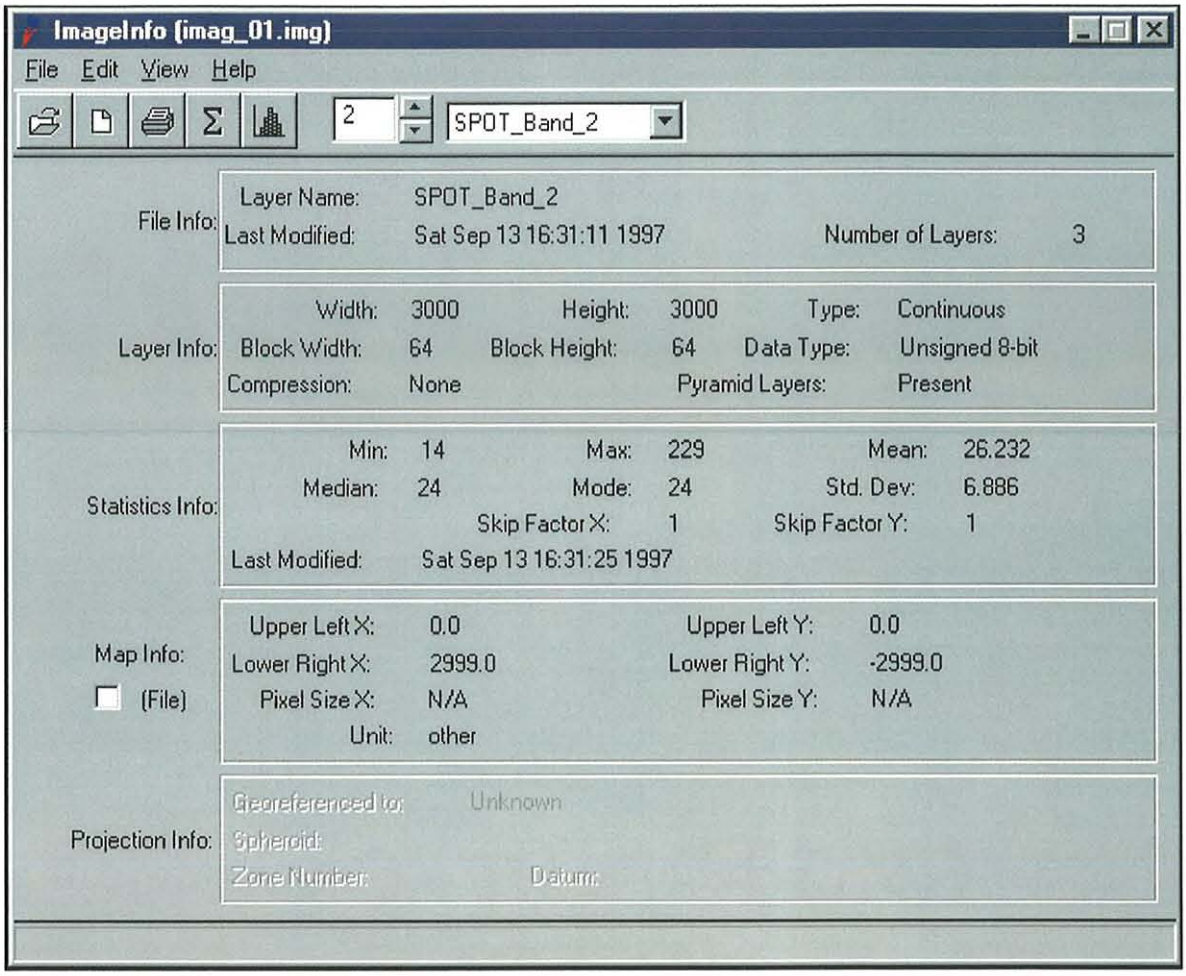
ImageInfo (imag_01.img)
File Edit View Help
2
SPOT_Band_2
File Info:
Layer Name: SPOT_Band_2
Last Modified: Sat Sep 13 16:31:11 1997
Number of Layers: 3
Layer Info:
Width: 3000
Height: 3000
Type: Continuous
Block Width: 64
Block Height: 64
Data Type: Unsigned 8-bit
Compression: None
Pyramid Layers: Present
Statistics Info:
Min: 14
Max: 229
Mean: 26.232
Median: 24
Mode: 24
Std. Dev: 6.886
Skip Factor X: 1
Skip Factor Y: 1
Last Modified: Sat Sep 13 16:31:25 1997
Map Info:
(File)
Upper Left X: 0.0
Upper Left Y: 0.0
Lower Right X: 2999.0
Lower Right Y: -2999.0
Pixel Size X: N/A
Pixel Size Y: N/A
Unit: other
Projection Info:
Georeferenced to: Unknown
Spheroid:
Zone Number:
Datum:

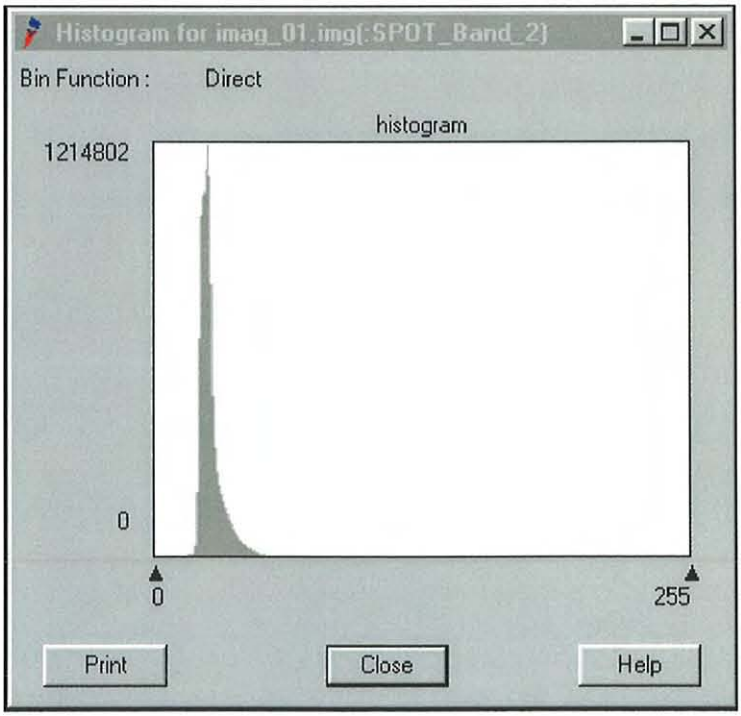
Histogram for imag_01.img(:SPOT_Band_2)
Bin Function : Direct
histogram
1214802
0
0
255
Print
Close
Help

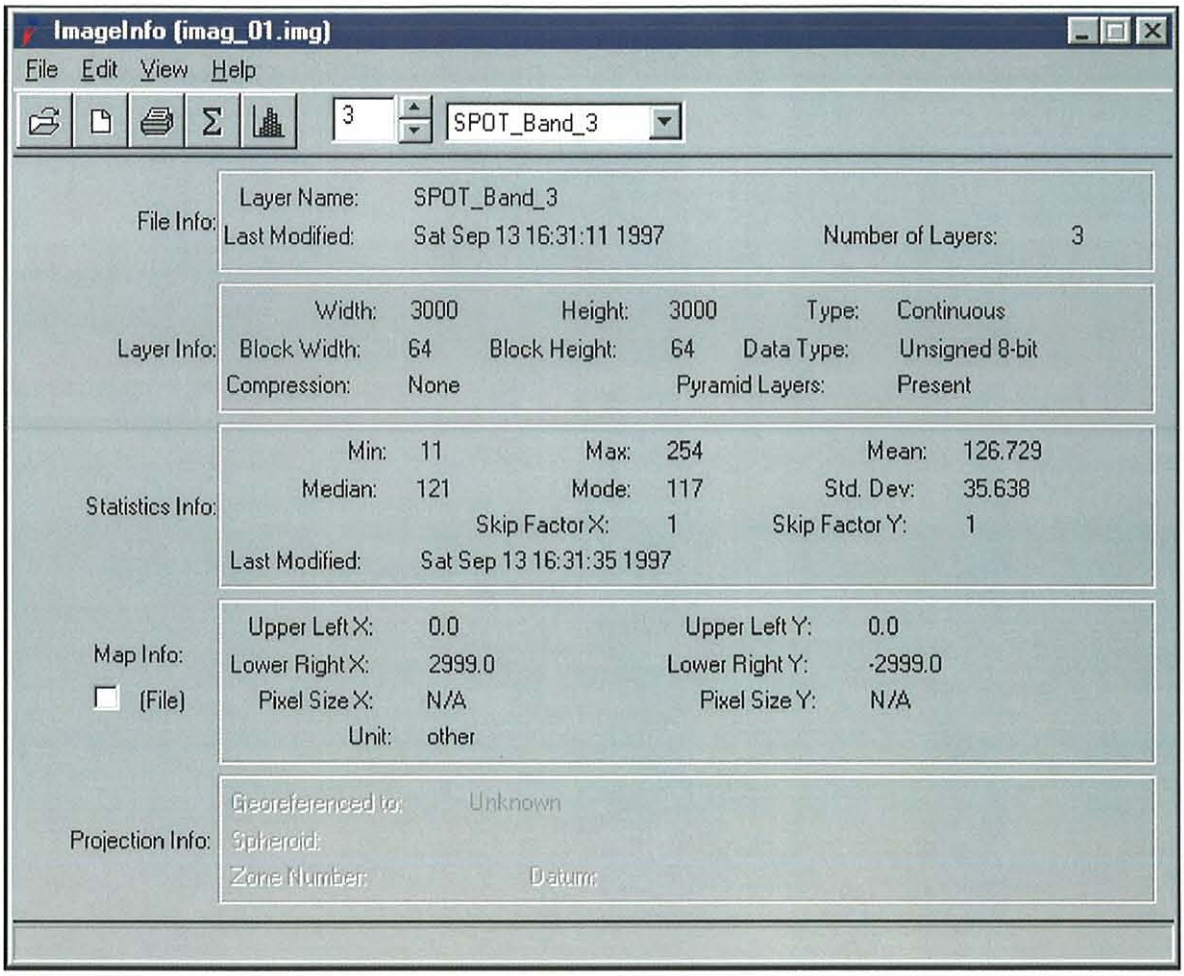
ImageInfo (imag_01.img)
File Edit View Help
3
SPOT_Band_3
File Info:
Layer Name: SPOT_Band_3
Last Modified: Sat Sep 13 16:31:11 1997
Number of Layers: 3
Layer Info:
Width: 3000
Height: 3000
Type: Continuous
Block Width: 64
Block Height: 64
Data Type: Unsigned 8-bit
Compression: None
Pyramid Layers: Present
Statistics Info:
Min: 11
Max: 254
Mean: 126.729
Median: 121
Mode: 117
Std. Dev: 35.638
Skip Factor X: 1
Skip Factor Y: 1
Last Modified: Sat Sep 13 16:31:35 1997
Map Info:
(File)
Upper Left X: 0.0
Upper Left Y: 0.0
Lower Right X: 2999.0
Lower Right Y: -2999.0
Pixel Size X: N/A
Pixel Size Y: N/A
Unit: other
Projection Info:
Georeferenced to: Unknown
Spheroid:
Zone Number:
Datum:

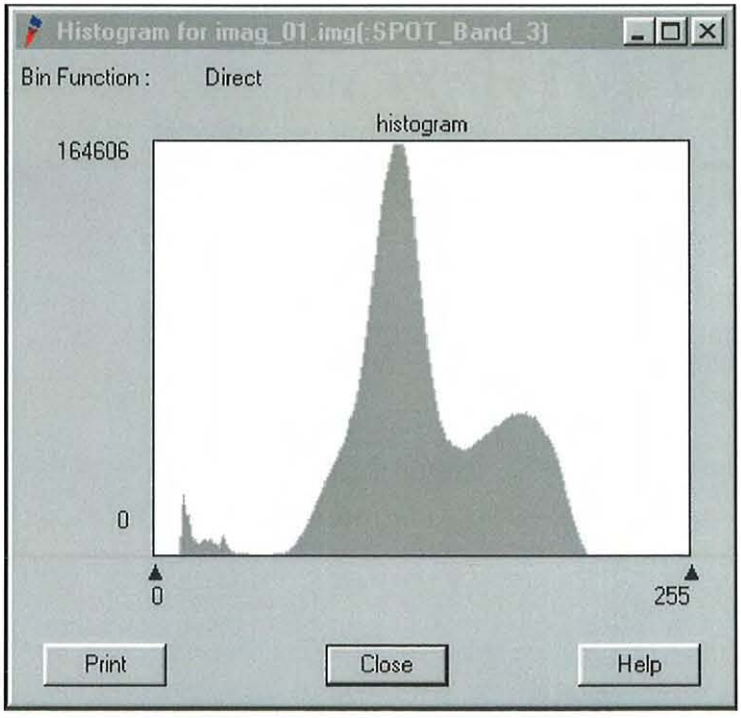
Histogram for imag_01.img(:SPOT_Band_3)
Bin Function : Direct
histogram
164606
0
0
255
Print
Close
Help

APPENDIX 2

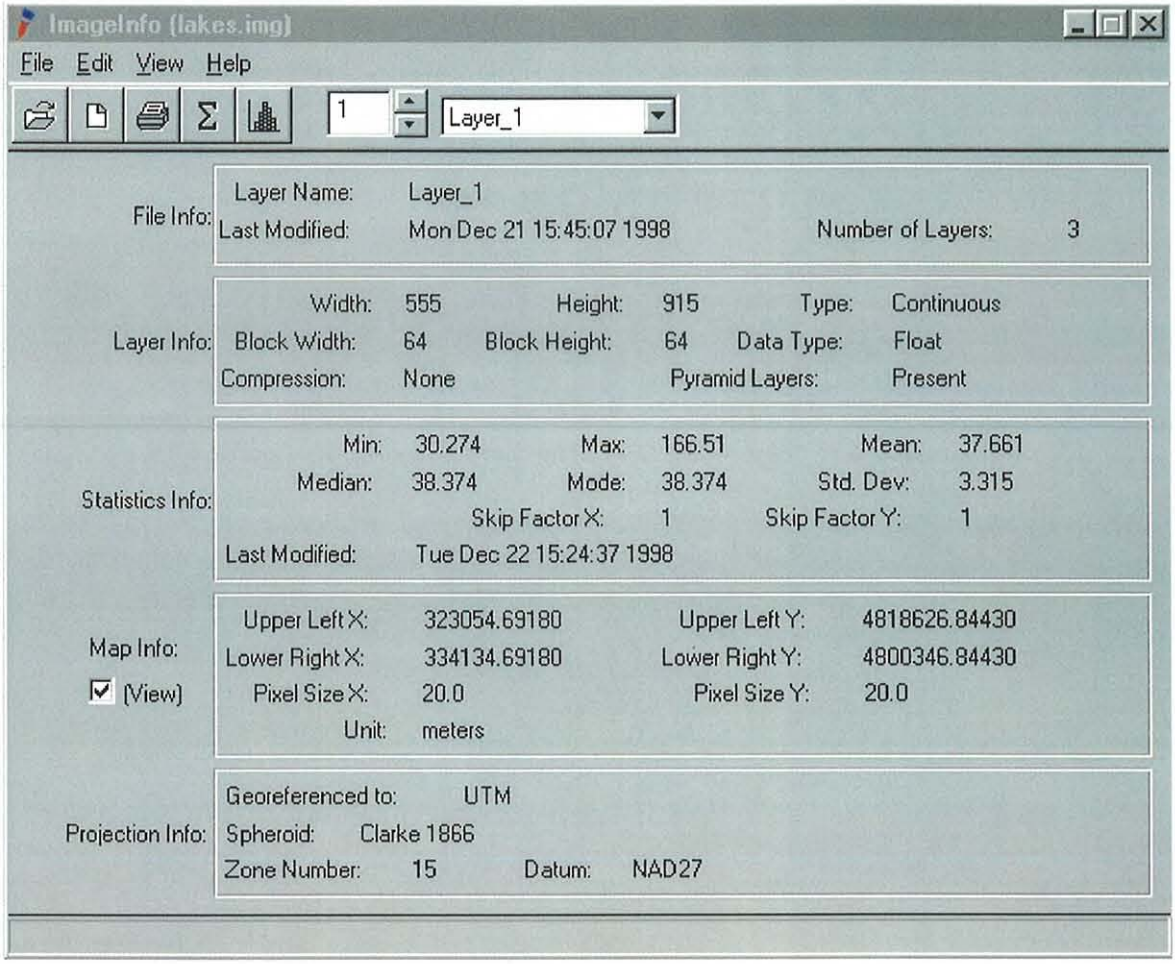
ImageInfo (lakes.img)
File Edit View Help
1
Layer_1
File Info:
Layer Name: Layer_1
Last Modified: Mon Dec 21 15:45:07 1998
Number of Layers: 3
Layer Info:
Width: 555
Height: 915
Type: Continuous
Block Width: 64
Block Height: 64
Data Type: Float
Compression: None
Pyramid Layers: Present
Statistics Info:
Min: 30.274
Max: 166.51
Mean: 37.661
Median: 38.374
Mode: 38.374
Std. Dev: 3.315
Skip Factor X: 1
Skip Factor Y: 1
Last Modified: Tue Dec 22 15:24:37 1998
Map Info:
(View)
Upper Left X: 323054.69180
Upper Left Y: 4818626.84430
Lower Right X: 334134.69180
Lower Right Y: 4800346.84430
Pixel Size X: 20.0
Pixel Size Y: 20.0
Unit: meters
Projection Info:
Georeferenced to: UTM
Spheroid: Clarke 1866
Zone Number: 15
Datum: NAD27

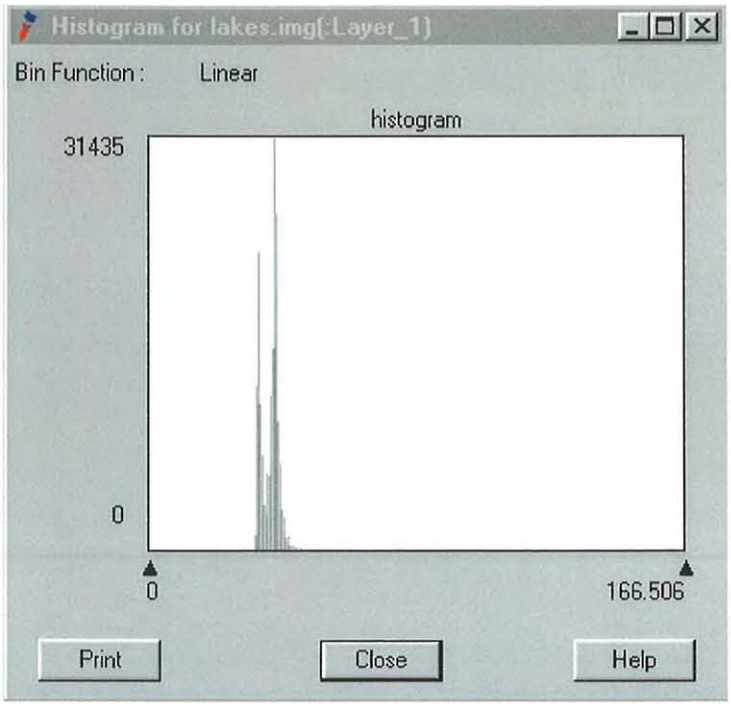
Histogram for lakes.img(:Layer_1)
Bin Function : Linear
histogram
31435
0
0
166.506
Print
Close
Help

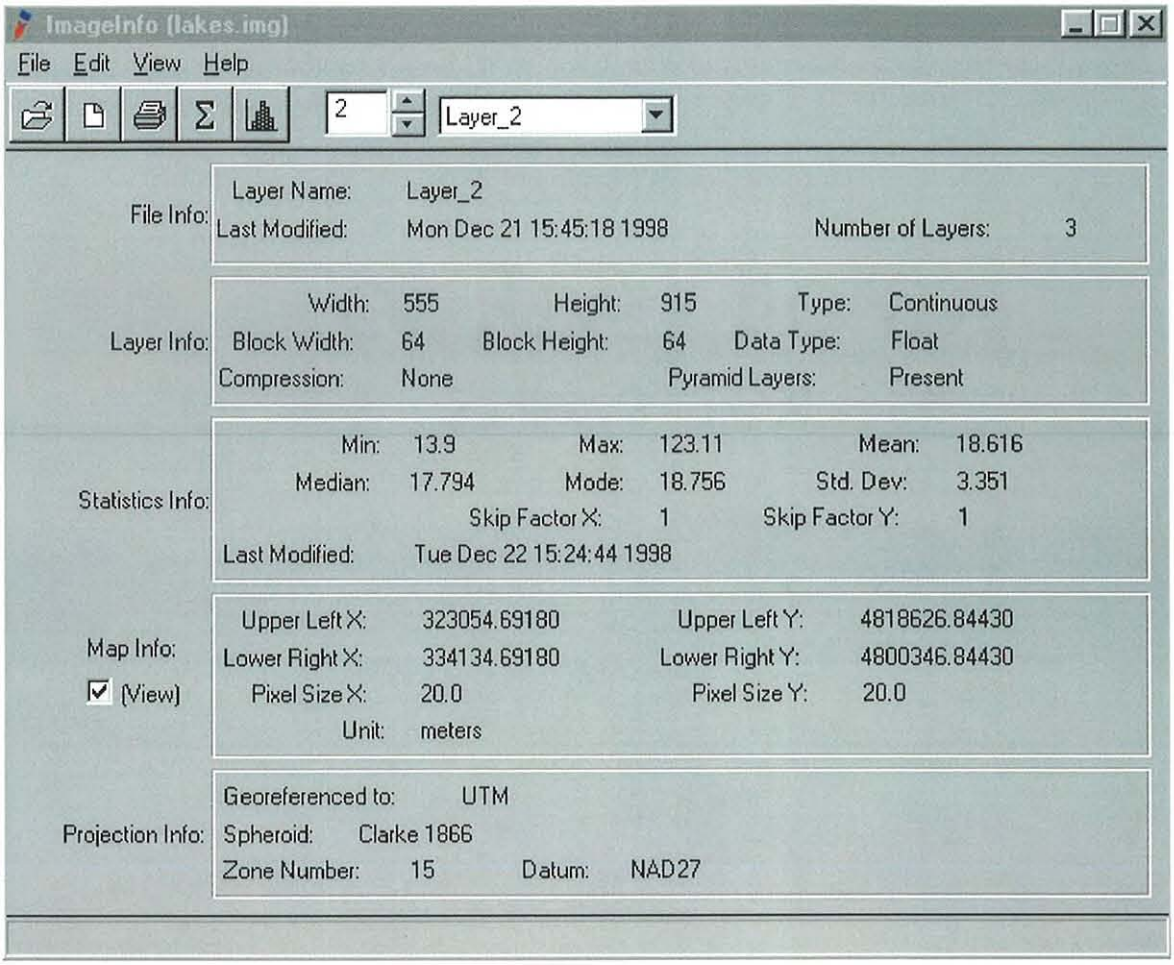
ImageInfo (lakes.img)
File Edit View Help
2
Layer_2
File Info:
Layer Name: Layer_2
Last Modified: Mon Dec 21 15:45:18 1998
Number of Layers: 3
Layer Info:
Width: 555
Height: 915
Type: Continuous
Block Width: 64
Block Height: 64
Data Type: Float
Compression: None
Pyramid Layers: Present
Statistics Info:
Min: 13.9
Max: 123.11
Mean: 18.616
Median: 17.794
Mode: 18.756
Std. Dev: 3.351
Skip Factor X: 1
Skip Factor Y: 1
Last Modified: Tue Dec 22 15:24:44 1998
Map Info:
(View)
Upper Left X: 323054.69180
Upper Left Y: 4818626.84430
Lower Right X: 334134.69180
Lower Right Y: 4800346.84430
Pixel Size X: 20.0
Pixel Size Y: 20.0
Unit: meters
Projection Info:
Georeferenced to: UTM
Spheroid: Clarke 1866
Zone Number: 15
Datum: NAD27

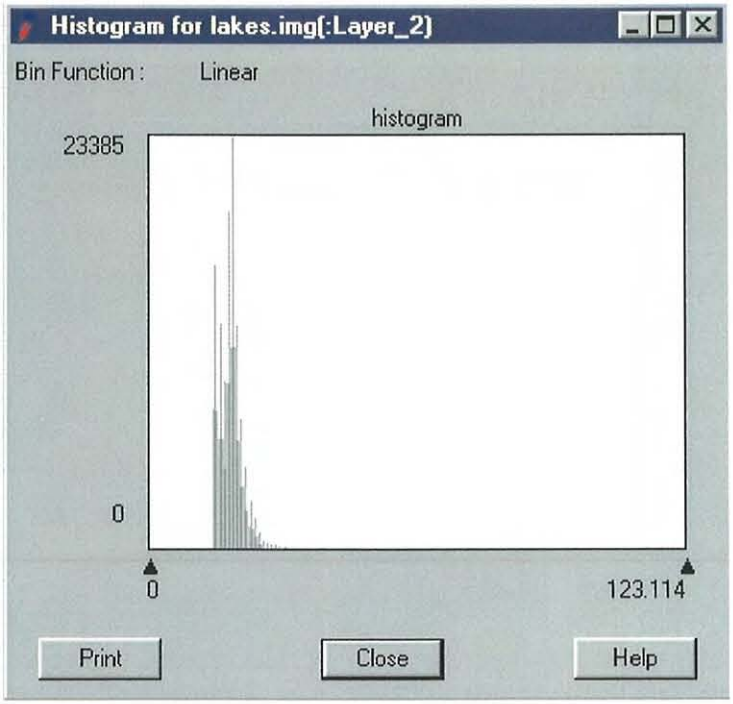
Histogram for lakes.img(:Layer_2)
Bin Function : Linear
histogram
23385
0
0
123.114
Print
Close
Help

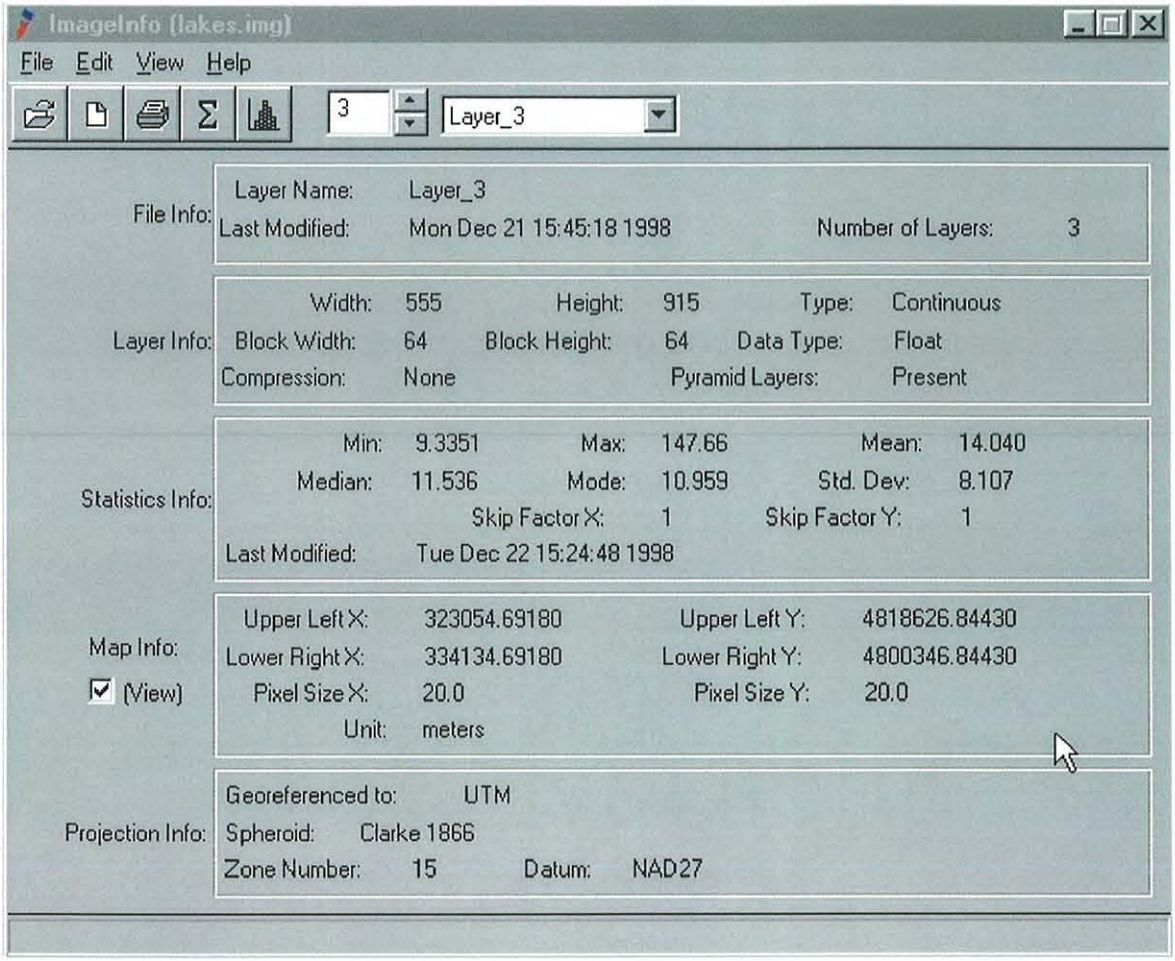
ImageInfo (lakes.img)
File Edit View Help
3
Layer_3
File Info:
Layer Name: Layer_3
Last Modified: Mon Dec 21 15:45:18 1998
Number of Layers: 3
Layer Info:
Width: 555
Height: 915
Type: Continuous
Block Width: 64
Block Height: 64
Data Type: Float
Compression: None
Pyramid Layers: Present
Statistics Info:
Min: 9.3351
Max: 147.66
Mean: 14.040
Median: 11.536
Mode: 10.959
Std. Dev: 8.107
Skip Factor X: 1
Skip Factor Y: 1
Last Modified: Tue Dec 22 15:24:48 1998
Map Info:
(View)
Upper Left X: 323054.69180
Upper Left Y: 4818626.84430
Lower Right X: 334134.69180
Lower Right Y: 4800346.84430
Pixel Size X: 20.0
Pixel Size Y: 20.0
Unit: meters
Projection Info:
Georeferenced to: UTM
Spheroid: Clarke 1866
Zone Number: 15
Datum: NAD27

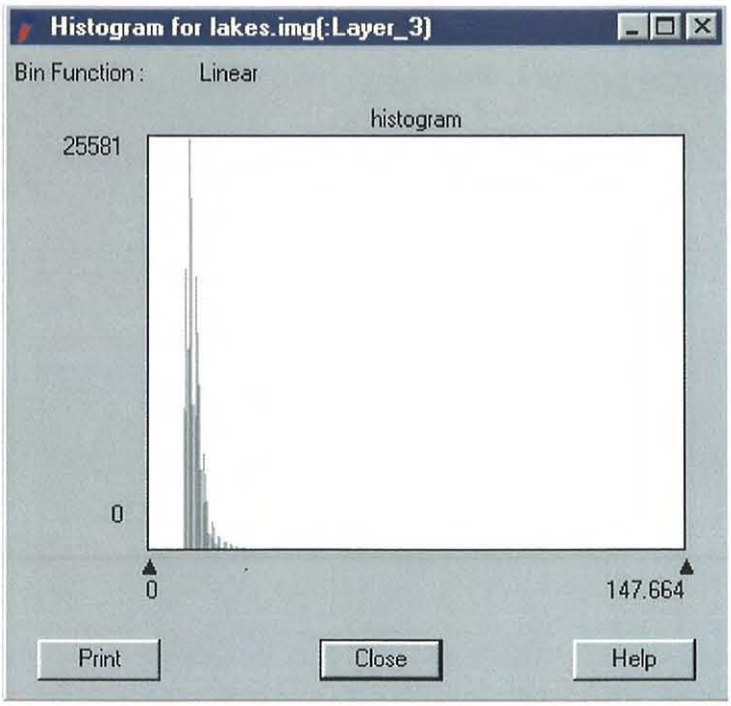
Histogram for lakes.img(:Layer_3)
Bin Function : Linear
histogram
25581
0
0
147.664
Print
Close
Help

LITERATURE CITED

Arar, E.J., and G.B. Collins, 1992. Method 445.0 In vitro Determination of Chlorophyll *a* and Pheophytin *a* in Marine and Freshwater Phytoplankton by Fluorescence, version 1.1, in U.S. EPA Methods for the Determination of Chemical Substances in Marine and Estuarine Environmental Samples. EPA /600/R-92/121.

Bachmann, R.W., 1990. Climatic Influences on Annual Variations in Water Transparency in Lake West Okoboji, *Proceedings from the Iowa Academy of Sciences*, 87(4):142-145.

Bachmann, R.W., and J.R. Jones, 1974. Water Quality in the Iowa Great Lakes: A Report to the Iowa Great Lakes Water Quality Control Plan, Iowa State University, Ames, Iowa 573pp.

Bachmann, R.W., and J.R. Jones, 1978. A Survey of Water Transparency in Iowa Lakes, *Proceedings from the Iowa Academy of Sciences*, 85(1):6-9.

Bachmann, R.W., R.V. Bovbjerg, and J.D. Hall, 1966. The Morphometry of Lake West Okoboji, *Proceedings from the Iowa Academy of Sciences*, 73:165-168.

Begni, G., 1982. Selection of the Optimum Spectral Bands for the SPOT Satellite, *Photogrammetric Engineering and Remote Sensing*, 48(10):1613-1620.

Bold, H.C., and M.J. Wynne, 1985. Introduction to the Algae: Structure and Reproduction, Prentice-Hall, Inc., Englewood Cliffs, 720pp.

Carr, N.G., and B.A. Whitton, eds., 1973. The Biology of Blue-Green Algae, University of California Press, Berkeley, 676pp.

Chacon-Torres, A., L.G. Ross, M.C.M. Beveridge, and A.I. Watson, 1992. The Application of SPOT Multispectral Imagery for the Assessment of Water Quality in Lake Patzcuaro, Mexico, *International Journal of Remote Sensing*, 13(4):587-603.

Crippen, R.E., 1989. A Simple Spatial Filtering Routine for the Cosmetic Removal of Scan-line Noise from Landsat TM P-Tape Imagery, *Photogrammetric Engineering and Remote Sensing*, 55(3):327-331.

Dekker, A.G., T.J. Malthus, and E. Seyhan, 1991. Quantitative Modeling of Inland Water Quality For High-Resolution MSS Systems, *IEEE Transactions on Geoscience and Remote Sensing*, 29(1):89-95.

Dekker, A.G., T.J. Malthus, M.M. Wijnen, and E. Seyhan, 1992. The Effect of Spectral Bandwidth and Positioning on the Spectral Signature Analysis of Inland Waters, *Remote Sensing of the Environment*, 41:211-225.

Dodd, J.D., R.M. Webster, G. Collins, and L. Wehr, 1968. A Consideration of Pollen, Diatoms and Other Remains in Postglacial Sediments, *Proceedings from the Iowa Academy of Sciences*, 75:197-209.

Gitelson, A.A., 1992. The Peak Near 700 nm on Radiance Spectra of Algae and Water: Relationships of its Magnitude and Position with Chlorophyll Concentration, *International Journal of Remote Sensing*, 13(17):3367-3373.

Gitelson, A.A., F. Szilagyi, and K.-H. Mittenzwey, 1993. Improving Quantitative Remote Sensing for Monitoring of Inland Water Quality, *Water Research*, 27(7):1185-1194.

Gitelson, A.A., S. Laaorawat, G.P. Keydan, and A. Vonshak, 1995. Optical Properties of Dense Algal Cultures Outdoors and Their Application to Remote Estimation of Biomass and Pigment Concentration in *Spirulina platensis* (Cyanobacteria), *Journal of Phycology*, 31:828-834.

Guyot, G. and X. Gu, 1994. Effect of Radiometric Corrections on NDVI-Determined from SPOT-HRV and Landsat-TM Data, *Remote Sensing of the Environment*, 49:169-180.

Guzzi, R., G.C. Maracci, R. Rizzi, and A. Siccardi, 1985. Spectroradiometer for Ground-Based Atmospheric Measurements Related to Remote Sensing in the Visible from a Satellite, *Applied Optics*, 24:2859-2864.

Jensen, J.R., 1996. Introductory Digital Image Processing: A Remote Sensing Perspective, Prentice Hall, Upper Saddle River, 319pp.

Jones, J.R., and R.W. Bachmann, 1974. Limnological Features of Some Northwestern Iowa Lakes, *Proceedings from the Iowa Academy of Sciences*, 81(4):158-163.

Jones, J.R., and R.W. Bachmann, 1978. Trophic Status of Iowa Lakes in Relation to Origin and Glacial Geology, *Hydrobiologia*, 57(3):267-273.

Jupp, D.L.B., J.T.O. Kirk, and G.P. Harris, 1994. Detection, Identification and Mapping of Cyanobacteria — Using Remote Sensing to Measure the Optical Quality of Turbid Inland Waters, *Australian Journal of Marine and Freshwater Research*, 45:801-828.

Kirk, J.T.O., 1994. Light and Photosynthesis in Aquatic Ecosystems, Cambridge University Press, Cambridge, 509pp.

Lathrop, R.G. Jr., and T.M. Lillesand, 1989. Monitoring Water Quality and River Plume Transport in Green Bay, Lake Michigan with SPOT-1 Imagery, *Photogrammetric Engineering and Remote Sensing*, 55(3):349-354.

Lillesand, T.M., and R.W. Kiefer, 1994. Remote Sensing and Image Interpretation, John Wiley & Sons, New York, 750pp.

Lee, R.E., 1989. Phycology, Cambridge University Press, Cambridge, 645pp.

Mayo, M., A.A. Gitelson, Y.Z. Yacobi, and Z. Ben-Avraham, 1995. Chlorophyll Distribution in Lake Kinneret Determined from Landsat Thematic Mapper Data, *International Journal of Remote Sensing*, 16(1):175-182.

Messina, J., 1996. What is Radiance? Ask Dr. SPOT Technical Column in *SPOTLight*.

Milton, E.J., 1987. Principles of Field Spectroscopy, *International Journal of Remote Sensing*, 8(12):1807-1827.

Mittenzwey, K.-H., A.A. Gitelson, and K.Y. Kondratiev, 1992. Determination of Chlorophyll *a* of Inland Waters on the Basis of Spectral Reflectance, *Limnology and Oceanography*, 37(1):147-149.

Morel A., and L. Prieur, 1977. Analysis of Variations in Ocean Color, *Limnology and Oceanography*, 22(4):709-722.

Nusch, E.A., 1980. Comparison of Different Methods for Chlorophyll and Pheopigment Determination, *Ergebnisse der Limnologie*, 14:14-36.

Price, J.C., 1987. Calibration of Satellite Radiometers and the Comparison of Vegetation Indices, *Remote Sensing of the Environment*, 21:15-27.

Quibell, G., 1992. Estimating Chlorophyll Concentration Using Upwelling Radiance from Different Freshwater Algal Genera, *International Journal of Remote Sensing*, 13(4):2611-2621.

Richardson, L.L., 1996. Remote Sensing of Algal Bloom Dynamics, *BioScience*, 46(7):492-501.

Rowan, K.S., 1989. Photosynthetic Pigments of Algae, Cambridge University Press, Cambridge, 334pp.

Rundquist, D.C., J.F. Schalles, and J.S. Peake, 1995. The Response of Volume Reflectance to Manipulated Algal Concentrations Above Bright and Dark Bottoms at Various Depths in an Experimental Pool, *Geocarto International*, 10(4):5-14.

Rundquist, D.C., L. Han, J.F. Schalles, and J.S. Peake, 1996. Remote Measurement of Algal Chlorophyll in Surface Waters: The Case for the First Derivative of Reflectance Near 690 nm, *Photogrammetric Engineering and Remote Sensing*, 62(2):195-200.

Santer, R., X.F. Gu, J.L. Deuze, C. Devaux, E. Vermote, and M. Verbrugghe, 1992. SPOT Calibration at the La Crau Test Site (France), *Remote Sensing of the Environment*, 41:227-237.

Schalles, J.F., A.A. Gitelson, Y.Z. Yacobi, and A.E. Kroenke, 1998. Estimation of Chlorophyll *a* from Time Series Measurements of High Spectral Resolution Reflectance in an Eutrophic Lake, *Journal of Phycology*, 34:383-390.

Starks, P.J., E.A. Walter-Shea, F.R. Schiebe, and B. L. Markham, 1995. Temperature Sensitivity Characterization of a Silicon Diode Array Spectrometer, *Remote Sensing of the Environment*, 51:385-389.

Starks, P.J., F.R. Schiebe, and J.F. Schalles, 1995. Characterization of the Accuracy and Precision of Spectral Measurements by a Portable, Silicon Diode Array Spectrometer, *Photogrammetric Engineering and Remote Sensing*, 61(10):1239-1246.

Stewart, W.D.P., ed., 1974. Algal Physiology and Biochemistry; Biological Monographs Volume 10, University of California Press, Berkeley, 989pp.

Turner Designs, 1995. TD-700 Laboratory Fluorometer Operating Manual, v. 1.2.

Van Stokkom, H.T.C., G.N.M. Stokman, and J.W. Hovenier, 1993. Quantitative Use of Passive Optical Remote Sensing Over Coastal and Inland Water Bodies, *International Journal of Remote Sensing*, 14(3):541-563.

Verdin, J.P., 1984. U.S. Department of the Interior, Bureau of Reclamation, Engineering and Research Center, Limnological Applications of Multispectral Remote Sensing. REC-ERC-84-2, 53pp.

Welschmeyer, N.A., 1994. Fluorometric Analysis of Chlorophyll *a* in the Presence of Chlorophyll *b* and Pheopigments, *Limnology and Oceanography*, 39(8):1985-1992.

Wetzel, R.G. and G.E. Likens, 1991. Limnological Analyses, Springer-Verlag, New York, 391 pp.

Wetzel, R.G., 1983. Limnology, Saunders College Publishing, Fort Worth, 767 pp.

Yacobi, Y.Z, M. Mayo, and A.A. Gitelson, 1995. Remote Sensing of Chlorophyll in Lake Kinneret Using High-Spectral-Resolution Radiometer and Landsat TM: Spectral Features of Reflectance and Algorithm Development, *Journal of Plankton Research*, 17(11):2155-2173.

Yacobi, Y.Z., U. Pollingher, Y. Gonen, V. Gerhardt, and A. Sukenik, 1996. HPLC Analysis of Phytoplankton Pigments from Lake Kinneret with Special Reference to the Bloom-Forming Dinoflagellate *Peridinium gatunense* (Dinophyceae) and Chlorophyll Degradation Products, *Journal of Plankton Research*, 18(10):1781-1796.